dietitianCE

Continuing Education for Nutrition Professionals

Dietary, Exercise, and Other Influences on Inflammatory Bowel Disease

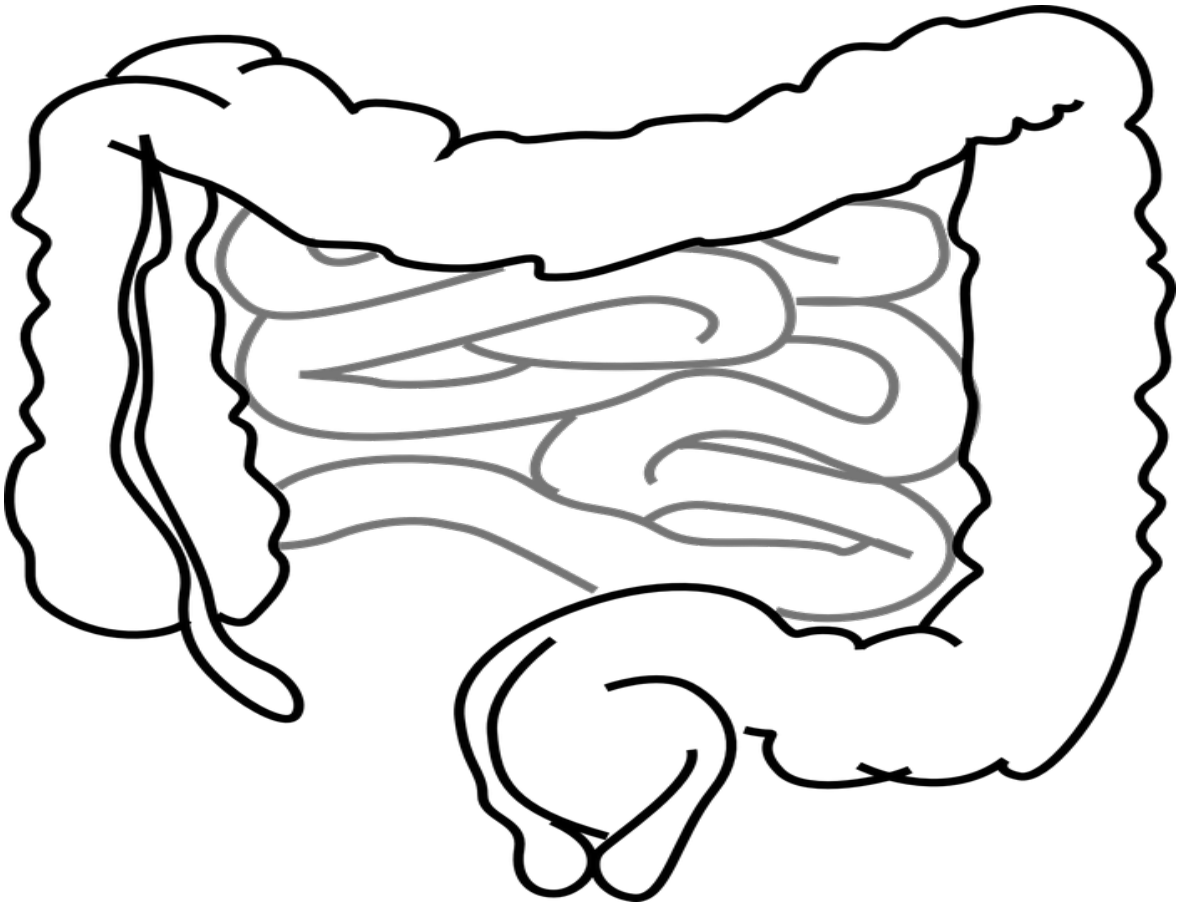

Colon epithelial cells luminal environment and physiopathological consequences: impact of nutrition and exercise

Abstract

The colonic epithelial cells represent a border between the colon luminal content, containing notably bacteria and a complex mixture of compounds, and the "milieu interieur" as defined by the French physiologist Claude Bernard. The physical-chemical composition of the luminal content, including luminal pH and bacterial metabolite, that obviously is not constant, is modified for instance according to the diet. Data obtained recently indicate that physical exercise may also modify the colonic luminal content. Evidence has indicated that modification of the luminal content characteristics has, indeed, consequences for the colonic epithelial cells, notably in terms of energy metabolism and DNA integrity. Although such alterations impact presumably the homeostatic process of the colonic epithelium renewal and the epithelial barrier function, their contribution to pathological processes like mucosal inflammation, pre-neoplasia, and neoplasia remains partly elusive. Open questions remain regarding the individual and collective roles of luminal changes, particularly in a long-term perspective. These questions are related particularly to the capacity of the bacteria metabolites to cross the mucus layer before entering the colonocytes, to the concentrations of metabolites in proximity of the colonic crypt stem cells, and to the capacity of colonocytes to detoxicate deleterious compounds, to take up and utilize beneficial compounds.

Keywords: Colon, Intestinal microbiota, Oxygen consumption, DNA damage, Barrier function, Exercise, Dietary protein

Background

The colonic epithelium can be viewed as a dynamic structure with a very rapid speed of renewal. Indeed, the colonic epithelium in mammals is renewed within few days. Stem cells residing within the base of the crypts are responsible for continuously producing transit cells that undertake differentiation following a limited number of cellular divisions. This renewal is made through highly coordinated and complex sequences of events beginning with mitosis of pluripotent stem cells situated at the bottom of the colonic crypts. The differentiated cells reach the surface of the colon, where they are removed by detachment-induced apoptosis named Anoïkis. The high division rate of stem cells and the corresponding high apoptotic rate of mature cells lead to the high cellular turnover of the colon epithelium. A dysfunction of oxygen consumption or mitochondrial dysfunction may compromise the epithelium homeostasis and consequently alters its barrier function [1].

Besides, the colonic epithelium is notably responsible for the physiological function of water, electrolyte, and various bacterial metabolites absorption from the lumen to the bloodstream. This absorption is made through absorptive colonocytes which are facing the luminal content, a complex and not fully characterized mixture of bacteria and their metabolites, water, undigested or partially digested dietary/endogenous compounds, particularly from endogenous and alimentary proteins that may be beneficial or deleterious for the epithelium, etc. Occasionally, the homeostatic processes of colonic epithelial self-renewing, possibly associated with disruption of normal functions, are affected, and such alterations may be associated with different physiopathological states including

diarrhea [2], mucosal inflammation, and preneoplasic/neoplasic lesions [3].

It is expected from the high energy consumption of the colonic epithelial cells that mitochondrial dysfunction may have a larger impact on their metabolism and physiology. Thus, the objectives of this mini-review are (i) to give some examples of the impact of nutrient intake, especially dietary protein, on the characteristics of the large intestine luminal content composition; (ii) to give a brief overview on the effects of changes of the colonic epithelial cell luminal environment on their physiology and metabolism, with a focus on the effects of some bacterial metabolites; (iii) to examine to what extent such changes, above the adaptive capacities of the colonocytes, may have consequences for the gut health; and finally (iv) to report on some recent results regarding the impact of physical exercise on the luminal environment of colonocytes.

Effects of the diet on the composition of the large intestine luminal content

Undigested or partially digested substrates from both endogenous (digestive secretions, exfoliated cells, mucins, etc.) and dietary sources can be metabolized by the bacteria belonging to the intestinal microbiota [4]. Dietary intervention studies with volunteers revealed that the macronutrient composition of the diet can impact the composition of the large intestine luminal content. Notably, it has been shown that dietary undigestible polysaccharides increase the fecal concentration of short-chain fatty acids (SCFA) [5], while diets with a high fat content increase bile acid secretion in the small intestine, leading to high fecal concentrations of microbiota-derived secondary bile acids, such as deoxycholic acid [6].

Although the digestion of alimentary protein is very efficient, approximately 90% efficiency, some nitrogenous material originating from non-digested proteins are transferred from the small intestine to the large intestine [7] and are degraded by the microbiota and by residual pancreatic enzymes to produce numeral metabolites and gases. These gases, especially, can be beneficial or deleterious for the intestinal epithelium in a concentration-dependent way [8, 9]. High-protein diets increase the fecal concentrations of amino acid-derived bacterial metabolites, such as branched-chain fatty acids, phenolic and indolic compounds, hydrogen sulfide (H_2S), and ammonia, among others [10]. Other parameters, such as colonic luminal pH, may also be modified by dietary changes. Ingestion of nondigestible carbohydrates decreases the fecal pH in adults [11], while consumption of high-protein/low carbohydrate diets increases this parameter [12]. Collectively, these studies indicate that the human rectal environment (inferred from feces analysis) is depending on the dietary composition.

Regarding the composition of the colonic microbiota, although considered as globally stable at the individual level [13], this composition can be, however, rapidly affected by environmental modifications, notably from dietary origin [14]. Although modifications of luminal bacterial metabolite composition in inflammatory bowel diseases have been reported [15], it is often a difficult task to determine if such modifications are causes or consequences of these diseases. In the same line of thinking, although intestinal microbiota dysbiosis has been observed in colorectal cancers [16], the respective causal links between the bacterial composition/bacterial metabolic capacity/bacterial metabolite composition and the related pathophysiological situations remain largely elusive.

In this overall context, our mini-review will present several changes in the luminal environment (bacterial metabolite composition, pH, osmolarity) which have been shown to impact, at least in vitro, the colonic epithelial cells with potential implications in digestive disease apparition and development [17].

Bacterial metabolites and colonic epithelium energy metabolism

The gastrointestinal tract consumes 20% of the whole body oxygen consumption while representing approximately 5% of body weight. Absorptive colonic epithelial cells utilize energy substrates from both the luminal and basolateral sides. Fuels from arterial origin are mainly amino acids including L-glutamine, L-glutamate, and L-aspartate, but also D-glucose [18].

SCFA (namely acetate, propionate, and butyrate) are major luminal fuels for colonocytes. These compounds are produced by the intestinal microbiota from undigestible polysaccharides [19] and several amino acids originating from undigested protein [20]. For instance, butyrate plays an important role on oxygen consumption in order to favor energy metabolism [21]. Data showing that butyrate uptake is impaired in the inflamed colonic mucosa. It has also been suggested that the reduction of butyrate availability may decrease the physiological functions of this SCFA, especially butyrate, in colonocytes [22]. In addition, to act as a luminal fuel in colonocytes, butyrate acts as a regulator of gene expression in these cells [23] (Fig. 1).

Hydrogen sulfide, which is produced by some intestinal bacteria from endogenous and exogenous sulfur-containing substrates, influences colonocyte health via mitochondrial metabolism and inflammation resolution. Evidences have suggested that, under specific conditions such as hypoxia, H_2S contributes to generate adenosine triphosphate (ATP) [24, 25]. Then, when oxygen is insufficient, colonocytes are capable of obtaining energy demand via sulfide oxidation ($S_2O_3^{2-}$). Indeed, this oxidation process is an adaptation of

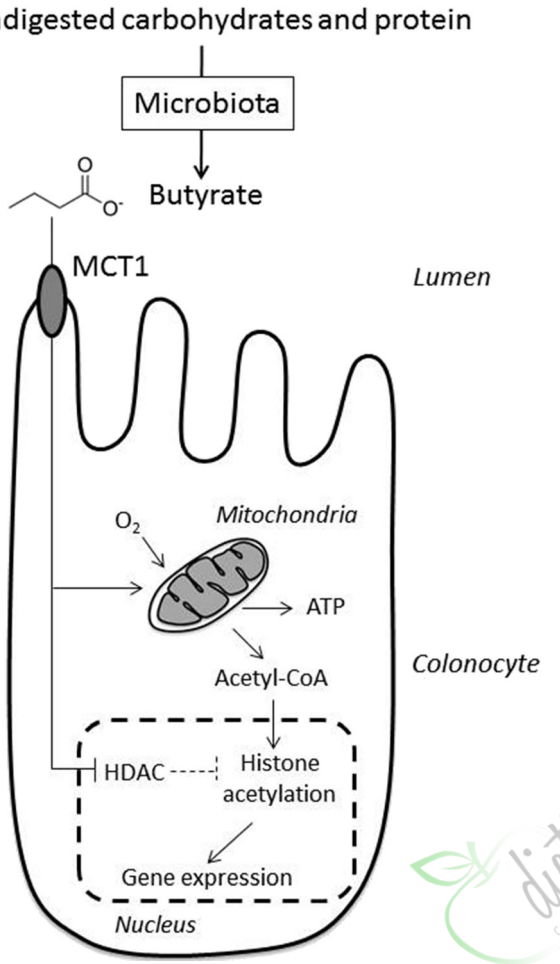

Fig. 1 Schematic representation of the microbiota-derived butyrate metabolism and effects on colonocytes. Butyrate, which is produced from undigested carbohydrates and some protein-derived amino acids, diffuses through the mucus layers before entering colonocytes. Butyrate enters the cell via MCT1 (monocarboxylate transporter 1) and is oxidized in the mitochondria allowing ATP production. A part of cytosolic acetyl CoA produced from butyrate is used for histone acetylation, while unmetabolized butyrate inhibits histone deacetylase (HDAC) activity. Increased histone acetylation then modulates gene expression in colonocytes

colonocytes, and it involves a sulfide quinone reductase (SQR) activity, which also contributes to colonocytes tolerance [26]. Besides, H_2S inflammatory signaling is dependent on its concentration and colonocytes' ability to detoxify this gas transmitter. At low concentrations, H_2S has been shown to upregulate cyclooxygenase-2 (COX-2) expression [27] and to reduce prostaglandin E_2 synthesis, chemokines, cytokines, and other protein expressions that are related to factor nuclear kappa B (NF-κB) pathway [28] (Fig. 2). COX-2 is important for maintenance of mucosal defense in the gastrointestinal tract, as well as in inflammation resolution [27]. Hydrogen sulfide is also capable of inhibiting phosphodiesterases via elevation of second messengers, such as cyclic AMP and/or cyclic GMP levels, which contribute to its anti-inflammatory role in colonocytes and lowering blood pressure [29]. ATP-sensitive potassium channel can be activated by H_2S, especially from endogenous origin, which may attenuate pain in colonic inflammation [30] and leukocytes activation [31]. Moreover, H_2S may interfere on leukocytes adherence, notably neutrophils, in vascular endothelium and diminishes both leukocyte recruitment and infiltration under tissue injury condition [31]. Those cells infiltrated by neutrophils can undergo apoptosis and be cleaned by macrophage type 2, which have anti-inflammatory phenotype [27, 31]. Therefore, it seems that H_2S, at low concentrations, plays an important role in inflammation resolution in colonocytes through several pathways, and this resolution, in turn, may also favor tissue repair (Fig. 2).

On the other hand, H_2S as well as p-cresol and ammonia, at excessive luminal concentrations, interferes with colonocyte respiration, at least in in vitro experiments. Hydrogen sulfide inhibits, above a threshold value, markedly, although in a reversible way, the colonocyte oxygen consumption and ATP production [32] (Fig. 2). This inhibition of cell respiration corresponds to the inhibition of the mitochondrial cytochrome C oxidase activity, one of the main components of mitochondrial respiration [33]. At concentration where H_2S inhibits oxygen consumption in colonocytes, this gaseous compound increases the expression of several inflammation-related genes [8]. The cytoplasmic concentration of this agent can increase the capacity of colonocytes of detoxifyed H_2S in the mitochondria and then impact gene expression in the nuclei (Fig. 2). Indeed, studies have shown H_2S detoxification impairment in patients with Crohn's disease [34] and also butyrate β-oxidation impairment in patients with ulcerative colitis [35]. Moreover, this metabolite was capable of supporting colonic tumor growth through stimulation of cell bioenergetics and cell proliferation [36]. Another bacterial metabolite, p-cresol, which is produced from L-tyrosine by the intestinal microbiota and which is present in the feces at low millimolar concentration, partially inhibits oxygen consumption in colonocytes [9]. Ammonia (considered as the sum of NH_4^+ and NH_3), which is produced by the bacterial microbiota from amino acid deamination and hydrolysis of urea by the bacterial ureases, is present at millimolar concentrations in the colonic luminal content [20]. Millimolar concentrations of ammonia dose-dependently inhibit SCFA oxidation [37] and basal oxygen consumption in colonocytes [38]. However, colonocytes appear to be able to face moderate increase of ammonia luminal concentration by metabolizing ammonia in L-glutamine and L-citrulline, respectively, in the cytosol and mitochondria of colonocytes [39, 40].

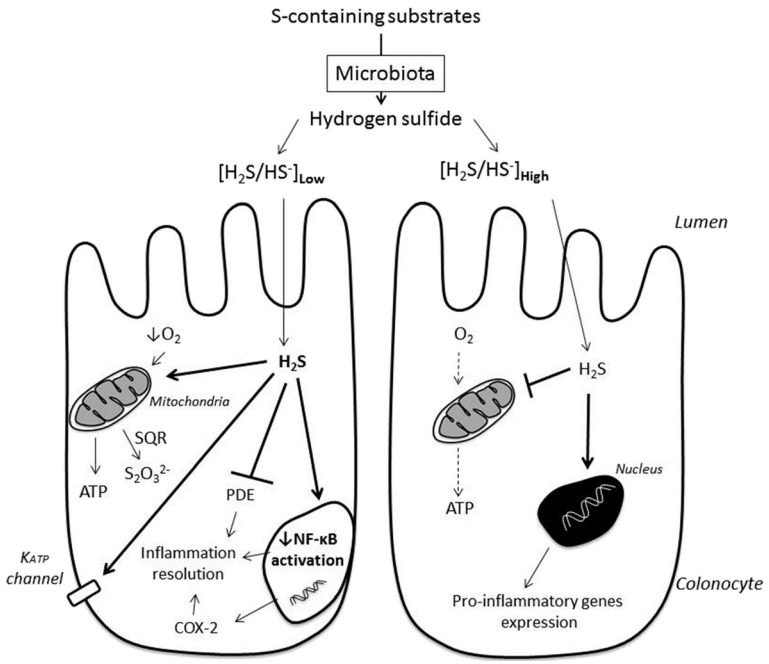

Fig. 2 Schematic representation of the microbiota-derived H_2S metabolism and effects on colonocytes. Hydrogen sulfide (H_2S) is produced from several dietary and endogenous sulfur-containing compounds and diffuses through the mucus layers and colonocyte apical membrane. Left panel: When H_2S concentration is low, mitochondria can detoxicate it through oxidation into thiosulfate ($S_2O_3^{2-}$) via sulfide quinone reductase (SQR) in the sulfide oxidizing unit. H_2S can also be used for ATP production when oxygen (O_2) is low. Moreover, H_2S is able to support inflammation resolution through inhibition of phosphodiesterases (PDE), downregulation of NF-κB pathway, and enhancement of cyclooxygenase-2 (COX-2) expression. In addition, H_2S is able to activate ATP-potassium sensitive channel (K_{ATP} channel), which may be involved with reduced pain and inflammation. Right panel: When H_2S is high, thus exceeding colonocyte detoxification capacity, it inhibits mitochondrial cytochrome c oxidase activity, leading to a decrease O_2 consumption. Raised concentration of the intra-cytoplasmic H_2S increases the expression of genes related to inflammation

Then, it appears that some bacterial metabolites, such as H_2S, at a given concentration, and SCFA are regulators of colonocyte metabolism. However, when present in the colonic luminal content at excessive concentrations, H_2S, p-cresol, and ammonia can act on colonocytes as "metabolic troublemakers" by acting, mainly, on the mitochondrial activity [41].

Possible links between physical exercise and intestinal microbiota

We are far away from the precise mechanisms that connect exercise and intestinal microbiota. It is supported that the exercise, especially the aerobic exercise, plays a role on intestinal microbiota by altering parameters that influence the intestinal microenvironment. Recently, a paper from our laboratory concerning exercise, nutrition, and intestinal microbiota [42] was published, and we will present below some topics.

Short-chain fatty acids

Exercise may increase acetate-, propionate-, and butyrate-producing bacteria species [43, 44]. Matsumoto et al. [45] were the first to show that voluntary exercise in animals is able to change SCFA production (mainly n-butyrate) in the cecum. In addition, this study reported alteration in the cecal microbiota profile after exercise with greater predominance of butyrate-producing bacteria species [45]. This shift in butyrate production and bacteria composition in the exercised group was also shown by Evans et al. [43].

The possible effect of aerobic exercise on the microbial composition is the environment change which has been connected to a pH decrease in the gut from SCFA production. SCFA contribute to decrease pH in the large intestine and decrease the transformation of primary to secondary bile acids promoting colonic acidification. Changes in the intestinal luminal pH may modify the environment in such way that it becomes more favorable for the proliferation of commensal bacterial species [42, 46].

After being absorbed by colonocytes, SCFA can participate in intestinal metabolism. Acetate and propionate are preferred for other organs, while butyrate is the major fuel for colonocytes. Specifically, butyrate can promote cell differentiation and cell cycle arrest and inhibit the enzyme histone deacetylase, [47]. Also, butyrate can improve mitochondrial metabolism via β-oxidation and

AMP-activated protein kinase (AMPK) activation in colonocytes [48].

Moreover, studies have shown that butyrate may induce mucin synthesis [49] and improve gut barrier integrity by increasing tight junction assembly [50–52]. Mucins are the protective layer consisting of glycoproteins that form the intestinal barrier which limit exposure of mucosa to toxins and bacteria. This mucin layer has been recognized to play an important role in the interaction with intestinal microbiota and may serve as a substrate for intestinal bacteria, such as the commensal species *Akkermansia muciniphila*. Because of this, the mucin layer contributes to modulate the microbial community composition [52].

Butyrate production in the large intestine is associated with production of heat shock protein 70 (Hsp70). Hsp70 maintains the functional and structural properties of intestinal epithelial cells in response to intense prolonged exercise [53]. Since exercise and butyrate stimulate epithelial cell Hsp70 production, this may provide structural and functional stability to intestinal epithelial cells undergoing unfavorable conditions.

Bile acids

Exercise has been reported to increase excretion of primary bile acids in the gastrointestinal tract. Since SCFA, specifically butyrate (that has been reported to be increased by exercise), diminishes the conversion of bile acids into secondary bile acids, physical activity may, consequently, favor the rising of primary bile acids concentrations in the intestinal luminal content [54, 55]. The primary bile acids have established anti-microbial activity [55]. In agreement with this hypothesis, Islam et al. [56] demonstrated that cholic acid induced substantial changes in the cecal microbiome composition by stimulating the growth of Firmicutes at the expense of Bacteroidetes and provoked outgrowth of several bacteria in the *Clostridia* and *Erysipelotrichi* classes. Antimicrobial activity of the bile acids may elicit selective pressure on the bacterial communities in exercised mice, leading to a shift of the intestinal microbiota composition [55, 56]. Besides, some bile acid-tolerant microbes are sulfur-reducing bacteria, such as *Bilophila wadsworthia*. In animal-based diet, for example, this species can thrive and favors inflammation via H_2S production [57].

Furthermore, secondary bile acids produced by intestinal microbiota influence mitochondrial metabolism. Intestinal microbiota can convert primary bile acids into secondary bile acids. The latter, in turn, interacts with mitochondria through farnesoid X receptor (FXR) and G-coupled membrane protein 5 (TGR5) [58]. These transcription factors regulate other proteins that are involved in fatty acid uptake and oxidation, such as peroxisome proliferator-activated receptor alpha (PPAR-α) and steroid response element binding protein 1-c (SREBP-1c) [59].

Hence, exercise is able to modulate both butyrate and bile acids exercise which are involved in intestinal metabolism and health homeostasis. In addition, it seems that they can be influenced by H_2S, especially when H_2S is produced via microbiota.

Bacterial metabolites and colonic epithelial cell DNA integrity

By using the sensitive H2AX genotoxicity test, p-cresol has been found to alter dose-dependently the DNA integrity in colonocytes without cytotoxic effects [9]. Phenol, which is produced by the intestinal microbiota from L-tyrosine, can react with nitrite, leading to the formation of the mutagenic compound p-diazoquinone [60].

Numerous other bacterial metabolites have been identified to alter DNA integrity in colonocytes. They include the fecal pentaenes, which are produced by the microbiota presumably from polyunsaturated ether phospholipids, and represent potent mutagens towards colonocyte DNA [61]. Deoxycholic acid produced in the colon by the intestinal microbiota is also acting as a DNA-damaging agent [62]. Acetaldehyde, which is produced from ethanol by the intestinal microbiota, is considered as a possible co-carcinogenic compound in the rectum [63]. From these examples of genotoxic bacterial metabolites, it is largely conceivable that long-term exposure of colonic crypt cells to excessive DNA-damaging bacterial metabolites would increase the risk of unrepaired DNA lesions in these cells [64].

Bacterial metabolites and colonic epithelial barrier function

Some bacterial metabolites have been suspected to affect, either positively or negatively, the colonic epithelial barrier function. For instance, it has been proposed that exogenous H_2S, by reducing disulfide bonds in mucus, would increase the permeability of the mucous layer to luminal compounds, including the heme compound originating notably from red meat consumption [65]. Interestingly, evidence has been presented indicating that altered mitochondrial function induced by uncoupling agents in colonocytes cause intestinal barrier dysfunction [66], raising the view that perturbed mitochondrial function is associated with impaired epithelial integrity. Conversely, endogenous H_2S may have beneficial effects on colonic mucus production [67]. Also, the bacterial metabolite indole, which is produced from L-tryptophan, has been shown to act as a beneficial luminal compound by increasing epithelial cell tight-junction resistance [68]. Lastly, butyrate is also

recognized as a bacterial metabolite which enhances the intestinal barrier function [69].

Bacterial metabolites and pH

The pH in the human large intestine is slightly acidic in the caecum while being close to neutrality in the left colon and rectum [70]. The luminal pH depends on the respective concentrations of a very complex mixture of acidic and alkaline compounds in the large intestine. Modifications of the luminal pH may affect colonic epithelial cell physiology. Interestingly, lower colonic luminal pH in patients with ulcerative colitis has been observed [71]. In an experimental rodent model with chemically induced colon carcinogenesis, lower luminal pH is associated with higher tumor yield and increased epithelial cell proliferation [72]. Conversely, a low pH inhibits the synthesis by the intestinal microbiota of the DNA-damaging secondary bile acids [73]. In addition, acidic extracellular pH has been shown to shift colorectal epithelial cell death from apoptosis to necrosis upon exposure to short-chain fatty acids [74]. Lastly, low external pH is able to increase markedly the expression of the multidrug resistance (MDR) protein in human colon carcinoma cell lines [75], thus rendering these cells more resistant to chemotherapeutic agents.

Then, it appears that a more acidic luminal pH is associated with both beneficial and deleterious effects on colonocytes. These effects are apparently different according to the status of colonocytes, i.e., healthy or neoplasic.

Physical exercise and colonic luminal content characteristics

Recent studies strongly suggest that physical exercise can impact the characteristics of the intestinal luminal contents and notably the microbiota composition. Matsumoto et al. [45] were among the first to report that physical exercise modifies intestinal microbiota composition. More recently, it has been shown that the effects of exercise on intestinal microbiota are partly independent from dietary changes [76]. Studies have suggested that moderate aerobic exercise may contribute to the growth of butyrate-producing bacteria [77]. The training status and intensity of exercise appear to impact the proliferation of specific bacteria, such as *Faecalibacterium prausnitzii*, beneficial bacteria for the digestive tract [78]. A study with human volunteers reported increased microbiota diversity and richness in elite rugby players when compared with control groups with low physical activity and low or high body mass index. Interestingly, these athlete volunteers reported high protein consumption compared to the sedentary controls and, despite of there is no H_2S-related data on this study, it seems that exercise and diet can change intestinal microbiota composition orthogonally [79]. This hypothesis is also supported by Kang et al. [80]. Also, the authors found that trained men presented a high level of SCFA on fecal samples when compared with sedentary men [79]. Likewise, Estaki et al. [81] analyzed the fecal microbiota of individuals with different fitness and demonstrated that cardiorespiratory fitness was positively correlated with increased intestinal microbial diversity and butyrate concentrations. The authors found a microbiome enriched in butyrate-producing bacteria, such as *Lachnospiraceae*, *Roseburia*, and *Clostridiales*, and high level of butyrate concentrations on individuals with high fitness.

So far, evidences have suggested an influence on the intestinal environment (mainly intestinal bacteria and their metabolites concentrations) by exercise, especially moderate aerobic exercise (60–65% VO_2max) [42–44, 50, 78, 80]. However, studies differ among themselves in relation to the methods applied and are no data related to the exercise effect on the luminal H_2S production/concentration.

Conclusion and future prospects

According to experimental studies with animal models and colonocytes, there is no doubt that changes in the luminal environment of colonic epithelial cells, and notably high concentrations of several bacterial metabolites, impact major aspects of their physiology and metabolism. Notably, such high concentrations of individual bacterial metabolites impact colonocyte energy metabolism, intestinal barrier, and inflammatory resolution and DNA integrity.

Several crucial unresolved questions remained, notably those related to the genotoxic effects of several bacterial metabolites in close vicinity with the colonic crypt stem cells, a parameter difficult to measure for obvious technical reasons. Indeed, since the crypt stem cells appear to be the cells at the origin of colorectal cancer [82, 83], the identification of the luminal compounds at the origin of mutations in these cells, as well as the threshold of concentrations above which genotoxic effects are observed, represents important parameters to be determined.

Another important point to take into consideration is related to the capacity of the bacterial metabolites to cross the mucus layers before entering colonocytes through the brush-border membranes. As a matter of fact, much experimental studies have been performed with colonocytes directly exposed to bacterial metabolites dissolved in the incubation medium. From that point of view, intraluminal colonic instillation of bacterial metabolites in anesthetized animals represents an experimental design which is closer to the physiological situation [8].

Finally, by better identifying the changes in the luminal environment, which are associated with both dietary

modifications and/or physical exercise and which increase or decrease the risk of alteration of the normal process of colonic/rectal epithelia renewal and functions, it will become possible to intervene rationally for limiting the risk of pathology from inflammatory and neoplasic type in these anatomical parts of the intestine.

High salt diet exacerbates colitis in mice by decreasing Lactobacillus levels and butyrate production

Abstract

Background: Changes in hygiene and dietary habits, including increased consumption of foods high in fat, simple sugars, and salt that are known to impact the composition and function of the intestinal microbiota, may explain the increase in prevalence of chronic inflammatory diseases. High salt consumption has been shown to worsen autoimmune encephalomyelitis and colitis in mouse models through p38/MAPK signaling pathway. However, the effect of high salt diet (HSD) on gut microbiota and on intestinal immune homeostasis, and their roles in determining vulnerability to intestinal inflammatory stimuli are unknown. Here, we investigate the role of gut microbiota alterations induced by HSD on the severity of murine experimental colitis.

Results: Compared to control diet, HSD altered fecal microbiota composition and function, reducing *Lactobacillus* sp. relative abundance and butyrate production. Moreover, HSD affected the colonic, and to a lesser extent small intestine mucosal immunity by enhancing the expression of pro-inflammatory genes such as *Rac1*, *Map2k1*, *Map2k6*, *Atf2*, while suppressing many cytokine and chemokine genes, such as *Ccl3*, *Ccl4*, *Cxcl2*, *Cxcr4*, *Ccr7*. Conventionally raised mice fed with HSD developed more severe DSS- (dextran sodium sulfate) and DNBS- (dinitrobenzene sulfonic acid) induced colitis compared to mice on control diet, and this effect was absent in germ-free mice. Transfer experiments into germ-free mice indicated that the HSD-associated microbiota profile is critically dependent on continued exposure to dietary salt.

Conclusions: Our results indicate that the exacerbation of colitis induced by HSD is associated with reduction in *Lactobacillus sp.* and protective short-chain fatty acid production, as well as changes in host immune status. We hypothesize that these changes alter gut immune homeostasis and lead to increased vulnerability to inflammatory insults.

Keywords: Salt, NaCl, Western diet, Colitis, Microbiota, Lactobacillus, Butyrate, MAPK-pathway

Background

The prevalence of chronic inflammatory diseases, such as multiple sclerosis (MS), rheumatoid arthritis, diabetes, and inflammatory bowel disease (IBD), has been steadily increasing over the past half-century [1]. Although multiple genetic factors have been identified to contribute to the risk of developing these disorders, genetic drift alone cannot explain the rapid increase in prevalence within this relatively short time interval [2]. Therefore, environmental factors, particularly related to dietary and hygiene habits, have been proposed as disease modifiers [3, 4]. The relationship between dietary habits and the increased prevalence of intestinal inflammatory disorders is of particular interest. Consumption of highly caloric processed foods, high in fat and simple carbohydrate content, and low in fiber content, has been steadily increasing in the "western world," where the incidence of chronic inflammatory diseases is the highest [5, 6]. Strong epidemiological evidences support the concept that diet underpins the rise in chronic inflammatory diseases such as IBD, diabetes, or asthma [3, 5, 6]. However, the exact mechanisms by which specific dietary changes increase susceptibility to inflammatory diseases, and whether they are indeed mediated by changes in microbiota composition

or function, are still unclear. Previous studies have shown that a high fat diet may have a direct pro-inflammatory effect, increasing the production of pro-inflammatory cytokines TNFα, IL-1β, and IL-6 [7]. Others have shown direct interactions between animal fat consumption, altered bile acid metabolism, and specific alteration in the gut microbiota, leading to increased colitis severity [8]. However, one characteristic element in the western diet that has been overlooked until recently is its high salt (sodium chloride, NaCl) content.

NaCl has been shown to induce pathogenic Th17 cells (IL-17-producing T-helper cells) in both human and mice naïve $CD4^+$ cell cultures in vitro. Mice receiving a salt-enriched diet developed a more severe form of experimental autoimmune encephalomyelitis (EAE), an animal model of MS, mediated by IL-17A and RORγt expressing Th17 cells [9, 10]. Interestingly, high NaCl intake has been associated with increased disease activity in MS patients [11]. Moreover, a longitudinal clinical study showed that high NaCl intake increases circulating monocytes and levels of plasma cytokines such as IL-6 and IL-23 [12]. A recent study has shown that exposing human *lamina propria* mononuclear cells (LPMC) to high concentrations of NaCl enhances TNF-α and IL-17A release in a p38-dependent manner, and that feeding mice a salt-enriched diet exacerbates experimental colitis [13]. While all these studies suggest a promoting role of high salt diet in driving a pro-inflammatory state, the underlying mechanisms are still not fully understood.

We hypothesized that a high salt diet impacts inflammation via the interaction with the gut microbiota. In fact, it is well established that diet determines the composition [14–16] and function [17, 18] of the gut microbiota. It has been recently shown that diet low in dietary fiber may be causing irreversible changes in gut microbiota with some species disappearing over generations [19]. Given that gut microbiota composition has been implicated in the pathophysiology of multiple immune-related disorders, such as IBD, diabetes, or asthma [20], and taking into account that diet shapes the gut microbiota, we investigated the ability of high salt diet (HSD) to modulate gut microbial composition and metabolism, and to influence vulnerability to intestinal inflammatory stimuli.

Methods

Mice

Six- to eight-week-old specific pathogen-free (SPF) male C57BL/6 mice (obtained from Taconic) were housed at the animal facility of McMaster University under 12 h light/dark cycles and standard conditions for temperature and humidity. All mice received irradiated control diet (7004, Teklad, with 20% of calories from protein, 29% from fat, and 51% from carbohydrates, containing 0.4% Na and 0.7% Cl) and sterile tap water ad libitum upon arrival. Experiments started 1 week after arrival in the central animal facility to allow the animals to habituate to the novel environment. Mice were then divided into two groups: (1) control diet—mice were fed with control diet for the entire course of the experiment; (2) HSD (high salt diet)—mice received the same diet supplemented with 4% NaCl (custom ordered from Teklad), plus 1% NaCl sterile water, ad libitum, during 4 weeks. For germ-free (GF) mice experiments, C57BL/6 mice were re-derived in McMaster Axenic Gnotobiotic Unit (AGU) by two-stage embryo transfer and kept in dedicated isolators during the entire course of the experiment. For the microbiota-transfer experiment, GF mice were colonized by oral gavage with 200 μl of cecal microbiota from a mouse fed with control diet or HSD and housed in dedicated individually ventilated racks.

DNA isolation and 16S rRNA Illumina sequencing

DNA was extracted from 100 mg of fecal content samples using the MagMAX DNA Multi-sample kit and the MagMAX Express-96 well magnetic particle processor (Thermofisher, Waltham, MA, USA) to achieve an automatic and standardized DNA extraction across samples. Briefly, fecal samples were mechanically homogenized with 2.8 mm ceramic beads (MoBio, Carlsbad, CA, USA; an additional 0.2 g of 0.1 mm glass beads were added), 100 μl of guanidine thiocyanate-EDTA-N-lauroyl sarcosine, and 800 μl of 200 mM $NaPO_4$. Samples were homogenized for 3 min at 300 rpm and were centrifuged 5 min at maximum speed. 200 μl of the extract was added to the MagMAX Express plate for further DNA extraction procedures according to manufacturer's instructions. Isolated DNA was kept at − 20 °C (or − 80 °C for longer storage). Polymerase chain reaction (PCR) amplification of the variable 3 (V3) region of the 16S rRNA gene was performed as previously described [21, 22]. Purified PCR products were sequenced using the Illumina MiSeq platform by the McMaster Genomics facility. Of note, we lost two samples during processing; one from baseline group and one from 4 weeks HSD group. The 16S rRNA samples metadata table is available in Additional file 1.

Illumina sequencing processing and analysis

Custom, in-house Perl scripts were developed to process the sequences after Illumina sequencing [23]. The sl1p pipeline is open source and publicly available at https://bitbucket.org/fwhelan/sl1p. Briefly, Cutadapt [24] was used to trim any over-read, and paired-end sequences were aligned with PANDAseq [25], with a 0.7 quality threshold. If a mismatch in the assembly of a specific set of paired-end sequences was discovered, they were culled. In addition, any sequences with ambiguous base calls were also discarded. Operational taxonomic units

(OTUs) were picked using AbundantOTU+ [26], with a clustering threshold of 97%. Taxonomy was assigned using the Ribosomal Database Project (RDP) classifier v.2.2 [27] against the Greengenes SSU reference database (2013 release) [28]. For all downstream analysis, we used Quantitative Insights Into Microbial Ecology (QIIME) [29]. We obtained a total of 2,839,134 reads after quality filtering, with an average of 76,733.351 reads/sample (range 34,470 to 144,746). OTU tables were filtered to exclude "root" and any OTU with less than 10 sequences in all samples, and finally rarefied to 30,000 reads/sample (OTU table is available in Additional file 1). Calculations of within-community diversity (α-diversity), between-community diversity (β-diversity), relative abundance taxonomic summaries, and the different statistical analyses were preformed using QIIME (scripts "alpha_rarefaction.py" and "beta_diversity_through_plots.py," respectively). The relationships between HSD and microbiota phylogeny were explored using Principal Coordinate Analysis on unweighted UniFrac metrics and abundance Jaccard index ("beta_diversity_through_plots" script, QIIME), and the dissimilarity distance between the diet groups was tested using ANOSIM statistical method ("compare_categories" script, QIIME). For relative abundance taxonomic summaries and further statistical analysis, OTUs with a representation of less than 0.1% in the community were excluded. The correlations between fecal microbiota composition (at the highest taxonomic levels (family and genus) and at OTU level) and the diet were assessed by Spearman's rank correlation coefficient with fisher *z*-transformation *p* value assignment method, using the "observation_metadata_correlation" script (QIIME), based on the attribution of a ranked value to the variable "Weeks of NaCl in diet", from "0" to "4." The "wash out" group was ranked "0." PICRUSt [30] was used to predict the altered KEGG pathways based on the 16S sequencing data. L3 KEGG pathways correlation with length of HSD was calculated based on Spearman's correlation using Prism GraphPad 6 (GraphPad software). Heatmaps were generated using the Heatmaps2 package (gplot) for R (version 3.3.2) (See R code script in Additional file 2). In the microbiota-transfer experiment, the OTUs were considered successfully transferred when present with an average of 2 reads or higher.

Short-chain fatty acids (SCFA) quantification

SCFA were quantified as previously published [31, 32]. Briefly, 20–50 mg of frozen cecal content was collected into a tube; previously treated with methanol. The cecal samples were diluted 1:1 (*w*:*v*) with HCl 3.7% (10× diluted) and homogenized. Then 10 μl of internal standards and 500 μl of diethyl ether were added to the samples, and the tubes vortexed for 15 min. The extract (400 μl) was transferred to a clean tube. This step was repeated until we obtained a total of 800 μl of diethyl ether-fecal extract, 60 μl of which was then transferred to a chromatographic vial with 20 μl of N-tert-butyldimethylsilyl-N-methyltrifluoroacetamide (MTBSTFA). The organic extract-MTBSTFA was incubated at room temperature for at least 1 h, before being analyzed using the GC-MS Agilent 6890 N GC coupled to Agilent 5973 N Mass Selective Detector, with the column DB-17HT (30 m × 0.25 mm ID, 0.15 mm film).

Experimental colitis

Additional groups of 6- to 8-week-old specific pathogen-free (SPF) male C57BL/6 mice (obtained from Taconic) and NIH Swiss mice (obtained from Harlan) were housed at the animal facility of McMaster University as described above. After a period of 4 weeks on HSD or control diet, mice were given 3.5% dextran sodium sulfate (DSS, MW 36-50 kDa; MP Biomedicals, Santa Ana, CA, USA) in drinking water for 5 days followed by regular water for the next 2 days. HSD mice were switched to control diet before starting DSS administration. Body weight and general health condition were assessed daily. At day 7, mice were euthanized and the colon was blindly evaluated using a previously validated score [33, 34]. Briefly, the colon was evaluated for muscle thickness, hyperemia and erythema, presence of blood in the stools, and stool formation (For details, see Additional file 2). Control mice (no DSS) received only water during the entire procedure. For germ-free (GF) mice, the DSS dose had to be lowered to a 2% solution due to their higher sensitivity to experimental colitis. For the microbiota adoptive transfer experiments in ex-germ free mice a 2.5% DSS solution was used, starting 5 days after colonization.

For Dinitrobenzene sulfonic acid (DNBS)-colitis, mice were anesthetized with isoflurane (3%) and were injected with 1 ml of saline subcutaneously. A custom-made polyester catheter was introduced 3.5 cm into the rectum and 100 μl of 50% EtOH containing 3.5 mg of DNBS (MP Biomedicals, Santa Ana, CA, USA) was injected. From that day, all mice received control diet with normal water containing 6% sucrose to prevent dehydration. At day 3 post-DNBS, mice were euthanized and blindly evaluated using a validated DNBS-colitis macroscopic score [35]. The colon was evaluated for adhesion to surrounding tissue, thickness, hyperemia, erythema, and stool consistency. Mucosal ulcers were quantified and measured (for details see Additional file 2). Mice from control group (no DNBS-colitis) were rectally injected with a 50% EtOH solution.

Tissue processing

Blood was collected via orbital bleeding and centrifuged at 5000 rpm for 10 min. The serum was separated and stored at − 80 °C. The colon (full length, from the rectum to the cecum) was excised and measured.

Colonic content was removed and 0.5–1.0 cm sections were dissected from mid-colon and either snap-frozen in liquid N_2 for MPO analysis, stored in RNA later (Ambion) for RNA extraction, or fixed in 10% buffered formalin for histology assessment (from the border of an ulcer when present). MPO was performed on frozen tissues as previously described [36], and its activity expressed in units per milligrams of tissue. For histology, colonic sections were embedded in paraffin, 48 h after being fixed in 10% formalin solution, and were stained with hematoxylin and eosin (H&E). Inflammation was blindly evaluated following an inflammation histology scoring system (see Additional file 2).

Gene expression

Total RNA was extracted and purified using RNeasy Mini Kit (Qiagen, Hilden, Germany) according to manufacturer's instructions, including the DNA removal step using the RNase-Free DNase Set (Qiagen). NanoString nCounter Gene Expression CodeSet for mouse inflammation genes (v2; 248 genes) and a custom CodeSet panel that included 68 genes related to immune, gut barrier, and neurobiology functions (see Additional file 2) were run according to manufacturer's instructions (NanoString Technologies Inc., Seattle, WA, USA). Data from nCounter was analyzed using nSolver 2.5 software (Nanostring Technologies Inc.) (Nanostring raw counts are provided in Additional file 3). The log2 ratios of gene expression were then uploaded into Ingenuity Pathway Analysis software (Qiagen) for further analysis. For Q-PCR gene expression, cDNA library was generated using the SuperScript III First-Strand Synthesis System (Invitrogen, Carlsbad, CA, USA), according to manufacturer's instructions, using Oligo-dT primers (Qiagen). Additional information on the primers is provided in Additional file 2.

Immune cells extraction

Mesenteric lymph nodes (mLN) were harvested aseptically, and the cells were released from the nodes using a 70-μm strainer with the help of a syringe plunger, and were suspended in RPMI medium. After washing, the cells were kept in complete RPMI medium on ice until further use.

Colonic and small intestinal (SI) *lamina propria* (LP) cell extraction was performed using established protocols [37]. Briefly, colon and SI were removed and kept in cold sterile Dulbecco's phosphate-buffered (DPBS) solution until further processing. All fatty tissue, content, and the payer's patches were removed. Sections of intestine were open longitudinally, were cut into 0.5–1 cm pieces, and were incubated in 2 mM Dithiothreitol (DTT)/Hank's solution (HBSS) on a horizontal shaker (240 rpm) for 15 min at 37 °C to remove the mucous layer. After vigorous vortexing, the tissues were strained with a sterile metal strainer and were incubated with a 5 mM EDTA/HBSS solution for 10 min at 37 °C (240 rpm) to remove the epithelial layer. After vigorous vortexing, the tissues were strained once again. This epithelial removal step was repeated 3–4 times. After removing the EDTA solution, the tissues were digested in 0.1% Collagenase solution (type VIII; Sigma-Aldrich, St. Louis, MO, USA) and DNAse (I recombinant, grade I; Roche, Basel, Switzerland; 0.05 mg/50 ml of digestion solution) to aid the release of the LP cells (15 min for SI and 25 min for colon, 37 °C). Supernatants were strained through a 40-μm cell strainer to separate LP cells from the remaining intestinal tissue and were washed thoroughly. The cell suspension was then purified by Percoll (GE Healthcare, Chicago, IL, USA) density gradient method. Briefly, the cell suspension was re-suspended in 35% Percoll solution and underlayed with a solution of 70% Percoll. The tubes were centrifuged at 4 °C, 670 G, for 30 min (without break and with slow acceleration). The purified cell suspension was removed from the interphase, was washed, and was resuspended in complete RPMI. For LP cells gene expression, the cell suspension was resuspended in RLT buffer (RNeasy Mini Kit, Qiagen) and was snap-frozen in liquid nitrogen.

Flow cytometry

Cells isolated from mLNs, colon LP and SI LP were divided into two groups for intracellular staining: (1) anti-IL17A + anti-RORγt; and (2) anti-FoxP3. Cells of the first group were stimulated for 4–5 h at 37 °C with PMA (50 ng/ml), ionomycin (750 ng/ml; both from Sigma-Aldrich), in the presence of 10 μg/ml of Brefeldin A (BD Biosciences, San Jose, CA, USA), to activate IL17A expression. After this period, all cells were washed with PBS solution and were stained for cell viability with Fixable Viability Dye eFluor® 780 (1:1000; eBiosciences, San Diego, CA, USA) for 30 min at RT. Cells were then stained with the following extracellular antibodies: anti-TCRb-PerCP-Cy5.5 (1:100; H57-597 clone; eBioscience) and anti-CD4 + -Pacific Blue (1:200, RM4-5 close, BD Biosciences) for 30 min at 4 °C. Cells were fixed and permeabilized with FoxP3 Fixation/Permeabilization Concentrate and Diluent (eBioscience) according to manufacturer's instructions and were stained for 90 min at 4 °C, with the following intracellular antibodies: anti-IL17A-APC (1:100; TC11-18H10.1 clone, Biolegend, San Diego, CA, USA) and anti-RORγt-PE (1:100; AFKJS-9 clone; eBioscience); or anti-FoxP3-FITC (1:100; FJK-16s clone; eBioscience). The data was acquired on LSR II cytometer (BD Bioscience) and was analyzed with FlowJo software (10.2 version) (TreeStar, Ashland, OR, USA).

Statistical analysis

Data analysis was carried out using GraphPad Prism 6 (GraphPad Software, La Jolla, CA, USA). Student's *t* test,

multiple *t* test, one-way ANOVA, or two-way ANOVA were used as appropriate. For ANOVA, samples were corrected for multiple comparisons using Tukey's test. For Nanostring data, including heatmaps, the statistical analysis was carried out using nSolver 2.5 software (Nanostring Technologies). Heatmaps were generated using Euclidean distance metric based on group average. $P < 0.05$ was considered as statistically significant. Values are presented as means ± SEM. The raw data of all experiments is available in Additional file 1.

Results

HSD alters gut microbiota composition

To investigate the impact of HSD on gut microbiota composition, we analyzed intestinal microbiota dynamics of mice fed with HSD for 4 weeks, with a follow-up at 1 week after the mice returned to the control diet. While fecal bacterial richness (observed species) and diversity (Chao1 diversity index) were not affected during the HSD, both α-diversity metrics decreased at 1 week follow-up (Additional file 4: Figure S1). Despite some variability within groups, we observed a significant modulation of fecal bacteria composition with time exposure to HSD, based on the phylogenetic distance metric unweighted UniFrac (UnwUF) and the non-phylogenetic abundance weighted Jaccard distance (AJac) (ANOSIM of UnwUF: $R = 0.416$, $p = 0.001$; ANOSIM of AJac: $R = 0.283$, $p = 0.003$) (Fig. 1a, Table 1). 1 week of HSD was not sufficient to significantly modulate the microbiota, but 4 weeks of HSD led to a significant shift in the composition, as revealed by ANOSIM pairwise analysis (UnwUF: $R = 0.480$, $p = 0.004$; AJac: $R = 0.036$, $p = 0.008$; Table 1). Interestingly, 1 week after returning to the control diet, fecal microbiota composition partially reverted to its original composition based on unweighted and weighted UniFrac metrics (Fig. 1a, Table 1 and Additional file 4: Figure S2).

In order to better understand the impact of HSD on the microbial community, we studied the correlation between HSD exposure and the taxonomic composition at genus and OTU level. Four bacterial genera were found to significantly correlate with HSD (Fig. 1b, c, Additional file 4: Table S1). *Lactobacillus* genus showed the strongest correlation by decreasing 2-fold of its relative abundance after 4 weeks of HSD and quickly normalizing after returning to the control diet ($r = -0.703$, $q = 0.003$). An unclassified genus belonging to the order *Clostridiales* also decreased relative abundance over 1-fold after 4 weeks of HSD and partially normalized 1 week after returning to control diet ($r = -0.605$, $q = 0.017$). Finally, unclassified genera belonging to the *Lachnospiraceae* family and the *Oscillospira* genus showed a positive correlation with HSD ($r = 0.614$, $q = 0.017$ and $r = 0.548$, $q = 0.042$, respectively) (Fig. 1b, c, Additional file 4: Table S1). Similarly, three fecal OTUs correlated with time of exposure to HSD (Fig. 1c, Additional file 4: Table S2): OTU #3, belonging to the genus *Lactobacillus* ($r = -0.707$, $q = 0.005$), OTU #9, belonging to the order *Clostridiales* ($r = -0.684$, $q = 0.005$), and OTU #25, belonging to the family Lachnospiraceae ($r = 0.609$, $q = 0.027$).

To test the stability of fecal microbiota and rule out spontaneous changes in microbial profiles during this age period, we analyzed microbiota composition in an additional group of control mice fed with control diet. There were no spontaneous changes in the microbiota genus affected by HSD such as *Lactobacillus*, *Oscillospira* and unclassified genus from *Clostridiales* and *Lachnospiraceae*, between weeks 8 and 12, in mice on control diet (Additional file 4: Figure S3). However, the microbiota profiles of mice on HSD and control diet clustered separately at both time points, likely consequence of the cage effect and low number of mice (Additional file 4: Figure S3).

HSD affects predicted microbial metabolic activity and luminal SCFA levels

To investigate whether the differences in fecal microbiota composition induced by HSD could impact its metabolic activity, we assessed inferred metagenomic KEGG pathways using PICRUSt [30]. Multiple pathways appeared to be affected, with three of them being strongly upregulated by HSD, including "fatty acid metabolism," "lysine degradation," and "arginine and proline metabolism," while "fructose and mannose metabolism" was downregulated (Fig. 1d). As HSD altered the relative abundance of several OTUs and genera of major SCFAs producers such as *Lachnospiraceae*, *Clostridiales*, and *Oscillospira*, and PICRUSt predicted changes in the metabolism of fatty acids, we sought to quantify luminal SCFA in mice on HSD. Out of the seven SCFA tested, only butyrate levels were significantly affected, showing a decrease after 4 weeks of HSD (Fig. 1e). We also observed a decrease in lactic acid concentration; however, this change did not reach statistical significance. Taken together, these results show that HSD modulates both composition and function of the gut microbiota.

HSD modulates colonic and small intestinal immune gene expression

We subsequently tested whether the HSD-induced changes in gut microbiota were affecting host's gut mucosal homeostasis. We assessed gene expression profile of colonic *lamina propria* immune cells with nCounter Mouse Inflammation V2 Panel (Nanostring). HSD altered the expression of 35 genes ($p < 0.05$) in mouse colonic *lamina propria* cell extract, with 11 transcripts being significantly upregulated and 24 being downregulated (Fig. 2a, b; See Additional file 4: Table S3

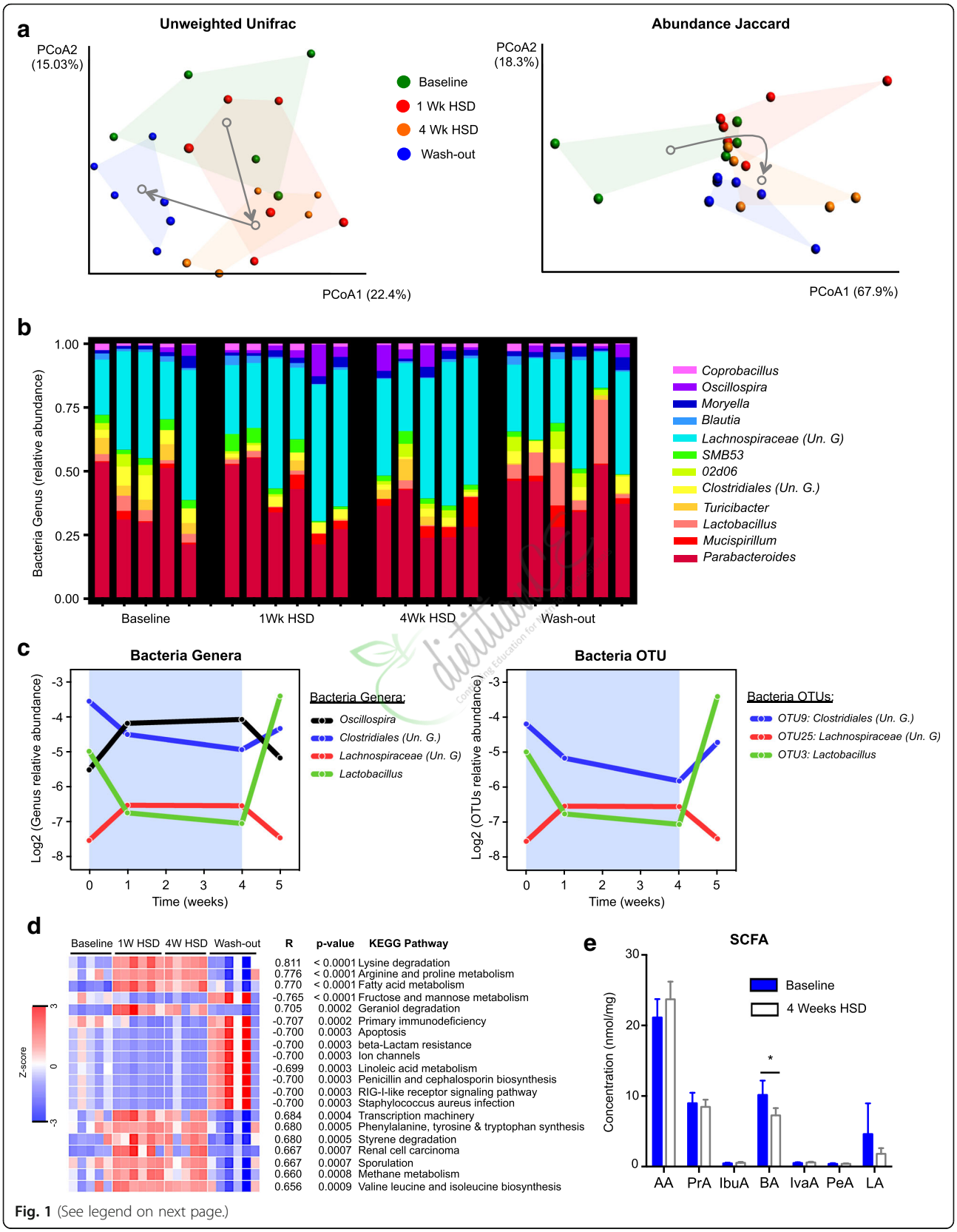

Fig. 1 (See legend on next page.)

(See figure on previous page.)
Fig. 1 High salt diet alters gut microbiota composition and function. **a** Principal coordinate analysis (PCoA) plots of unweighted UniFrac metric (left panel) and abundance Jaccard index (right panel) of fecal microbiota composition over time exposed to HSD. Gray arrows indicate the direction of the significant microbiota composition that shifts between groups. **b** Summary of the relative abundance of microbial genera present in 99.9% of the community overtime exposure to HSD. **c** Relative abundance of fecal bacterial genera (left panel) and OTUs (right panel) that significantly correlate with HSD ($q < 0.05$). The blue background represents the period exposed to HSD. **d** Heatmap of the 20 most significant KEGG pathways that correlate with HSD in fecal microbiota. **e** SCFA quantification at 0 and 4 weeks after HSD. Un. G (Unclassified Genus). AA (acetic acid), PrA (propionic acid), IbuA (isobutyric acid), BA (butyric acid), IvaA (isovaleric acid), PeA (pentanoic acid), LA (lactic acid). Values are presented as means ± SEM. $n = 5$–6 mice/group. *$p < 0.05$

for the full list of affected genes). Some of these genes were selected for validation by q-PCR (Fig. 2c). A considerable part of the affected transcripts were chemokines, cytokines, or their receptors (Additional file 4: Table S3). Among these, the cytokine IL-7 and the receptor IL-1rap were upregulated by HSD (0.47 and 0.19 log2 ratio, respectively), while all other cytokines and chemokines were downregulated. Of note, we observed the downregulation of several chemokines (and chemokine receptors) important for the chemotaxis of monocytes/macrophages, dendritic cells, neutrophils, and NK cells, such as Ccl3, Ccl4, Cxcl10, Cxcl2, Ccr7, and Cxcr4 (Additional file 4: Table S3), indicating a possible impairment of their migration. The most significant change observed was the upregulation of Rac1 (Ras-related C3 botulinum toxin substrate 1) transcript (log2 ratio = 0.41, $p = 0.0001$), a member of Rho family GTPases with broad functions, from innate immunity processes to leukocyte chemotaxis and barrier function.

In order to identify possible functional pathways affected by HSD we integrated our gene expression data with publicly available databases results using Ingenuity Pathway Analysis (IPA) bioinformatics platform. The upregulation of the genes Map2k6, Map2k1, Mapk3, Atf2, and IL1rap was predicted by IPA to stimulate several pro-inflammatory canonical pathways such as "acute phase response signaling," IL-6, and Mapk signaling (Additional file 4: Table S4). The roles of macrophages and IL-17 signaling were also strongly predicted to be affected by HSD (Additional file 4: Table S4). Even though IL-17A cytokine itself was not found to be significantly affected by HSD in *lamina propria* colonic cell extracts, IPA identified multiple genes related to IL-17 signaling to be affected, such as Mapk3, Map2k1, Map2k6, and the transcription factor Atf2 (all upregulated), as well as Cxcl10, Hras, and Ptgs2 (all downregulated). When analyzing functions affected by HSD in the colon, IPA predicted downregulation of leukocyte migration and movement (Fig. 2d, Additional file 4: Table S5). This was expected since HSD suppressed the expression of many chemokines and cytokines responsible for immune cells chemotaxis. On the other hand, the functions related to leukocyte viability and maturation were predicted to be upregulated, based on the expression of genes like IL-7, Map2k1, and Mapk3 (Fig. 2d, Additional file 4: Table S5).

Although the focus of our study was the effect of HSD on colonic microbiota and immune function, we also assessed its effect on small intestine recognizing that that most of the Na^+ and Cl^- is absorbed in this compartment. We observed a significant change in the expression of 11 genes ($p < 0.05$), including the upregulation of IL17A and Defa-rs1, as well the downregulation of IL12a and Cxcr4 (Additional file 4: Figure S4 and Table S6). Only two genes (Cxcr4 and Mef2c_Mm) were affected similarly in both colonic and small intestinal *lamina propria* cell extracts, emphasizing the distinct nature of the immune milieu of each gut compartment. IPA identified three canonical pathways related to bacteria recognition, toll-like receptors and IL-17 signaling to be most affected in the small intestine (Additional file 4: Table S7). While "recruitment of leukocytes" ($z = 0.196$, $p = 4.01E\text{-}05$) was upregulated, "proliferation of lymphocytes" ($z = -2.398$, $p = 5.44E\text{-}06$) was downregulated.

Table 1 ANOSIM statistical analysis of distance metrics on the effect of HSD on fecal microbiota composition

	Unweighted UniFrac		Abundance Jaccard index	
	ANOSIM *R*	ANOSIM *p*	ANOSIM *R*	ANOSIM *p*
All groups	0.416	0.001	0.283	0.003
Baseline vs 1 week HSD	0.144	0.133	0.211	0.108
Baseline vs 4 weeks HSD	0.480	0.004	0.360	0.008
Baseline vs wash out	0.341	0.034	0.197	0.106
1 week HSD vs 4 weeks HSD	0.277	0.052	0.528	0.006
4 weeks HSD vs wash out	0.525	0.007	0.075	0.237

HSD increases RORγt$^+$IL17$^+$ T-cells in mLNs but not in intestinal lamina propria

To better understand the effect of HSD on lymphocyte function, we phenotyped T-cell populations in the small intestinal and colonic *lamina propria* and in mesenteric lymph nodes (mLNs) using flow cytometry. HSD led to a 2-fold increase of RORγt$^+$IL17A$^+$ cells in the mLNs but not in small intestinal or colonic *lamina propria* (Additional file 4: Figure S5A). However, we consistently observed a mild but not statistically significant increase of this cell population in the colon across all experiments. No change was observed in the expression of

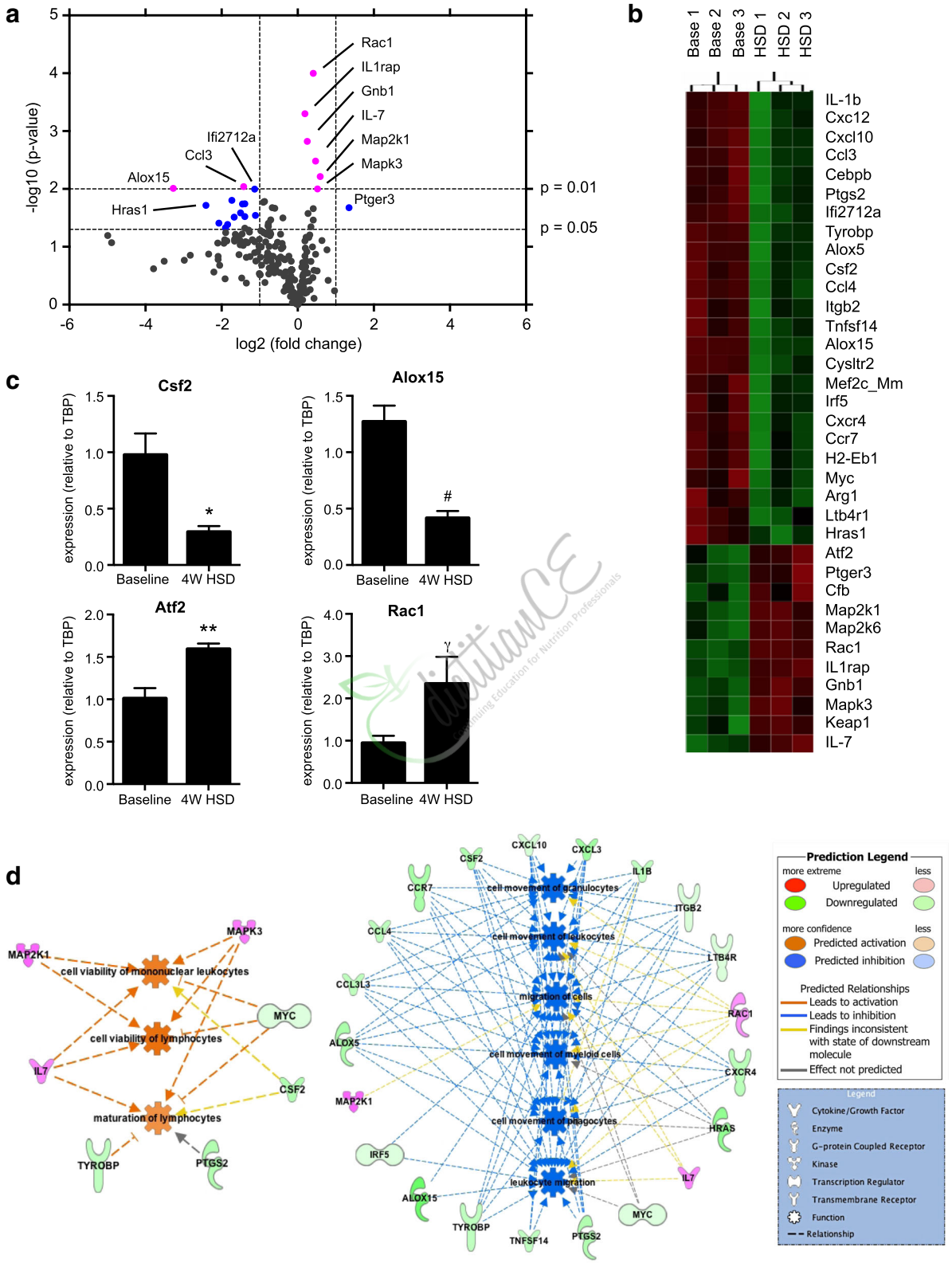

Fig. 2 (See legend on next page.)

(See figure on previous page.)
Fig. 2 High salt diet modulates immune expression in colonic *lamina propria*. **a** Volcano plot of gene expression in colonic *lamina propria* total cell extract of mice receiving HSD or control diet for 4 weeks, $n = 9$ mice/group. Pink dots: genes with $p < 0.01$. Blue dots: genes with $0.01 < p < 0.05$, fold change > 2. **b** Heatmap of immune genes that changed with HSD ($p < 0.05$). Based on group average, Euclidean distance metric. **c** qRT-PCR analysis of differentially expressed genes in the two groups. Values are presented as means ± SEM, $n = 5$–6 colon/group, $^{*}p < 0.05$, $^{**}p < 0.01$, #$p < 0.001$, γ$p = 0.065$. **d** Gene-cell function networks obtained from Ingenuity Pathway Analysis. On the left, network with the genes that contribute to the predicted inhibition of functions related to immune cell migration, and, on the right, network with the genes that contribute to the predicted upregulation of the immune cell viability and maturation

IFNγ by CD4+ T-cells in mice on HSD (data not shown), nor in the frequency of $CD4^{+}FoxP3^{+}$ T-cells, even though, for the latter, we noticed a small increase of this cell type across tissues in all experiments (Additional file 4: Figure S5B). Taken together, these results show that HSD affects the gut mucosal immune compartment.

HSD exacerbates DSS colitis

To investigate how the changes in gut microbiota and immune function affect vulnerability to inflammatory insults, we used DSS and DNBS colitis models. We confirmed that mice on HSD developed a more severe DSS colitis when compared to mice on control diet, as previously described [13], characterized by an increased rectal bleeding, diarrhea, and general inflammation of the colonic tissue (Fig. 3a). HSD induced higher weight loss on day 5 of DSS administration, when compared to DSS mice on control diet, a difference that was maintained until the end of the experiment, on day 7 (Fig. 3b), indicating an accelerated onset and increased severity of colitis. Colon shortening, normally used as indicator of colitis severity, was greater in HSD mice compared to control diet mice (Fig. 3c). MPO activity, reflecting neutrophil infiltration, was increased 2-fold in the colon of mice on HSD after DSS administration when compared to mice on control diet (Fig. 3d). Furthermore, there was a significant difference in mortality between the two groups, with 5% of mice on control diet meeting the endpoint criteria prematurely, while this number increased to 19% in mice on HSD (Fig. 3e).

To better understand the immune responses during DSS colitis, we assessed the expression of a group of genes related to immune and barrier function using a customized Nanostring gene expression codeset (see list of genes in Additional file 2). HSD altered the expression of nine genes in the colon of mice on DSS, when compared to DSS mice on control diet (Fig. 3f). HSD decreased expression of genes involved in the maintenance of mucosal barrier such as Tjp1 (tight junction protein ZO-1), Muc2 (Mucin 2), Tff3 (trefoil factor 3), and Ocln (Occludin). On other hand, HSD mice had an increased expression of MMP9 (Matrix Metalloproteinase 9) and Cnlp (Cathelcidin-related antimicrobial peptide), genes expressed by innate immune cells such neutrophils and macrophages and previously described to be over-expressed in gut inflammatory conditions [38, 39]. HSD also reduced expression of two genes strongly expressed by epithelial cells: F2rl1 (protease activated receptor 2) and 5-HT (serotonin). This finding might be a consequence of the severe epithelial damage observed in colitis. Thus, the altered gene expression profile supports the notion that HSD exacerbates DSS colitis.

These results were reproduced using another mouse strain; NIH Swiss mice also developed a more severe DSS colitis after 4 weeks of HSD, confirming that HSD induces susceptibility to experimental colitis in multiple mouse strains (Additional file 4: Figure S6).

HSD exacerbates DNBS-colitis

To confirm the increased sensitivity to colonic inflammation in mice on HSD, we used the DNBS model. Similar to the DSS colitis model, we chose a concentration of DNBS that would induce a mild form of colitis (3.5 mg of DNBS/mouse), in order to appreciate the effect of diet on worsening of experimental colitis. Similar to the results obtained with DSS-induced colitis, mice that were previously exposed to a 4-week HSD developed more severe colitis after rectal injection of DNBS (Fig. 4a). HSD mice had higher number of ulcers that were larger in size, when compared to control diet mice. Figure 4b, c shows that HSD mice developed ulcers that affected the entire colonic wall, up until the serosa with large clusters of cellular infiltrates, and, in some cases, a total loss of the epithelial layer. Strikingly, while none of the control diet mice met the endpoint criteria to be euthanized at this mild DNBS concentration, the mortality of HSD mice after DNBS administration reached 25% (Fig. 4d). Taken together, these results show that HSD exacerbates both DSS- and DNBS-colitis.

HSD exacerbates experimental colitis in a gut microbiota-dependent manner

We hypothesized that HSD exacerbates colitis through induction of gut dysbiosis as it decreases levels of beneficial bacteria, such as *Lactobacillus*, and decreases butyrate, a SCFA important for gut immune homeostasis and previously shown to be protective in colitis. To test this hypothesis, we administered 2% DSS to germ-free (GF) mice after 4 weeks of HSD. DSS administration induced

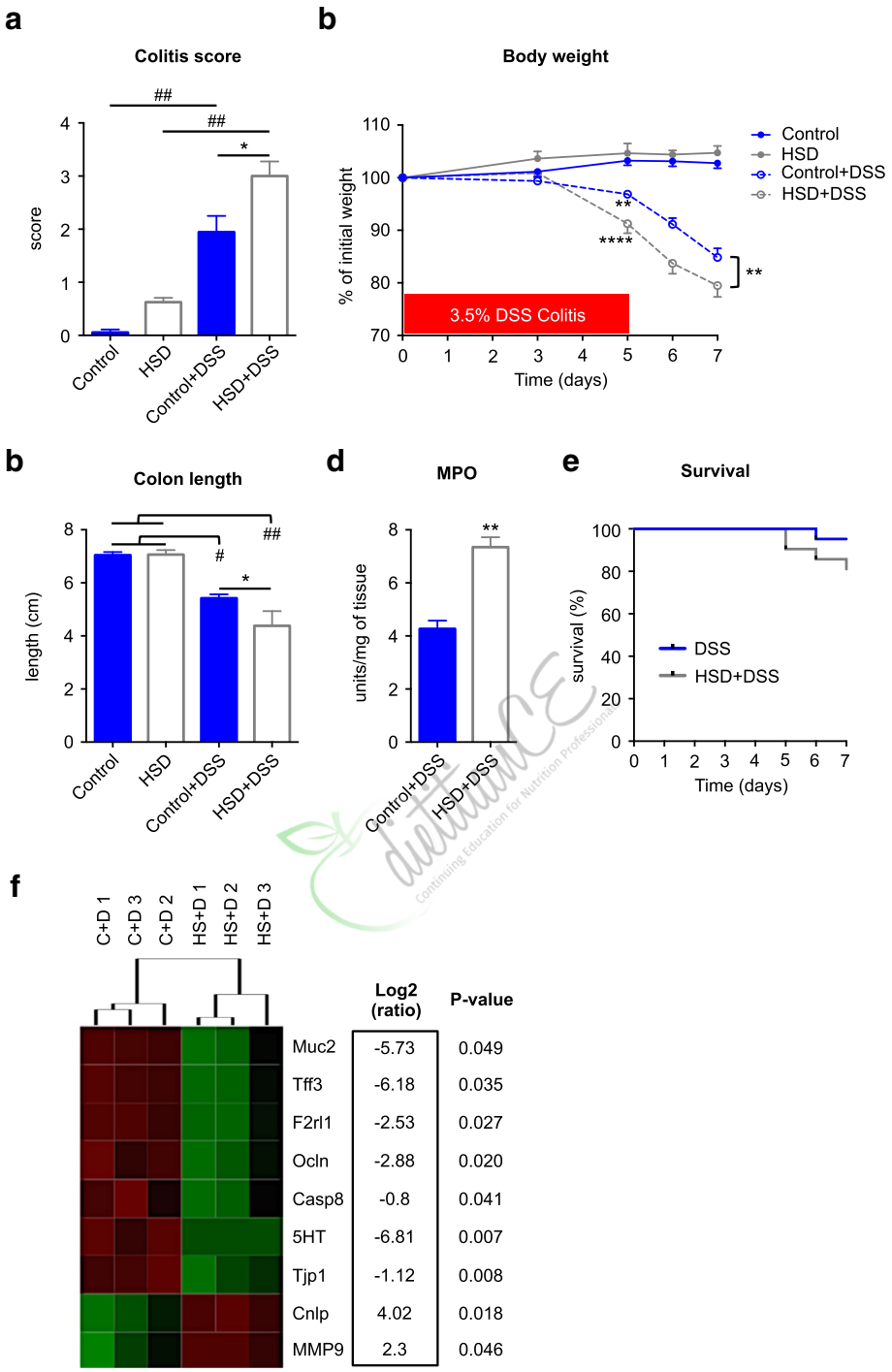

Fig. 3 High salt diet exacerbates DSS colitis. **a** DSS colitis macroscopic scores at endpoint (day 7) in four groups of mice: control (control diet, no DSS), HSD (high salt diet, no DSS), control+DSS (control diet, DSS in water), HSD + DSS (high salt diet, DSS in water). **b** Body weight changes during DSS administration. **c** Colon length at endpoint. **d** Colonic MPO of the two groups of mice receiving DSS. **e** Survival curve of the two groups of mice with DSS colitis. **f** Heatmap of differentially expressed genes ($p < 0.05$) in the colon of mice with DSS colitis: C + D (control diet+DSS), HS + D (HSD + DSS). The heatmap was generated based on group average using Euclidean distance metric. Colitis scores, weight change, colon length, and MPO are presented as means ± SEM; $n = 8–9$ mice/group. *$p < 0.05$, **$p < 0.01$, #$p < 0.001$, ##$p < 0.0001$

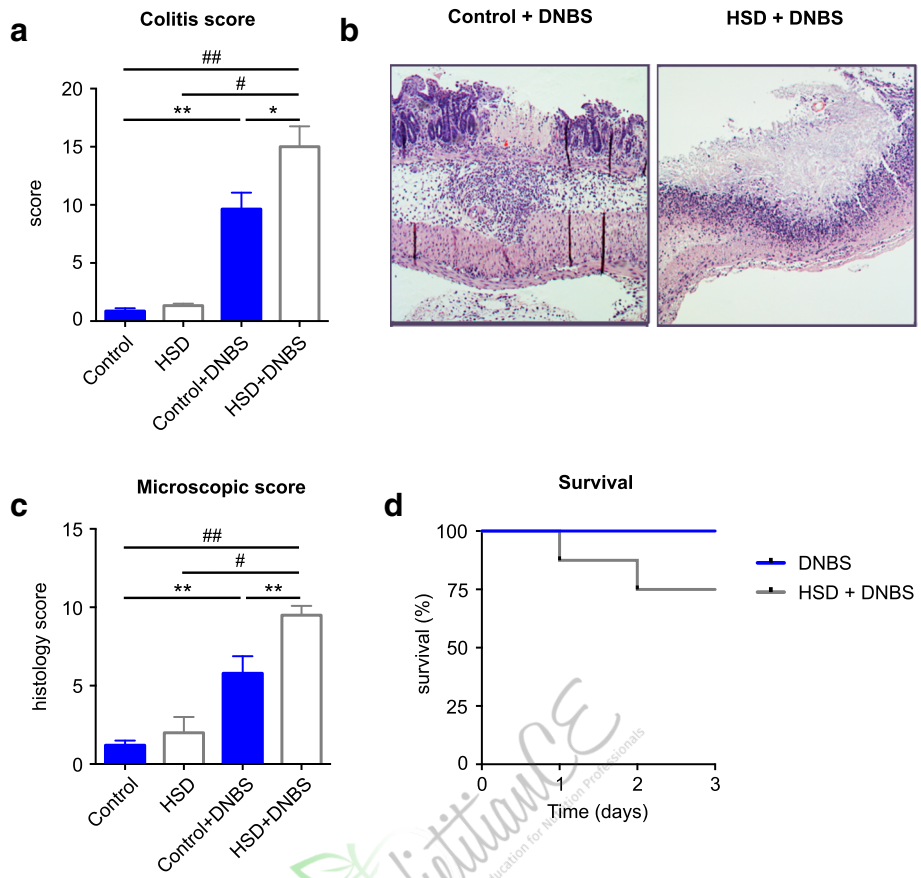

Fig. 4 High salt diet exacerbates DNBS colitis. **a** DNBS colitis macroscopic scores at endpoint (day 3) in four groups of mice: control (control diet, 50% EtOH vehicle), HSD (high salt diet, 50% EtOH vehicle), DNBS (control diet, DNBS in 50% EtOH vehicle), HSD + DNBS (high salt diet, DNBS in 50% EtOH vehicle). **b** Representative H&E-staining of colonic section of DNBS mice highlighting the ulcers in the mucosa. **c** Histological scores in colonic sections. **d** Survival curve of the two groups with DNBS colitis. Colitis and histology scores are presented as means ± SEM; $n = 5–9$ mice/group. $^{*}p < 0.05$, $^{**}p < 0.01$, $\#p < 0.001$, $\#\#p < 0.0001$

colitis in GF mice (Fig. 5a, b), with increase in macroscopic scores and decreased colon length compared to control mice not exposed to DSS. However, there were no differences in macroscopic scores, colon length, MPO, or histology scores between GF mice on HSD and those on control diet after DSS-colitis (Fig. 5a–d). We assessed the expression of a group of relevant genes using a customized Nanostring gene expression codeset. DSS administration altered expression of 25 genes in GF mice on control diet (Additional file 4: Table S8) that were related to immune, barrier, and neural function such as Mapk1, Nfkb1, CD11c, and GABA B, confirming that the administration of DSS altered gut physiology, even in the absence of microbiota. However, out of the 68 tested genes, only 1 gene, Reg3ɣ, was found to be differentially expressed between HSD and control diet groups after DSS administration (log2 ratio = − 1.15; $p = 0.032$). These results suggest that the colonic microbiota is a key factor in exacerbation of colitis by HSD.

To test whether HSD-associated microbiota alone can confer increased vulnerability to inflammatory insult, we transferred the microbiota from mice on HSD or control diet to GF mice. The recipient mice received control diet during the entire course of the experiment and were exposed to 1 cycle of DSS, starting at day 5 post-colonization (Fig. 6a). We observed no differences in colitis severity, including weight loss, colon length, and macroscopic scores between the two groups of mice (Fig. 6f–h). However, when analyzing the fecal microbiota profiles, we found that prior to DSS administration, both groups of recipient mice had similar microbial profiles, closer to control donor, based on abundance Jaccard index (Fig. 6b, c). Further analysis has confirmed that there were no differences between the microbiota genera of both recipient groups (Additional file 4: Table S10), including genera affected by HSD such as *Lactobacillus* (Fig. 6d). When analyzed in detail, the OTUs successfully transferred from control diet-microbiota

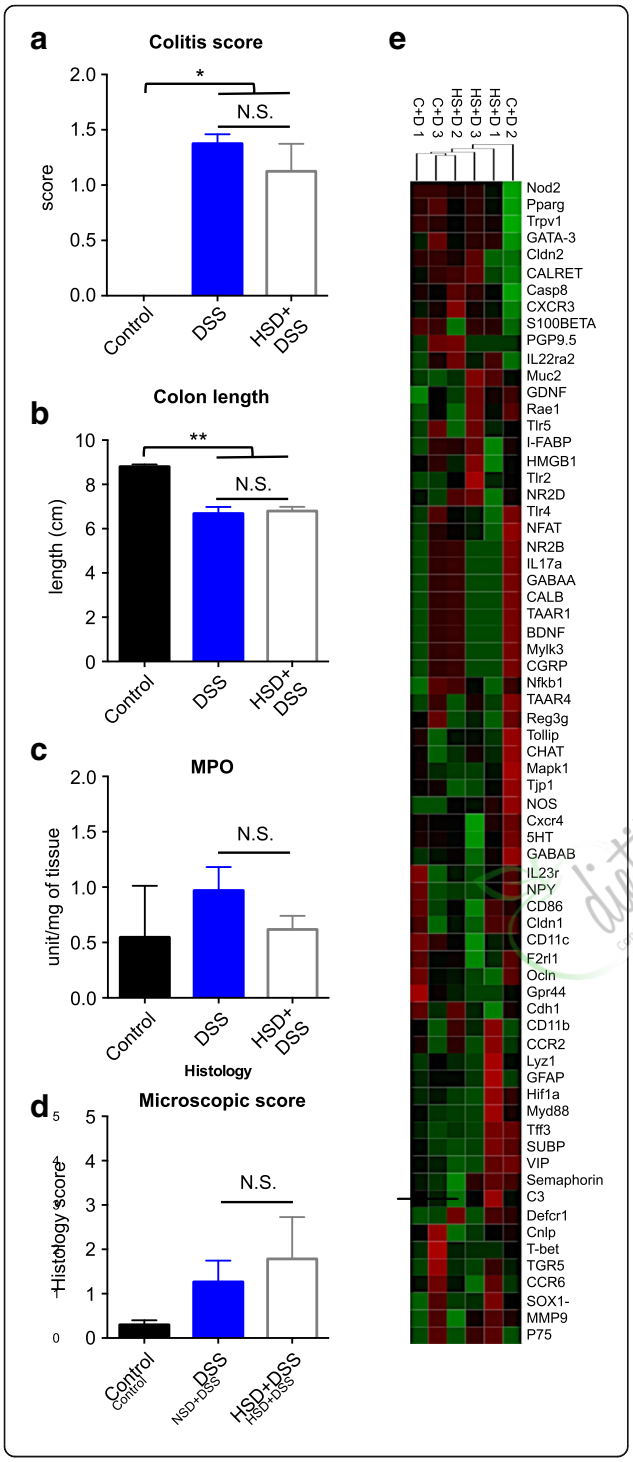

Fig. 5 The effect of high salt diet on exacerbation of colitis is dependent on gut microbiota. **a** DSS colitis macroscopic scores at endpoint (day 7) in three groups of mice: control (no DSS colitis), DSS (control diet, DSS in water), HSD + DSS (high salt diet, DSS in water). **b** Colon length of mice at endpoint. **c** Colonic MPO. **d** Histological scores of the DSS colitis. Values are presented as means ± SEM; $n = 3$–6 mice/group. *$p < 0.05$, **$p < 0.01$. **e** Heatmap of the gene expression of 68 genes related to immune, gut barrier, and neural function, in the colon tissue of germ-free mice after DSS administration, on control diet or HSD: C + D (control diet + DSS), HS + D (HSD + DSS). The heatmap was generated based on group average using Euclidean distance metric

accounted for 98.0% of the entire donor's community, while the OTUs from HSD-microbiota accounted for 75.9% of the donor's microbiota community (Table 2). From the 15 most abundant OTUs of each microbiota-type, that accounted for 99% of control diet microbiota and 95% of HSD microbiota, we verified that only 7 OTUs from HSD microbiota were detected in the recipient mice, while from control diet-microbiota 12 OTUs were present (Fig. 6e, Table 2). These results demonstrate that a significant proportion of the HSD OTUs did not successfully colonize the gut of recipient mice when these were fed control diet, suggesting that a constant exposure to high levels of NaCl in the diet is necessary to maintain the HSD signature microbiota profile. Taken together, similar colitis severity observed in the two microbiota-similar recipient groups supports our hypothesis that microbiota composition and function is a major determinant of colitis severity.

Discussion

In addition to host genetic make-up, environmental factors such as diet and microbiota composition have been shown to play a crucial role in the development of inflammatory diseases. Here, we show that high content of NaCl in diet modulates gut microbiota composition and function, namely, decreasing the relative abundance of *Lactobacillus* spp and levels of the SCFA butyrate, promoting a pro-inflammatory state in the gut. We demonstrate that the gut microbiota is a key mediator in the exacerbation of experimental colitis by HSD, supported by the fact that the detrimental effect of HSD was not observed in GF mice.

To understand the impact of HSD in the modulation of gut microbiota, we fed mice with a diet supplemented with 4% NaCl for 4 weeks and analyzed fecal microbiota dynamics during and after HSD. The NaCl concentration employed here simulates the concentration of a typical high salt diet [13, 40], which was shown to exacerbate the development of several immune disorders in mice [9, 10, 13]. Importantly, 4 weeks of 4% NaCl diet do not affect mouse blood pressure [9]. HSD altered gut microbiota composition and function, mainly decreasing colonic *Lactobacillus* spp. relative abundance and SCFA butyrate

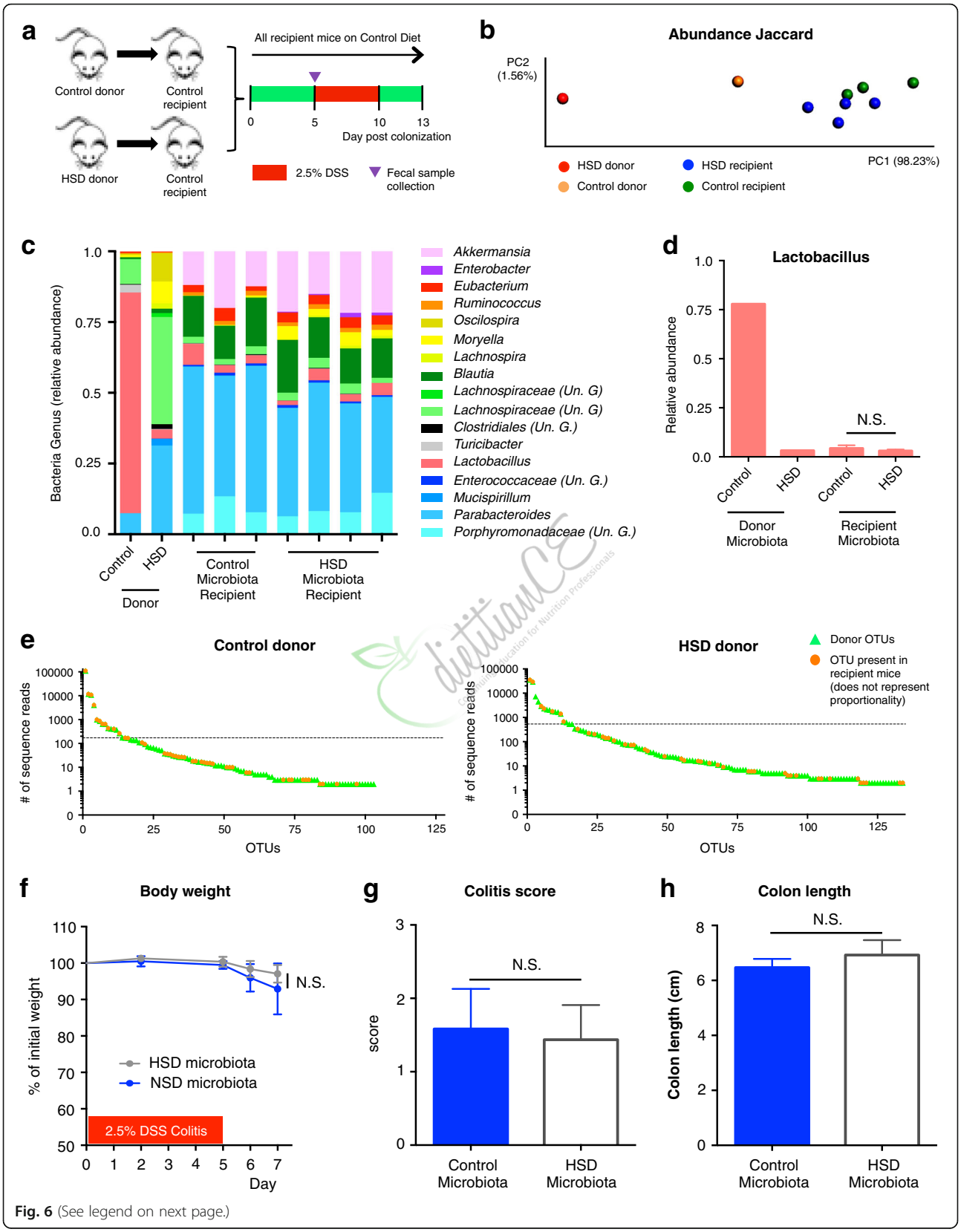

Fig. 6 (See legend on next page.)

(See figure on previous page.)
Fig. 6 HSD-signature microbiota requires constant exposure to high salt diet for its maintenance. **a** Experimental design. **b** Principal coordinate analysis (PCoA) of abundance Jaccard index from fecal microbiota composition data. **c** Summary of the relative microbial genera present in 99.9% of the community. Un. G (Unclassified Genus). **d** Relative abundance of *Lactobacillus* genus. **e** Total read count of each OTU present in the indicated donor fecal microbiota (in green triangles). Orange dots indicate the OTUs that were present in recipient mice at day 5 post-colonization. The horizontal dashed line separates the 15 most abundant OTUs from the others. **f** Body weight during DSS administration. **g** Macroscopic scores of DSS colitis at endpoint. **h** Colon length at endpoint

levels, two factors that have been implicated in the maintenance of a healthy gut physiology. This is in agreement with a very recently published study by Wilck et al. showing that high salt diet alters gut microbiota, mainly by decreasing levels of *Lactobacillus murinus*, leading to induction of T helper 17 cells [41] and that supplementation with *L. murinus* can abrogate the pro-inflammatory effect of HSD. In addition to butyrate, lactic acid also appeared to decrease after HSD, although not significantly. Interestingly, it has been shown that lactic acid is used by some butyrate-producing bacteria for the production of high concentrations of butyric acid [42], thus it is plausible that the decrease observed in *Lactobacillus* spp. is, at least in part, indirectly responsible for the significant decrease of butyric acid. Several species of *Lactobacillus* genus have been shown to play a role in host's gut mucosal immune and barrier function [43]. A recent study showed that *Lactobacillus reuteri* ameliorates colitis in mice by increasing the colon mucus thickness [44]. Butyrate plays an essential role in gut homeostasis as it serves as the primary energy source for colonocytes and is important for maintaining tissue barrier function [45]. Moreover, it has been directly implicated in colonic Tregs' differentiation [46, 47], intestinal macrophage function [48], and colonic inflammation down-regulation [49]. Furthermore, a recent study has shown that butyrate deficiency is directly associated with colitis [50], while small clinical studies have shown that butyrate treatment improves colitis [51, 52].

We hypothesized that the changes in gut microbiota driven by HSD, in the absence of any additional inflammatory insult, would affect intestinal immune homeostasis. Our data revealed a strong impact of HSD on mucosal immunity, both in the colon and small intestine. Even though Na^+ and Cl^- ions are thought to be absorbed in the small intestine, HSD had a stronger impact in the colon, when considering the number of affected genes (35 genes in the colon and 11 genes in the small intestine). This is in line with a recent study showing that HSD increased sodium luminal concentration in the colon but not in the small intestine [53], which may partially explain the different impact of HSD on small intestinal and colonic mucosal immunity.

Table 2 OTU count analysis of microbiota transplant experiment

	# of OTUs		
	Total from donor	Successfully transferred to recipient	Transferred from 15 most abundant OTUs
CTL microbiota	103	43 (98.0%)*	12
HSD microbiota	134	43 (75.9%)*	7

*Coverage of the donor microbiota community based on read counts

Many of the altered genes were related to immune cell trafficking, cell viability, and signal transduction elements. Rac1 gene, which was increased by HSD, has been associated with ulcerative colitis in many studies. Several polymorphisms that lead to the increase of Rac1 expression have been shown in patients with UC [54] and Rac1 is the target of a commonly used IBD treatment azathioprine [55]. Moreover, mice with a Rac1 conditional deletion in neutrophils and macrophages are resistant to DSS-colitis, showing reduced neutrophil migration and reduced levels of IL1β and KC [54]. Furthermore, the genes Mapk3, Map2k1, Map2k6, Atf2, and Hras1, together with Rac1, were also integrated by IPA to be part of the upregulated "LPS-stimulated MAPK signaling" as well as part of other MAPK-related canonical pathways (Additional file 4: Table S7). This is of particular interest, not only because MAPK signaling pathway has been shown to be induced by NaCl [9, 10, 13], but also because microbiota-derived molecules such as LPS, flagellin, DNA, RNA, and others can lead to the activation of MAPK signaling pathways by selectively binding to various pattern recognition receptors on innate immune cells [56, 57]. In agreement with previous reports, we found that IL-17 signaling pathway was predicted to be affected by HSD in both colonic and small intestine tissues [9, 10, 13].

Surprisingly, we found that HSD downregulated the expression of multiple chemokines, cytokines, and its receptors in the colonic *lamina propria*. This was unexpected considering that previous studies have shown that NaCl induces macrophage chemotaxis in vitro [58] and that macrophages infiltrate the skin of rodents fed with HSD in response to the storage of Na^+ in this organ, a mechanism important to maintain interstitial electrolyte and volume homeostasis [59]. However, several other studies have shown downregulation of the expression of chemokine receptors in neutrophils and other granulocytes, upon TLR engagement in a p38-MAPK signaling-dependent manner, with cells remaining partially functionally competent; a potential mechanism regulating cell positioning and activation [60, 61]. Considering that HSD induced changes in colonic microbiota and upregulation of MAPK signaling pathways in the colon, it is conceivable that the observed downregulation of

chemokine receptors and other molecules is a result of mucosal granulocytes TLR engagement. Downregulation of cytokines and chemokines could compromise the colonic immune barrier and promote a pro-inflammatory response or impaired resolution of inflammation after the intestinal injury induced by DSS and DNBS.

To investigate the effect of HSD-induced alterations in mucosal immune function and gut microbiota, we used two different models of experimental colitis. We confirmed that HSD exacerbates colitis in mice [13] and showed enhanced colonic barrier disruption after DSS in mice fed with HSD. In fact, Ocln and ZO-1, two components of the tight junction (TJ) structure, were significantly downregulated, as well as Muc2, a protein secreted by goblet cells (GC) and essential for the structure of the mucus layer in the intestine, and Tff3, also mostly expressed by GC, with a key role in mucus layer stability and mucosal repair [62]. On the other hand, Mmp9 and Cnlp were upregulated in HSD mice after DSS-colitis. Even though Cnlp has been proposed to have a protective role [63], the level of this peptide has been shown to be elevated in DSS colitis and patients with ulcerative colitis [64, 65]. Mmp9 is markedly elevated in intestinal tissues of IBD patients, and it has been proposed to be a biomarker of disease activity [66–68]. Mmp9 is also elevated in DSS colitis and has been shown to contribute to the severity of colitis by increasing intestinal epithelial TJ permeability [68]. Cnlp and Mmp9 are highly expressed by active neutrophils; therefore, their upregulation could also reflect the increased infiltration of these cells in the inflamed colonic tissue of HSD mice after DSS administration. We reproduced the colitis results in a different mouse strain and showed that HSD leads to a similar exacerbation of DSS colitis in NIH Swiss as in C57BL/6 mice, suggesting that HSD-mediated exacerbation of experimental colitis is independent of mouse genotype. Further supporting our results, several studies have recently reported increased severity of colonic inflammation not only in models of chemically induced colitis [13, 69], but also in IL-10 KO mice, which spontaneously develop colitis, and in *Salmonella typhimurium* infected mice, while on HSD [53].

In order to test whether gut microbiota plays a role in the HSD-dependent exacerbation of gut injury, we induced DSS colitis in GF mice. While DDS induced colitis in both groups of germ-free mice, there was no worsening of the colonic inflammation in mice fed a HSD. This suggests that the increased susceptibility to colitis induced by a HSD is critically dependent on the presence of the microbiota. In subsequent experiments, we found no difference in colitis severity when transferring gut microbiota from SPF mice on a HSD into germ-free recipients. Although seemingly counterintuitive, the results are in accordance with our previous data as we found that at the beginning of DSS administration (5 days post-colonization), the microbiota of all recipient mice had converged to a similar profile, regardless of the donor microbiota. This is in sharp contrast with our SPF mice experiment, where we observed a marked dysbiosis prior to commencing DSS and subsequently worse colitis in mice previously on high salt diet. In our transfer experiment, most of the abundant OTUs from the control diet donor were transferred to the recipient mice while only a minority of abundant HSD donor OTUs were detected in the recipient mice. These differences in microbiota profiles could be partially attributed to technical issues, including freezing and thawing, and exposure to oxygen, as we did not use fresh cecal content samples for colonizations. However, we believe that the major factor accounting for this difference was the fact that recipient mice were given control diet, which did not allow establishment of HSD microbiota profiles. Thus, the microbiota transfer experiment supports the notion that HSD-induced dysbiosis, and its altered metabolic activity, is a major determinant of the sensitivity to inflammatory insult in this model and that a constant exposure to HSD is necessary to maintain the "pro-inflammatory" microbiota profile.

Even though it has been previously shown that NaCl can directly affect immune cells in vitro, we hypothesize that these direct effects do not play a major role in our in vivo model. Taking into consideration that (i) dysbiosis, including the depletion of *Lactobacillus* and butyrate, is known to affect mucosal immune homeostasis, and that (ii) the mucosal milieu in the colon, which harbors the highest microbial density along the GI tract, was more affected by HSD than small intestine, and that (iii) multiple immune pathways affected by HSD are strongly modulated by microbial products, we hypothesize that changes in the immune system are a consequence of the disruption of the gut microbiota by HSD. This notion is further supported by the lack of changes in colonic mucosal immune milieu in germ-free mice on HSD (Additional file 4: Table S9).

Taken together, this study provides an example of how environmental factors, such as diet, play a key role in shaping gut microbial communities that influence host physiology and predisposition to disease.

Conclusion

We have demonstrated that consumption of a diet with high salt content results in alteration of gut microbiota composition and function that may be pro-inflammatory by virtue of the loss of *Lactobacillus* spp. and reduced production of the protective SCFA butyrate. Our findings indicate that the maintenance of the pro-inflammatory microbiota is dependent on a continued high salt intake and is associated with changes in gut immune homeostasis, predisposing mice to the development of a more severe

form of experimental colitis. Our study suggests that high concentrations of dietary salt, similar to those found in the western diet, contribute to the increased prevalence of chronic inflammatory disorders through microbiota-dependent mechanisms. This finding has implications for the management of patients with IBD and other inflammatory disorders and should be further investigated as it provides an easy candidate for dietary therapeutic interventions.

A probiotic complex, rosavin, zinc, and prebiotics ameliorate intestinal inflammation in an acute colitis mouse model

Abstract

Background: An altered gut microbiota balance is involved in the pathogenesis of inflammatory bowel disease (IBD), and several probiotic strains are used as dietary supplements to improve intestinal health. We evaluated the therapeutic effect of 12 probiotics in combination with prebiotics, rosavin, and zinc in the dextran sodium sulfate (DSS)-induced colitis mouse model.

Methods: The probiotic complex or the combination drug was administered orally to mice with DSS-induced colitis, and the body weight, disease activity index, colon length, and histopathological parameters were evaluated. Also, the combination drug was applied to HT-29 epithelial cells, and the expression of monocyte chemoattractant protein 1 (MCP-1) was evaluated by real-time polymerase chain reaction.

Results: Administration of the combination drug attenuated the severity of DSS-induced colitis. Moreover, the combination drug significantly reduced the levels of the proinflammatory cytokines tumor necrosis factor-α, interleukin (IL)-6, IL-1β, and IL-17, and significantly increased the levels of Foxp3 and IL-10 in colon sections. Additionally, treatment with the combination drug reduced MCP-1 expression in HT-29 cells. Treatment with the combination drug decreased the levels of α-smooth muscle actin and type I collagen compared with vehicle treatment in mice with DSS-induced colitis.

Conclusion: These results suggest that the combination of a probiotic complex with rosavin, zinc, and prebiotics exerts a therapeutic effect on IBD by modulating production of pro- and anti-inflammatory cytokines and the development of fibrosis.

Keywords: Inflammatory bowel disease, Gut microbiota, Probiotics, Fibrosis

Background

Inflammatory bowel disease (IBD), which comprises Crohn's disease (CD) and ulcerative colitis (UC), is a chronic, progressive, and destructive inflammatory condition of the gastrointestinal tract caused by multiple genetic and environmental factors [1]. The pathogenesis of IBD is related to a breakdown of intestinal homeostasis, which results in uncontrolled immune responses to the gut microbiota by intestinal epithelial cells and immune cells, leading to complications, such as perforating ulcers and fibrosis [2–5]. Intestinal fibrosis is a common complication and a nonspecific feature of IBD. Increased deposition of collagen causes excessive fibrosis, progressive tissue architectural distortion, dysfunctional wound healing, and luminal narrowing [6, 7].

The interplay between the microbiota and immune cells is important in the pathogenesis of IBD [8]. Interleukin (IL)-17-producing Th17 cells are involved in mucosal immune responses [9, 10]. The IL-17 mRNA level is increased in inflamed mucosa from IBD patients, and the disease severity of IBD is correlated with the IL-17 level in peripheral blood mononuclear cells from UC patients [11, 12]. Furthermore, IL-17 deficiency does not cause colonic inflammation in IBD animal models [13, 14]. T regulatory (Treg) cells play roles that are the opposite of those played by Th17 cells in autoimmune diseases, including in IBD [15]. Treg cells maintain immune-cell homeostasis by suppressing the functions of other immune cell types, particularly Th17 cells. IL-10, which is secreted by Treg cells, is essential for intestinal homeostasis; indeed, IL-10 deficiency leads to the spontaneous development of colitis in mice [16].

Probiotics are live microorganisms that benefit host health when administered in adequate amounts [17]. Probiotics promote maintenance of the gut barrier function and modulation of the host immune system; therefore, dietary supplements containing probiotics may be beneficial for IBD [18–20]. *Lactobacillus*, *Bifidobacterium*, and *Enterococcus* strains are commonly used as probiotics [21–23].

A prebiotic is a non-viable food substance that confers a health benefit on the host by promoting selective growth of beneficial bacteria and is associated with modulation of the intestinal microbiota [24]. A synbiotic, a mixture of a probiotic and prebiotic, has the advantages of both probiotics and prebiotics [25, 26].

In this study, we combined 12 probiotics with prebiotics, rosavin (extracted from *Rhodiola rosea* L.), and zinc. The therapeutic effect of this combination drug in mice with dextran sodium sulfate (DSS)-induced colitis was investigated. The combination drug modulated the production of both proinflammatory cytokines (IL-6, IL-1β, and IL-17) and an anti-inflammatory cytokine (IL-10) in mice with DSS-induced colitis. Furthermore, the combination drug ameliorated intestinal fibrosis.

Methods

Mice

Eight-week-old male C57BL/6 mice were purchased from Orient Bio Inc. (Seongnam, Korea). The animals were housed under specific pathogen-free conditions at the Institute of Medical Science of the Catholic University of Korea and were maintained under controlled temperature (21–22 °C) and light (12/12-h light/dark cycle) conditions. The mice were fed standard mouse chow and water. All experimental procedures were approved by the Department of Laboratory Animals, Institutional Animal Care and Use Committee (IACUC) of the School of Medicine, the Catholic University of Korea and conformed with all National Institutes of Health (USA) guidelines (Permit number: CUMC 2016-0244-01).

Probiotic complex, prebiotics, rosavin and zinc

The probiotic complex (Lot#171121), prebiotics (Chicory fiber, Lot#RCRRW6ARW6), and rosavin (Lot#88843) were purchased from CNS Pharm Korea Co., Ltd (Seoul, Korea). The probiotic complex comprises *Lactobacillus acidophilus*, *Lactobacillus casei*, *Lactobacillus fermentum*, *Lactobacillus paracasei*, *Streptococcous thermophilus*, *Bifidobacterium longum*, *Bifidobacterium bifidum*, *Bifidobacterium breve*, *Lactobacillus rhamnosus*, *Lactobacillus plantarum*, *Lactobacillus helveticus*, and *Lactobacillus salivarius*. The probiotic complex was resuspended in saline at 25 mg/mL and killed by heating at 80 °C for 30 min. Zinc was purchased from Sigma-Aldrich (MO, USA, #205532).

Induction of colitis and drug administration

C57BL/6 mice were divided into three groups (5 mice in each group) and were group-housed in cage. Groups of mice were administrated 3% DSS (MP Biomedicals, Santa Ana, CA, USA) in drink water. To measure the amount of DSS consumption, DSS-dissolved drinking water (3% DSS) was replaced daily and measure the amount left of drinking water. Each mouse drank about 15 mL of 3% DSS water during the 4 days. Mice were randomly assigned to three groups (n = 5/group) as follows: Vehicle-treated mice were administered DSS in drinking water. Probiotics complex-treated mice were administered the probiotics complex (100 mg/mouse) in drinking water, and combination drug-treated mice were administered the probiotics complex, prebiotics, zinc, and rosavin (100 mg/mouse; probiotics complex [1.25 mg], prebiotics [15 mg], zinc [3 mg], and rosavin [20 mg]) daily beginning 3 days after DSS administration. Body weight and disease activity index (DAI) score were monitored

daily. Data are representative of two independent experiments with similar results.

Assessment of inflammation

The severity of colitis was assessed daily by determining the percentage body weight change and DAI. The DAI was calculated as described previously [27]. Body weight loss (score: 0, none; 1, 0–5%; 2, 6–10%; 3, 11–15%; 4, 16–20%; 5, 21–25%; and 6, 26–30%), stool consistency (score: 0, normal stools; 1, soft stools; and 2, liquid stools), and rectal bleeding (score: 0, negative fecal occult blood; 1, positive fecal occult blood; and 2, visible rectal bleeding) were assessed daily in each mouse.

Histopathological analysis

Colon tissue Sections (5-μm thick) were fixed and embedded in 10% (v/v) neutral-buffered formalin (Sigma-Aldrich, St. Louis, MO). Histological analysis was performed on H&E stained colitis tissue and scored by two experimenters in a blinded fashion. Stained sections were examined under a photomicroscope (Olympus, Tokyo, Japan) (magnifications: 100×). The histological scoring system was used for evaluation of the degree of colitis [28]. Loss of epithelium, crypt damage, depletion of goblet cells, and infiltration of inflammatory cells were assessed in these sections. Histological evaluation and scoring of loss of epithelium (0, no loss of epithelium; 1, 0–5% loss of epithelium; 2, 5–10% loss of epithelium; and 3, > 10% loss of epithelium), crypt damage (0, no damage; 1, 0–10% loss of crypt; 2, 10–20% loss of crypt; 3, > 20% loss of crypt), depletion of goblet cells (0, none; 1, mild; 2, moderate; and 3, severe), and infiltration of inflammatory cells (0, none; 1, mild; 2, moderate; and 3, severe) were performed. Total histological score were ranged from 0 to 12.

Immunohistochemistry

Sections were treated with 3% (v/v) H_2O_2 in methanol to block endogenous peroxidase activity. Immunohistochemistry was performed using the Envision Detection™ kit (DAKO, Glostrup, Denmark, #5007). Tissue sections were incubated with primary antibodies against IL-10 (Santa Cruz Biotechnology, Santa Cruz, CA, USA, #SC-1783), Foxp3 (Santa Cruz Biotechnology, Santa Cruz, CA, USA, #SC-28705), tumor necrosis factor (TNF)-α (Abcam, Cambridge, UK, #ab6671), IL-1β (Abcam, Cambridge, UK, #ab9722), IL-17 (Abcam, Cambridge, UK, #ab79056), IL-6 (Abcam, Cambridge, UK, #ab7737), α-smooth muscle actin (α-SMA) (Abcam, Cambridge, UK, #ab7817), and type I collagen (Col-I) (Abcam, Cambridge, UK, #ab6308) for 2 h at room temperature. Sections were then incubated with a horseradish peroxidase (HRP)-conjugated secondary antibody for 30 min. The final colored products were developed using chromogen diaminobenzidine, and the sections were examined under a photomicroscope (Olympus, Tokyo, Japan). Positive cells were enumerated visually by four individuals, and the mean values were calculated.

Stimulation of HT-29 cells

HT-29 cells were seeded in 24-well plates at an initial density of 5×10^4 cells per well and allowed to adhere for 12 h. HT-29 cells were maintained in RPMI-1640 supplemented with 10% fetal bovine serum. After 12 h, the medium was replaced by a fresh one and the cells were pretreated with combination drug for 2 h and then the cells were incubated in the presence of lipopolysaccharide (LPS; 1 μg/mL, Sigma-Aldrich) for 2 days. The supernatants were assayed for monocyte chemoattractant protein 1 (MCP-1) levels.

Enzyme-linked immunosorbent assay

The levels of MCP-1 in HT-29 cell culture supernatants were measured by sandwich enzyme-linked immunosorbent assay (ELISA; R&D Systems). Horseradish peroxidase–avidin (R&D Systems) was used for color development. Absorbance at 405 nm was measured using an ELISA microplate reader (Molecular Devices, Sunnyvale, CA, USA).

Statistical analysis

All statistical analyses were performed using GraphPad Prism (version 4 for Windows; GraphPad Software). Normally distributed continuous data were analyzed using the parametric Student's *t* test. Differences in mean values among groups were subjected to analysis of variance (ANOVA) followed by Bonferroni post hoc test. Data are presented as means ± standard deviations (SDs). A value of $p < 0.05$ (two-tailed) was considered to indicate statistical significance.

Results

Effect of the combination drug on DSS-induced colitis

To investigate the therapeutic effects of probiotics complex and the combination drug, the probiotics complex and the combination drug in drinking water were administered to mice daily after DSS administration. Mice in the vehicle-treated DSS-induced colitis group showed marked weight loss from day 5 as a result of severe colitis (Fig. 1a). However, treatment with the probiotic complex ($p < 0.05$) or the combination drug ($p < 0.001$) ameliorated the loss of body weight. The DAI score, which combines weight loss, changes in stool consistency, and bleeding, was significantly lower in the probiotic complex—($p < 0.05$) and combination drug-treated groups ($p < 0.001$) compared to the

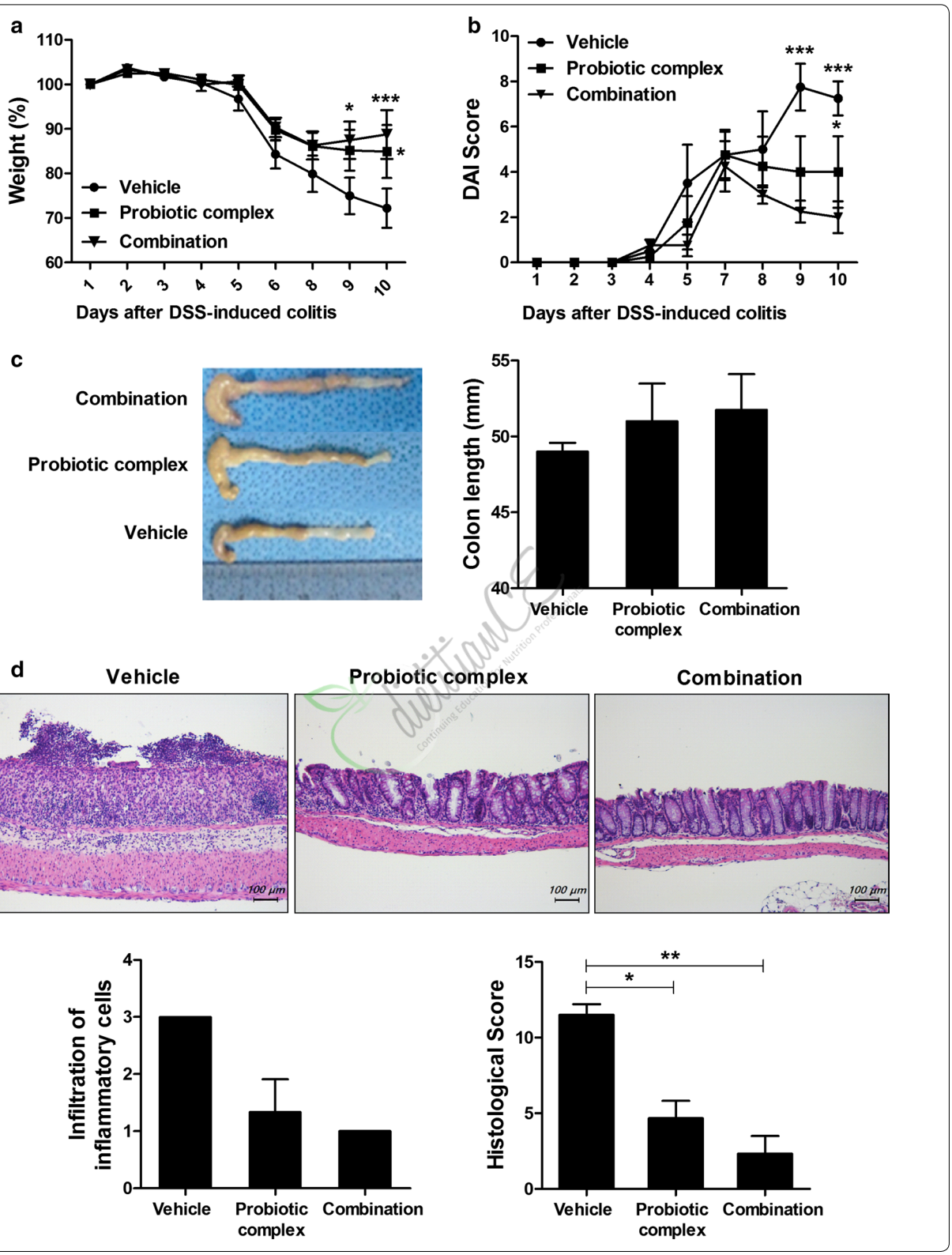
a
Weight (%)
110
100
90
80
70
60
Vehicle
Probiotic complex
Combination
*
***
*
1
2
3
4
5
6
8
9
10
Days after DSS-induced colitis
b
DAI Score
10
8
6
4
2
0
Vehicle
Probiotic complex
Combination
***
***
*
1
2
3
4
5
7
8
9
10
Days after DSS-induced colitis
c
Combination
Probiotic complex
Vehicle
Colon length (mm)
55
50
45
40
Vehicle
Probiotic complex
Combination
d
Vehicle
Probiotic complex
Combination
100 µm
100 µm
100 µm
Infiltration of inflammatory cells
4
3
2
1
0
Vehicle
Probiotic complex
Combination
Histological Score
15
10
5
0
**
*
Vehicle
Probiotic complex
Combination

(See figure on previous page.)
Fig. 1 The combination drug ameliorated DSS-induced colitis. C57BL/6 mice were treated orally with 3% DSS in distilled water ad libitum from days 0 to 4 and thereafter received regular drinking water. On day 3 after DSS administration, the probiotic complex or the combination drug (100 mg/mouse) was administered orally (n = 5/group). **a** Changes in body weight expressed as percentages of body weight on day 0. **b** With the exception of day 7, the DAI was monitored daily. Data are means ± SDs of four independent experiments. **c** Colon length of mice with DSS-induced chronic colitis on day 10. Macroscopic images of the colon (left panel). Colon length (right panel). **d** Representative hematoxylin and eosin-stained images of the colon on day 10. Scale bar, 100 μm. $^{*}p < 0.05$, $^{**}p < 0.01$, $^{***}p < 0.001$. Vehicle *vs.* probiotic complex or combination drug treatment

vehicle-treated group (Fig. 1b). Treatment with the probiotic complex or the combination drug prevented the decrease in colon length evident in the vehicle-treated group (Fig. 1c). Microscopic examination of the colon revealed that the probiotic complex and the combination drug restored the mucosal architecture compared with vehicle treatment. The histological score was decreased in the probiotic complex—($p < 0.05$) and combination drug-treated groups ($p < 0.01$) (Fig. 1d). The combination drug exerted a greater therapeutic effect than did the probiotic complex.

Effect of the combination drug on proinflammatory cytokine and chemokine expression

The effect of the probiotic complex and the combination drug on colitis was assessed by immunostaining

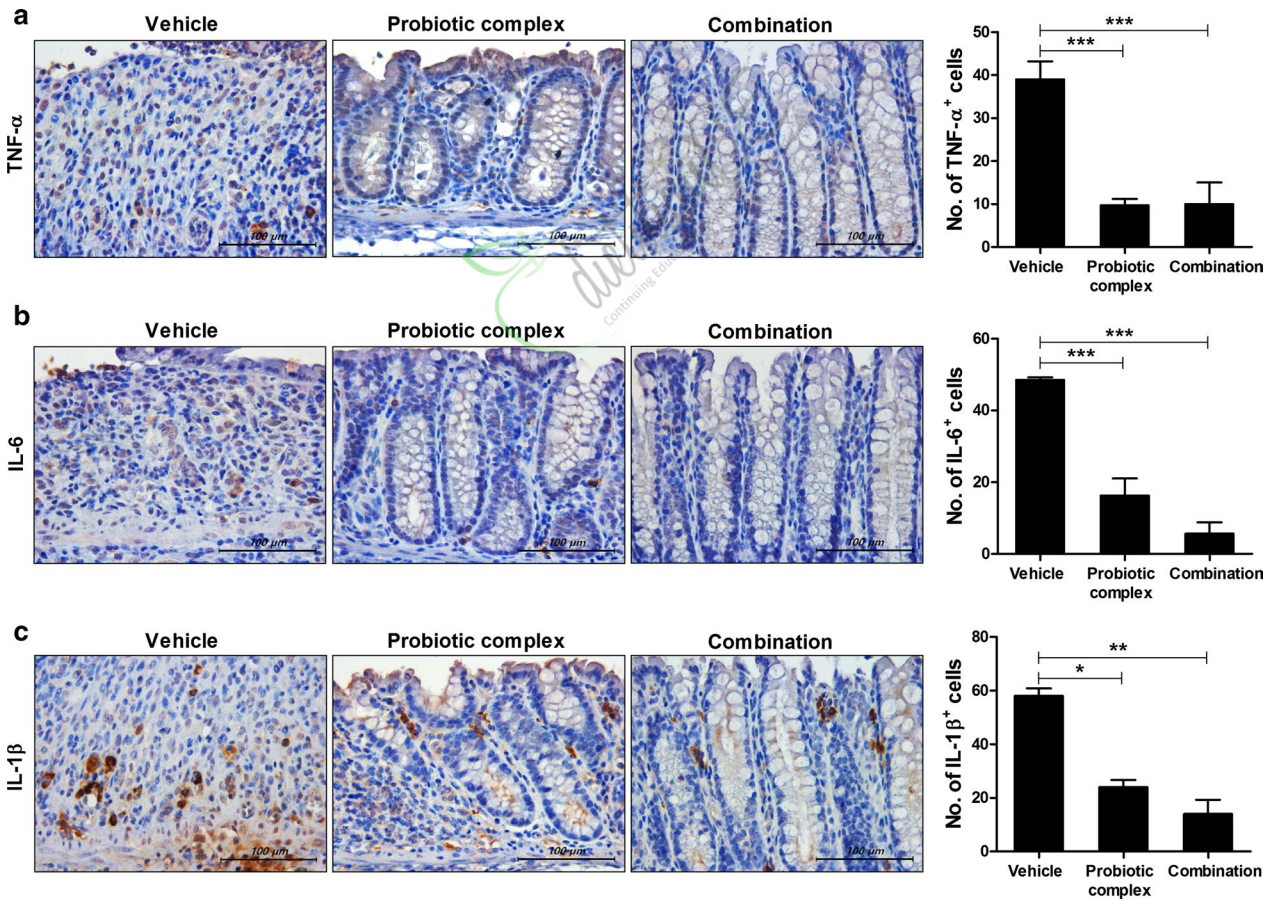

Fig. 2 The combination drug reduced proinflammatory cytokine levels. C57BL/6 mice were treated orally with 3% DSS in distilled water ad libitum from days 0 to 4 and thereafter received regular drinking water. On day 3 after DSS administration, the probiotic complex or the combination drug (100 mg/mouse) was administered orally (n = 5/group). On day 10 after DSS administration, colon tissue sections were stained with antibodies against TNF-α (**a**), IL-6 (**b**), and IL-1β (**c**). Representative histological features are shown, and the results are presented as mean ± SD numbers of antibody-positive cells (n = 5/group). Scale bar, 100 μm. $^{*}p < 0.05$, $^{**}p < 0.01$, $^{***}p < 0.001$. Vehicle vs. probiotic complex or combination drug treatment

colon sections for inflammatory cytokines (Fig. 2). Colon tissue from vehicle-treated mice had higher levels of TNF-α, IL-6, and IL-1β than did colon tissue from mice treated with the probiotic complex or the combination drug; the latter exerted the greatest effect on colitis ($p < 0.001$, $p < 0.001$, and $p < 0.01$, respectively). To assess the immune modulatory effects of combination drug, the HT-29 cell line, a human colorectal adenocarcinoma cell line, was pretreated with combination drug for 2 h and then incubated in the presence of LPS for 48 h. The level of MCP-1, which regulates migration and infiltration of monocytes/macrophages [29], in HT-29 cells was decreased by treatment with the combination drug ($p < 0.01$) (Fig. 3).

Effect of the combination drug on IL-17, Foxp3, and IL-10 levels

Th17 cells infiltrate the inflamed intestine, where they trigger and amplify inflammation [8]. To investigate the effect of the probiotic complex and the combination drug on IL-17, Foxp3 (a transcription factor for Treg cells [30]), and IL-10 levels, colon sections were subjected to immunohistochemical staining. The colon tissue of mice treated with the probiotic complex or the combination drug exhibited a lower IL-17 level than did the colon tissue of vehicle-treated mice ($p < 0.05$) (Fig. 4a). In contrast, Foxp3 and IL-10 levels were significantly increased in the colon tissue of mice treated with the combination drug compared to those treated with vehicle ($p < 0.05$ and $p < 0.001$, respectively) (Fig. 4b, c). Treatment with the probiotic complex also increased the expression of Foxp3 and IL-10, albeit not significantly so.

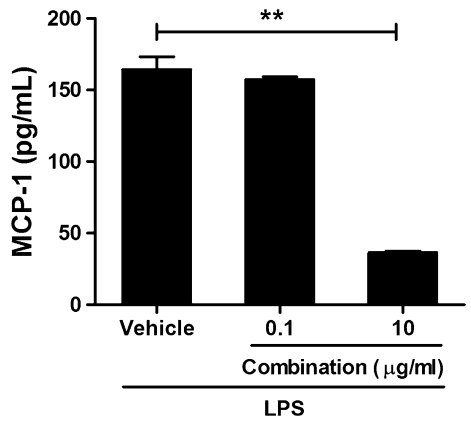

Fig. 3 The combination drug reduced the MCP-1 level in HT-29 cells. HT-29 cells were treated with the combination drug in the presence of LPS (1 μg/mL) for 48 h. MCP-1 mRNA and protein levels were determined by RT-PCR and ELISA, respectively. $^{**}p < 0.01$ by Student's *t* test. Vehicle vs. combination drug treatment

Effect of the combination drug on colitis-associated intestinal fibrosis

To investigate the antifibrotic effects of the probiotic complex and combination drug, colon sections were stained with Masson's trichrome (Fig. 5a). Treatment with the probiotic complex or the combination drug suppressed the area of blue staining in the colonic muscular layer compared with vehicle treatment. To evaluate the effect of the probiotic complex or the combination drug on the number of myofibroblasts in the colonic mucosa and submucosa, immunohistochemical staining for α-SMA, a marker of fibroblast differentiation to myofibroblasts, was performed on day 10. The number of α-SMA+ myofibroblasts was significantly decreased in the colons of mice treated with the probiotic complex or the combination drug compared with the vehicle-treated mice ($p < 0.01$) (Fig. 5b). Furthermore, the number of Col-1+ cells was significantly decreased in the colons of mice treated with the probiotic complex or the combination drug compared with vehicle-treated mice ($p < 0.01$) (Fig. 5c).

Discussion

The aim of this study was to elucidate the effect of a combination of a probiotic complex, prebiotics, rosavin, and zinc in a DSS-induced colitis mouse model. Treatment with the combination drug attenuated the severity of colitis; suppressed the body weight loss, reduction in colon length and DAI score; and reduced the histological changes evident in vehicle-treated mice. The combination drug decreased the levels of proinflammatory cytokines and chemokines and increased the levels of Foxp3 and IL-10 in colon tissue. Furthermore, treatment with the combination drug suppressed colitis-associated intestinal fibrosis.

Gut microbiota dysbiosis plays a key role in the pathogenesis of IBD. Probiotics, live microorganisms that benefit host health, are commonly used to control chronic gastrointestinal inflammation in IBD patients. *Lactobacillus* and *Bifidobacterium* species are widely used as probiotics [31]. Administration of *Lactobacillus plantarum* LP ameliorates the severity of colitis in IL-10-knockout mice [32]. *Lactobacillus paracasei* LS2 isolated from the Korean food, kimchi, reduces colitis disease by decreasing the number of Th1 cells and macrophages in the lamina propria [33]. Treatment with *Lactobacillus acidophilus* reduces the STAT3 and phosphorylated STAT3 levels in colon tissue from mice with DSS-induced colitis and increases the number of Treg cells among intestinal intraepithelial and lamina propria lymphocytes in a 2,4,6-trinitrobenzene sulfonic acid-induced colitis model [21, 34]. Treatment with *Bifidobacterium longum* ameliorates colorectal colitis in rats by altering the methylation

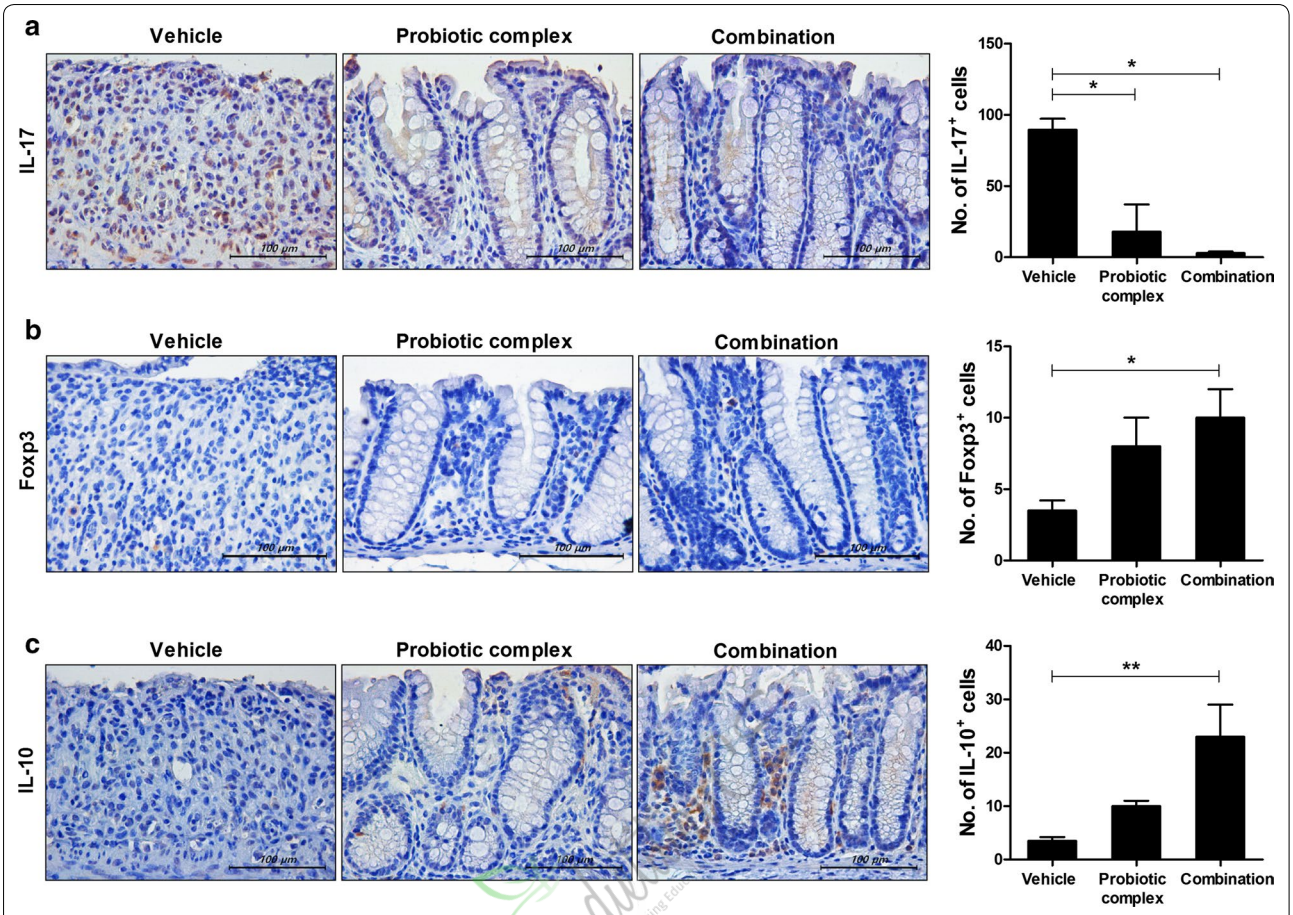

Fig. 4 The combination drug reduces IL-17 and Foxp3 levels. C57BL/6 mice were treated orally with 3% DSS in distilled water ad libitum from days 0 to 4 and thereafter received regular drinking water. On day 3 after DSS administration, the probiotic complex or the combination drug (100 mg/mouse) was administered orally (n = 5/group). On day 10 after DSS administration, colon tissue sections were stained with antibodies against IL-17 (**a**), Foxp3 (**b**), and IL-10 (**c**). Representative histological features are shown, and the results are presented as mean ± SD numbers of antibody-positive cells (n = 5/group). Scale bar, 100 μm. $^{*}p < 0.05$, $^{**}p < 0.01$. Vehicle vs. probiotic complex or combination drug treatment

level of the Foxp3 promoter, resulting in an increased number of Treg cells [35]. Moreover, *Streptococcus thermophilus* suppresses bacterial translocation, which reduces gastrointestinal bleeding and weight loss [36].

Much research has focused on the use of gut microbiota for the treatment of IBD. Treatment with lactobacilli and bifidobacteria promoted recovery of DSS-induced intestinal injury and inflammation in a mouse model of colitis [37]. *Lactobacillus casei* and *Bifidobacterium lactis* ameliorated injury to the intestinal mucosa and liver in a 2,4,6-trinitrobenzene sulfonic acid-induced colitis model [38]. Also, treatment with a probiotic combination that included lactobacilli, bifidobacteria, and streptococci reduced the levels of proinflammatory cytokines in colitis [39]. In this study, we evaluated the efficacy of a combination of 12 probiotics (lactobacilli, bifidobacteria, and streptococci) with prebiotics, rosavin, and zinc for the treatment of IBD. *Rhodiola rosea* is a widely used plant for traditional medicine and it was reported that it has anti-oxidant, neuroprotective, anti-diabetic and anti-inflammatory effects [40–42]. Rosavin is a typical compound of *Rhodiola rosea* and recent study revealed that it inhibits TNF-related apoptosis-inducing ligand expression via extracellular signal-regulated kinase phosphorylation in T cells [43]. Zinc is absorbed in the small intestine, functions as a cofactor for enzymes, such as alkaline phosphatase, and is essential for growth, immunity, and tissue repair [44, 45]. Furthermore, zinc involves in the regulation of cell proliferation via affecting metalloenzymes and hormonal signaling. Reduced zinc availability influences survival of animal [46]. Zinc deficiency is commonly seen in IBD patients due to inadequate zinc intake or poor absorption from the gastrointestinal tract [45, 47, 48]. In the present study, oral administration of the combination drug showed therapeutic effects in a DSS-induced colitis model. Notably, the combination

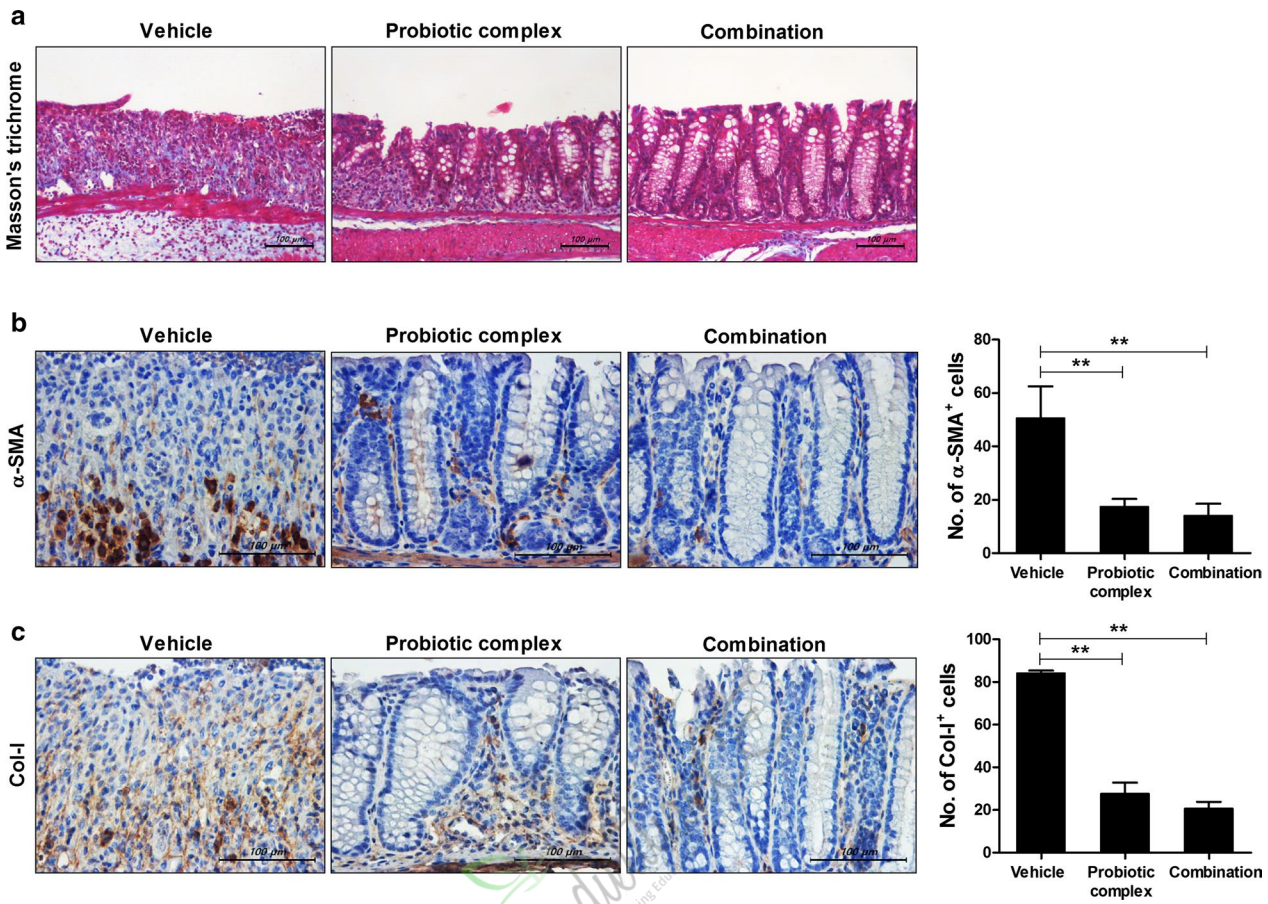

Fig. 5 The combination drug reduces colitis-associated intestinal fibrosis. C57BL/6 mice were treated orally with 3% DSS in distilled water ad libitum from days 0 to 4 and thereafter received regular drinking water. On day 3 after DSS administration, the probiotic complex or the combination drug (100 mg/mouse) was administered orally (n = 5/group). At 10 days after DSS administration, colon tissue sections were stained with Masson's trichrome (**a**). Representative histological features are shown. **b**, **c** Colon tissue was subjected to immunohistochemical staining for α-SMA (**b**) and Col-I (**c**). Representative histological features are shown, and the results are presented as mean ± SD numbers of antibody-positive cells (n = 5/group). $^{**}p < 0.01$. Vehicle vs. probiotic complex or combination drug treatment

drug resulted in a greater decrease in the levels of pro-inflammatory cytokines (TNF-α, IL-6, IL-1β, and IL-17) and greater increases in the levels of the anti-inflammatory cytokine IL-10 and transcription factor Foxp3 in colon tissue compared with the probiotic complex alone. Further studies should investigate the mechanisms underlying the effect of the combination drug on intestinal homeostasis.

The combination drug also improved DSS-induced intestinal fibrosis. Fibrosis develops from chronic inflammation and is caused by the accumulation of extracellular matrix components, which causes stricture formation and organ dysfunction [6, 7]. Fibrosis is a major and frequent complication in IBD patients, for which no specific therapy is available [49]. The combination drug decreased the α-SMA and type I collagen levels compared with vehicle treatment. Recently, there have been attempts to treat fibrosis using cytokine-targeted therapy. IL-10 deficiency accelerates kidney inflammation and fibrosis in the unilateral ureteral obstruction mouse model, and treatment with IL-10 ameliorates lung fibrosis [50, 51]. In contrast, IL-17 exerts pro-fibrotic effects in the lung, liver, and heart [52]. IL-17 deficiency reduces fibrosis in models of skin inflammation, and treatment with IL-17 enhances cardiac fibroblast proliferation and migration in pulmonary fibrosis models [53, 54].

DSS-induced colitis model used in this study is very popular for the IBD research because of its rapidity, simplicity, reproducibility and controllability. However, the limitation of this model is that T or B cell responses are not required for the development of colitis unlike human disease [55]. In addition, luminal bacteria play a role in the development of this robust colitis [56]. Therefore, additional studies are needed to determine the complex

role of combination of a probiotic complex with rosavin, zinc, and prebiotics on the gut-immune axis.

Conclusion

In conclusion, treatment with the combination of a probiotic complex, prebiotics, rosavin, and zinc attenuated colitis, significantly decreased the levels of proinflammatory cytokines, and significantly increased the levels of Foxp3 and IL-10 in colon tissue. Furthermore, treatment with the combination drug decreased the levels of α-SMA and Col-I compared with vehicle treatment. Therefore, the combination of a probiotic complex with rosavin, zinc, and prebiotics may be important therapeutics for IBD by modulating the inflammatory cytokines and fibrosis.

Low dose Naltrexone for induction of remission in inflammatory bowel disease patients

Abstract

Background: Around 30% of patients with inflammatory bowel disease (IBD) are refractory to current IBD drugs or relapse over time. Novel treatments are called for, and low dose Naltrexone (LDN) may provide a safe, easily accessible alternative treatment option for these patients. We investigated the potential of LDN to induce clinical response in therapy refractory IBD patients, and investigated its direct effects on epithelial barrier function.

Methods: Patients not in remission and not responding to conventional therapy were offered to initiate LDN as a concomitant treatment. In total 47 IBD patients prescribed LDN were followed prospectively for 12 weeks. Where available, endoscopic remission data, serum and biopsies were collected. Further the effect of Naltrexone on wound healing (scratch assay), cytokine production and endoplasmic reticulum (ER) stress (GRP78 and CHOP western blot analysis, immunohistochemistry) were investigated in HCT116 and CACO2 intestinal epithelial cells, human IBD intestinal organoids and patient samples.

Results: Low dose Naltrexone induced clinical improvement in 74.5%, and remission in 25.5% of patients. Naltrexone improved wound healing and reduced ER stress induced by Tunicamycin, lipopolysaccharide or bacteria in epithelial barriers. Inflamed mucosa from IBD patients showed high ER stress levels, which was reduced in patients treated with LDN. Cytokine levels in neither epithelial cells nor serum from IBD patients were affected.

Conclusions: Naltrexone directly improves epithelial barrier function by improving wound healing and reducing mucosal ER stress levels. Low dose Naltrexone treatment is effective and safe, and could be considered for the treatment of therapy refractory IBD patients.

Keywords: Crohn's disease, Ulcerative colitis, Naltrexone, Endoplasmic reticulum stress, Wound healing

Background

Inflammatory bowel disease (IBD) is a chronic inflammatory disorder, which includes Crohn's disease (CD) and ulcerative colitis (UC). The aim of therapy is to induce sustained remission, a state of long lasting quiescent disease. Several drugs exist to induce and maintain remission, and these drugs are usually prescribed in a step-up fashion. Nevertheless, even when using this step-up strategy, a subset of patients will fail to reach or maintain remission even with the most potent therapies, often due to drug intolerance or loss of efficacy. For instance, yearly loss of efficacy rates are 13–24% in patients treated with anti-tumor necrosis factor α (anti-TNFα) agents [1, 2]. In general, such a state of therapy refractoriness occurs in 35–60% of all IBD patients and severely limits treatment options, often resulting in surgery or corticosteroid dependency [3, 4]. Thus, for this subset of patients, alternative treatments remain of continued interest.

The etiology of IBD is complex, with genetic predisposition, an altered microbiome, environmental

factors and a weakened epithelial barrier function triggering a chronic mucosal immune response. Targeting these different causes with medication is the current challenge in IBD treatment. Previous research suggests that the endogenous opioid system also plays a role in gut immunity [5, 6]. For instance, in IBD patients, the μ-opioid receptor (MOR) is overexpressed in mucosal T-lymphocytes and monocytes, and ex vivo stimulation of MOR with the agonist DALDA reduced TNFα in mucosal biopsies from IBD patients [7]. In addition, DALDA also showed anti-inflammatory responses in a mouse model of colitis through inhibition of T cell proliferation and cytokine (including TNFα) production [8]. Another opioid known to modulate MOR responses is Naltrexone. While being a MOR *anta*gonist, which blocks endogenous opioid effects when used at high concentrations [9], administration of low dose Naltrexone (LDN) is postulated to result in upregulation of endogenous encephalin and endorphin levels and to have a positive modulatory effect on the MOR [10, 11]. Thus, the use of LDN in clinical settings is gaining interest, with Crohn's disease, multiple sclerosis and fibromyalgia described as potential targets for treatment with LDN [12–14]. In both mouse and rat models of IBD, LDN alleviated inflammation, in part by reducing pro-inflammatory cytokine production [15, 16]. Interestingly, we and others have shown that endoplasmic reticulum (ER) stress in intestinal Paneth cells is one of the contributing factors in IBD [17–19], and it was recently reported that Naltrexone attenuates inflammation in a mouse liver injury model by reducing ER stress [20, 21].

Pilot studies in patients with CD showed a positive effect of LDN therapy, with 15 of 17 patients showing a clinical response [22]. A subsequent randomized, placebo-controlled, double blind study in 34 patients found a response rate of 88% in the LDN group versus 40% in the placebo group after 12 weeks of therapy [23]. In addition LDN was also shown to be safe in pediatric IBD patients, and resulted in significantly reduced PCDAI scores, with 25% of patients achieving remission and 67% showing improvement of disease [24]. The above results suggest that LDN is an effective therapy for CD patients, although the exact mechanism remains unclear. Based on these promising results, patients started to request LDN therapy due to its favorable side-effect profile, and at the Erasmus MC we decided to start prescribing LDN to therapy refractory IBD patients with active disease. The aims of this study were to assess the clinical effect of LDN and to investigate whether LDN has a direct modulatory effect on intestinal epithelial barrier function.

Methods

Clinical cohort

A prospective cohort of patients with therapy refractory IBD (CD or UC) that started LDN therapy was formed. The decision to start LDN therapy was made by the treating physician, after fully informing the patient of the possible benefits and drawbacks. All patients were prescribed 4.5 mg Naltrexone once daily. Patients were instructed to administer one dose of LDN before bedtime.

Upon initiation of LDN therapy, patients were followed according to usual care at the outpatient clinic, with contact (in person or via telephone) after 4, 8 and 12 weeks. During these visits self-assessed disease activity and adverse events were recorded. Patients were offered endoscopic evaluation and assessment of laboratory values after 12 weeks of treatment or at time of discontinuation of LDN therapy, whichever occurred earlier. This study was approved by the Ethical Committee of the Erasmus MC (MEC-2014-656).

Clinical data collection

During the follow-up, demographic data (e.g. age, gender) and IBD related data (e.g. year of diagnosis, concomitant and previous IBD related therapies, Montreal phenotype classification) were recorded. Additionally, where available, data on diagnostic tests, particularly endoscopic evaluations, performed prior to the start of LDN therapy (with a 1 week window) and during the follow-up period were recorded. All patients that completed at least 1 assessment of disease activity were included in the cohort.

Clinical outcome measures

Clinical outcomes were based on patient self-assessments and outpatient assessments, where available. Patients were considered non-responders if no clinical improvement occurred in the first 4 weeks of LDN therapy. Patients were considered to have clinical response if self-assessed disease activity decreased within the first 4 weeks of LDN therapy, and lasted for at least 4 weeks in total. Of secondary interest were the rates of adverse events during LDN therapy. Endoscopy results were scored based on the most severe area of inflammation. Endoscopic findings in all IBD patients were scored on a scale from 0 to 3, representing no inflammation to severe inflammation respectively.

Cell lines

Colorectal cancer cell lines HCT116 and CACO-2 were cultured in Dulbecco's Modified Eagles Medium (DMEM, Lonza, Basel, Switzerland) supplemented with 100 U/mL penicillin, 100 mg/mL streptomycin (Life technologies, Bleiswijk, NL) and 10% Fecal Calf Serum (FCS,

Sigma-Aldrich, St. Louis, USA). Cells were maintained at 37 °C in a 5% CO_2 humidified setting.

Organoid culture

Non-inflamed intestinal biopsies were collected from two IBD patients undergoing routine endoscopy for their disease. Organoids were prepared as described [25, 26], see Additional file 1 for details.

Cell viability assay

Cell viability was assessed using MTT assays as described [27], see Additional file 1: Methods. Each experiment was performed twice in triplicate.

Wound healing assay

Wound healing assays were performed as described [28], see Additional file 1. The concentration of Naltrexone used was based on in vivo dosages (4.5 mg per ± 60 kg bodyweight). Experiments were performed thrice in duplicate, with two measure-sites per scratch.

Western blotting

Western blotting was performed as described [29], with modifications (see Additional file 1). HCT116 and CACO-2 cells were treated with Tunicamycin (2 µM), lipopolysaccharide (10 µg/mL LPS) or *E. coli* (paraffin-fixed DH5α, 6.25e5/mL) in the presence or absence of 1 µg/mL Naltrexone. Organoids were treated with LPS in the presence or absence of 1 µg/mL Naltrexone. Experiments were performed at least twice.

Immunohistochemistry

FFPE tissue sections were immunohistologically stained for GRP78, as described [17, 30], see Additional file 1. Antigen retrieval was performed by boiling the slides in 600 mL of 10 mM sodium citrate buffer, pH 6.0 for 15 min. Slides were blocked by incubating in 10% goat serum in PBS and incubated with GRP78 antibody (BiP, Cell Signaling Technology, Danvers, MA) diluted in blocking buffer (1:100) overnight at 4 °C. Rabbit envision (DAKO, Heverlee, Belgium) was used as secondary antibody.

Reverse transcriptase polymerase chain reaction (rt-PCR)

We used rt-PCR to determine MOR expression on the IEC cell lines, using Ribosomal protein (*RP2*) primers were used as control [26], see Additional file 1.

Enzyme linked immunosorbent assay (ELISA)

Cells were plated at 0.2×10^6 per well in 24 wells plates. Upon attachment to the plate, cells were treated as described in the text and supernatant was harvested after 24 h. Experiments were performed twice, in duplicate. Cytokine levels in supernatants from IECs and patient sera were determined by ELISA (Ready-SET-Go!® eBioscience, San Diego, CA) as per manufacturer's instructions. All samples were tested in duplicate in the ELISAs.

Statistical analysis

Continuous variables were reported as medians with interquartile range (IQR). Comparisons in continuous variables were performed with the Mann–Whitney U test. For comparisons of categorical variables, Fisher's exact test was used. For in vitro and ex vivo experiments, normality of distribution was assessed with D'agostino and Pearson Omnibus normality test. When passing normality test or when there were insufficient numbers to calculate normality, parametric testing was performed, otherwise, non-parametric tests were employed. Student T-tests were performed for comparisons of two groups. For comparisons of more than two groups, ANOVA with post hoc testing (Tukey's multiple comparison test) was performed. For all tests, one or two-sided (as appropriate) p-values < 0.05 were considered statistically significant, graphs show mean ± SEM. Analyses were performed using Graphpad Prism 5.0.

Results

Patient characteristics

From July 2010 till August 2014, 47 patients were treated with LDN, of which 19 (40.4%) were male and 28 were female. Median treatment and follow-up duration after start of LDN was 3 months (IQR 3–5 months). Of the 47 patients, 28 (59.6%) were diagnosed with CD and 19 with UC. Three patients had previously undergone surgery (2 ileocecal resections and 1 subtotal colectomy, all in CD patients). The full baseline patient characteristics are described in Table 1.

All participants were either steroid dependent or steroid refractory and had previously been treated with at least one other drug, and all patients showed clinical signs of disease activity at initiation of LDN therapy. Notably, 41 patients (87.2%) had previously received at least one anti-TNFα agent, and 19 (40.4%) had been treated with two anti-TNFα agents. The 6 patients not exposed to anti-TNFα had refused anti-TNFα therapy due to fear of possible side effects. The full details on the previous and concomitant treatments at start of LDN therapy are described in Table 2. Seven patients (14.9%) reported adverse events due to LDN, including vivid dreams (N = 4), drowsiness (N = 2) and headache (N = 1). Two patients discontinued LDN therapy after 2 weeks, due to drowsiness. Vivid dream complaints improved when LDN was administered in the morning instead of at bedtime.

Table 1 Baseline patient characteristics

General characteristics				
Diagnosis, N (%)	UC, 19 (40%)		CD, 28 (60%)	Combined, 47
Gender (M/F)	10/9		9/19	19/28
Median age at diagnosis (years, IQR)	31 (27–44.5)		23 (16.8–32.5)	27 (18–39.5)
Median age at start of LDN (years, IQR)	42 (33.5–52)		35.5 (25.5–53.5)	40 (27.5–52.5)
Median disease duration at start of LDN (years, IQR)	6.9 (3.2–12.4)		7.8 (3.8–16.5)	7.0 (3.8–13.4)
CRP mg/L, median (IQR)	7 (2–27)		6 (2–7)	6 (2–9)
Endoscopic score (median, IQR)	2.0 (1.0–2.0)		2.0 (2.0–2.0)	2.0 (1.25–2.0)
Disease characteristics				
Disease extent or phenotype [montreal classification, % (N)]	E1	11% (2)	L1	7% (2)
	E2	63% (12)	L2	32% (9)
	E3	26% (5)	L3	61% (17)

CD Crohn's disease, *CRP* C-reactive protein, *IQR* inter-quartile range, *LDN* low dose Naltrexone, *UC* ulcerative colitis

Table 2 Medical therapies used prior to start of LDN and concomitantly with LDN

	UC, 19	CD, 28	Combined, 47
Prior and concomitant therapies			
Therapies prior to LDN, N (%)			
5-ASA	17 (89%)	14 (50%)	31 (66%)
Steroids	19 (100%)	28 (100%)	47 (100%)
Immunosuppressives	18 (95%)	27 (96%)	45 (96%)
Anti-TNF	16 (84%)	25 (89%)	41 (87%)
Other	5 (26%)	2 (7%)	8 (15%)
Concomitant therapies at start of LDN, N (%)			
5-ASA	7 (37%)	3 (11%)	10 (21%)
Steroids	6 (32%)	18 (64%)	24 (51%)
Immunosuppressives	8 (42%)	9 (32%)	17 (36%)
Anti-TNF	5 (26%)	3 (11%)	8 (17%)
Other	1 (5%)	2 (7%)	3 (6%)
None	4 (21%)	7 (25%)	11 (23%)

Steroids refer to any form of corticosteroids. Immunosuppressives refer to thiopurines or methotrexate. Other refers to tacrolimus, cyclosporine, thioguanine or blinded trial drugs

anti-TNF anti-tumor necrosis factor, *CD* Crohn's disease, *LDN* low dose Naltrexone, *UC* ulcerative colitis

LDN therapy shows clinical and endoscopic efficacy in IBD patients

Of the 47 patients, 35 (74.5%) achieved a clinical response. Of those 35 patients, 12 patients had a response of at least 3 months (25.5% of total cohort, 8 CD, 4 UC), whereas a short-lived (between 4 and 12 weeks) improvement was seen in the remaining 23 patients (48.9% of total cohort, 13 CD, 10 UC). There was no statistically significant difference between CD and UC patients in the number of patients that achieved either response or remission ($p=1.000$ and $p=0.515$ respectively).

The median endoscopic score at baseline amongst all patients was 2 (IQR 1.25–2.0). In 12 patients, consecutive endoscopies were performed both at baseline and at 12 weeks or at time of relapse, whichever occurred earlier. These consecutive endoscopies were performed in 6 patients with response (3 CD, 3 UC) and 6 patients with remission (1 CD, 5 UC). Between these two groups, no significant difference was observed in baseline endoscopic score (median 1.67, range 1–3 versus 1.83, range 0–3 for response and remission respectively $p=0.676$). However, patients achieving clinical remission had a significantly greater improvement in endoscopic score compared to patients not reaching clinical response (median change − 1.5, range − 2 to 0 versus 1.0, range 0–2, $p=0.005$, Fig. 1). Complete endoscopic remission upon treatment with LDN was seen in 5 out of 6 patients with clinical remission.

Naltrexone improves wound healing in intestinal epithelial cell layers

Having shown clinical effect of Naltrexone in patients, we next sought to establish whether Naltrexone has a direct effect on epithelial cell function. After testing for the presence of MOR (Fig. 2a), we investigated the effect of Naltrexone on wound healing in layers of HCT116 and CACO2 colonic epithelial cell lines. Figure 2b shows that scratch wounds inflicted in HCT116 cell cultures are healed significantly faster when cells are treated with Naltrexone as compared to vehicle control ($p=0.0001$ at $t=24$; $p=0.0001$ at $t=48$). In CACO2 cells, which migrate much faster than HC116, all wounds were healed at $t=48$ and the effect of Naltrexone on wound size was less clear ($t=24$ h, $p=0.085$, Fig. 2b, right panel). Possibly, the lower MOR expression levels observed in CACO2 cells accounts for the lesser effect of Naltrexone in this cell line. However, when comparing

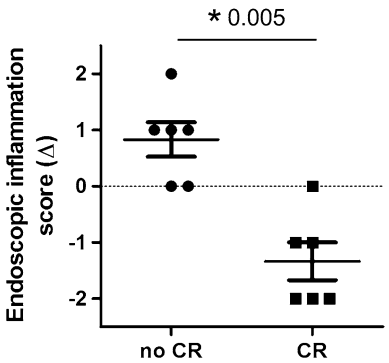

Fig. 1 Changes in individual endoscopic inflammation scores values. The change in endoscopic score value for patients in clinical remission after week 12 and patients not in clinical remission after week 12 are displayed. Each dot represents an individual. The horizontal line represents the group median. The difference in group medians is statistically significant (− 1.5 versus 1.0, for clinical remission and not in clinical remission respectively, p = 0.005)

the migrated distance of cells, it was evident that Naltrexone stimulated epithelial cell migration, in both HCT116 (361 ± 24 vs 656 ± 52 pixels, p = 0.085) and CACO2 (465 ± 26 vs 310 ± 50 pixels, p = 0.0083, Fig. 2c). This effect of Naltrexone on wound healing was not due to an increased cellular proliferation, as total viable cell numbers were not affected by Naltrexone up to a concentration of 100 µg/mL (Additional file 2: Figure S1A–C).

Naltrexone does not affect interleukin 8 (IL-8) cytokine levels in epithelial cells and patient sera

In vivo, epithelial cells produce an array of cytokines in response to inflammatory stimuli, which in turn can attract immune cells and perpetuate inflammation in IBD patients. We therefore investigated whether cytokine production by epithelial cells is directly affected by Naltrexone. Cells were stimulated with bacteria in the absence or presence of Naltrexone, and supernatants were tested for the presence of the pro-inflammatory cytokines IL-6, IL-8 and TNFα after 24 h. As shown in Fig. 3, treatment of cells with bacteria significantly increased IL-8 production in both HCT116 and CACO2 cells (44 ± 4 to 92 ± 14 pg/mL in HCT116, p = 0.0001, Fig. 3a and 17 ± 1 to 25 ± 3 pg/mL in CACO2, p = 0.0001, Fig. 3b). However, neither basal levels nor bacteria-stimulated levels of IL-8 were significantly affected by Naltrexone treatment. IL-6 and TNFα levels were undetectable (not shown).

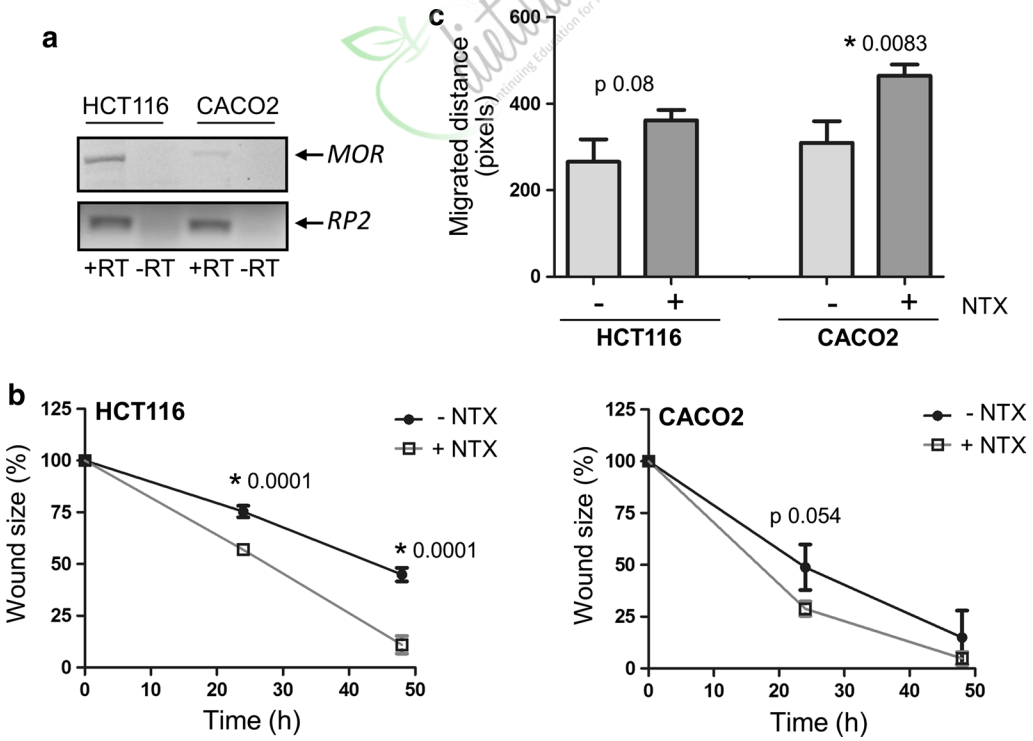

Fig. 2 Naltrexone improves epithelial wound healing. **a** Expression of the µ-opioid receptor (MOR) was tested by rt-PCR, using -RT (i.e. RNA) controls. Ribosomal protein 2 (RP2) was used as cDNA quality control. **b** HCT116 (left panel) and CACO2 (right panel) cultures were scratched in the presence or absence of 1 µM Naltrexone (NTX), and wounds were photographed at t = 0, 24 and 48. Mean percentage wound size of three independent experiments is shown. **c** Migration of wound edges at t = 24 in pixels presented as mean of three experiments

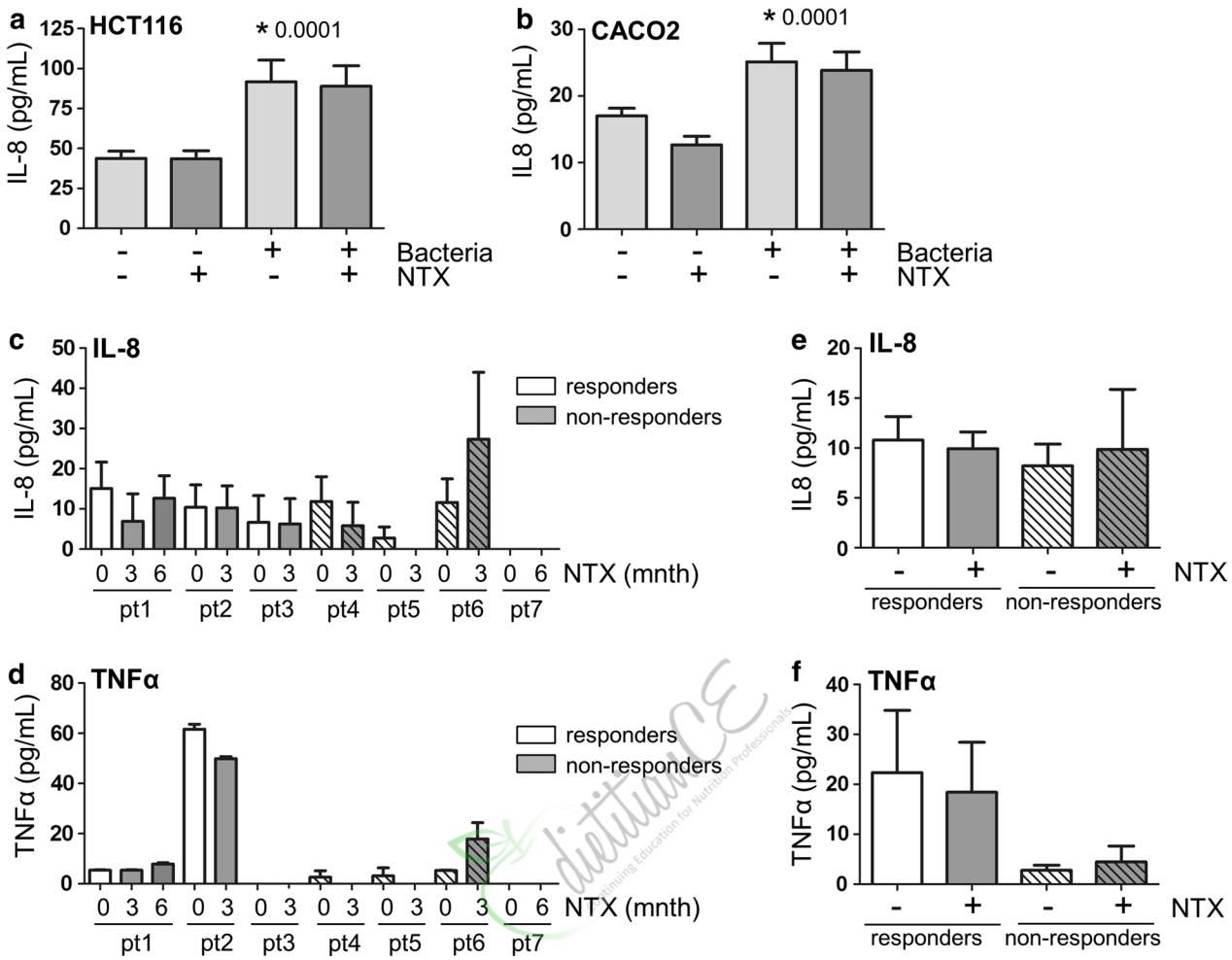

Fig. 3 Naltrexone does not affect IL-8 levels in epithelial cell lines and patient sera. Stimulation of HCT116 (**a**) and CACO2 (**b**) cell layers for 24 h with bacteria results in significantly increased IL-8 levels in culture supernatants as determined by ELISA. Co-treatment with 1 μg/mL Naltrexone does not affect basal levels or bacteria-induced levels of IL-8 production in these cell lines. **c**–**f** Serum from patients was taken before low dose Naltrexone (NTX) treatment, and 3 or 6 months into treatment. IL-8 was detectable in 6 of 7 patients **c** by ELISA, whereas TNFα was detectable in 5 patients (**d**). There was no significant difference in the mean IL-8 (**e**) or TNFα (**f**) levels between responders and non-responders to low dose Naltrexone

Next we tested whether IL-8 or TNFα systemic levels in patients were modulated by Naltrexone treatment in vivo. Paired serum samples (before and after initiation of treatment) were available of 7 patients, 3 responders and 4 non-responders. IL-8 was detected in 6 patients (Fig. 3c), whereas TNFα could be measured in serum from 5 out of 7 patients (Fig. 3d). No consistent up or down modulation of either IL-8 or TNFα was observed, nor were there significant differences in these cytokine levels between responders and non-responders to Naltrexone (Fig. 3e, f). Together, these data suggest that Naltrexone does not positively impact on inflammation through modulation of intestinal epithelial cell cytokine production.

ER stress is intestinal epithelium is reduced by Naltrexone

As ER stress in the mucosa has been associated with the development of IBD, and Naltrexone was previously shown to reduce ER stress-induced inflammation in a model of liver damage, we next investigated whether Naltrexone has a direct effect on ER stress in intestinal epithelium. ER stress was chemically induced in intestinal epithelial cell lines by Tunicamycin (Fig. 4a and Additional file 3: Figure S2), as demonstrated by a strong upregulation of the ER stress marker GRP78. Interestingly, Naltrexone was able to reduce these levels in both cell lines. Chemical stimulation of cells with Tunicamycin causes inhibition of the UDP-*N*-acetylglucosamine-dolichol phosphate *N*-acetylglucosamine-1-phosphate

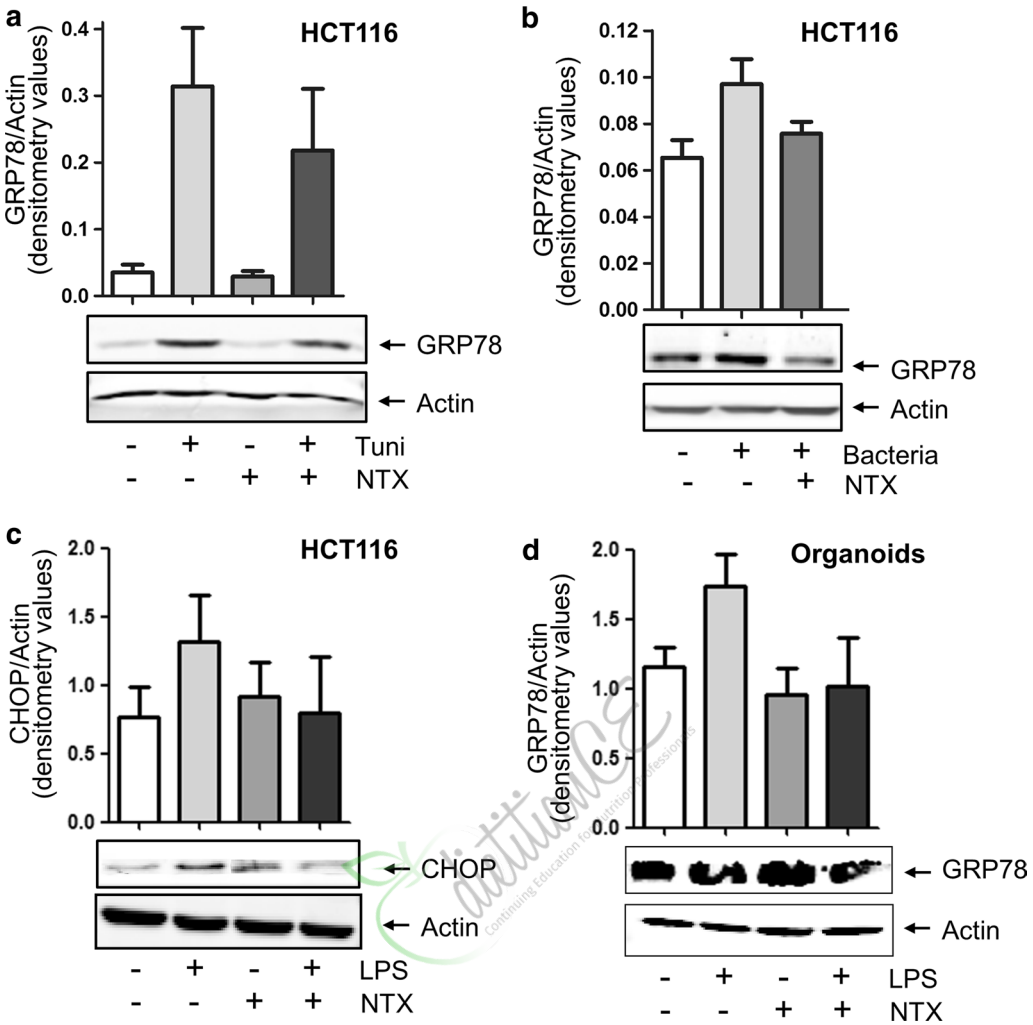

Fig. 4 ER stress in epithelial cell lines is decreased by Naltrexone. **a** ER stress was induced in HCT116 cells by treatment with 2 µM Tunicamycin (Tuni), resulting in an upregulation of GRP78 expression levels as detected by Western Blot analysis. Co-treatment of cells with 1 µg/mL Naltrexone (NTX) reduces the amount of Tunicamycin-induced GRP78 expression. Upper graph: mean densitometry values of two independent experiments, GRP78 expression is corrected for Actin, to control for equal loading. Representative example is shown in the bottom panels. **b** Treatment of HCT116 cells with bacteria results in a significant upregulation of GRP78 expression as detected by Western blot analysis, which is reduced by co-treatment cells by treatment of cells with 1 µg/mL Naltrexone. Mean densitometry values of four independent experiments is shown. **c** Treatment of HCT116 cells with LPS results in a significant upregulation of CHOP expression as detected by Western blot analysis, which is reduced by co-treatment cells by treatment of cells with 1 µg/mL Naltrexone. Mean densitometry values of three independent experiments is shown. **d** Treatment of organoids with LPS results in a significant upregulation of GRP78 expression as detected by Western blot analysis, which is reduced by co-treatment cells by treatment of cells with 1 µg/mL Naltrexone. Mean densitometry values are shown of experiments performed on organoids derived from two individual donors, with two independent experiments each

transferase (GPT) and subsequent accumulation of unfolded glycoproteins in the ER; a non-physiological process likely to result in much higher ER stress levels than are probable in vivo. To investigate ER stress in a more physiologically relevant setting, we incubated intestinal epithelial cells with bacteria (representative examples shown in Fig. 4b and Additional file 3: Figure S2A). A significant upregulation of GRP78 expression was observed in HCT116 cells treated with *E. coli* (0.065 ± 0.007 to 0.097 ± 0.01, $p = 0.0025$, Fig. 4b), which again was significantly reduced by co-treatment of cells with Naltrexone (0.076 ± 0.005, $p = 0.0025$). In CACO2 cells, Naltrexone diminished bacteria-induced GRP78 expression in three out of three experiments, although this did not reach statistical significance as bacteria-induced ER stress was low in these cells (Additional file 3: Figure S2A). In order to further confirm ER stress pathway activation with a different physiological stimulus, we

also induced ER stress in HCT116 cells with lipopolysaccharide and investigated expression levels of CHOP, a downstream target of the ER stress pathway. Figure 4c shows that CHOP levels induced by LPS were reduced by co-treatment with Naltrexone (1.315 ± 0.592 to 0.801 ± 0.710, $p = 0.027$). Again, the effect was less clear for CACO2 cells (Additional file 3: Figure S2C).

While cell lines are an easy and common model system to study epithelial cell function, such cell lines may show different cellular effects due to transforming mutations. We therefore generated organoids from colonic biopsies from two IBD patients, representing IBD epithelial tissue. Stimulation of these organoids with LPS again induced GRP78 expression (4 out of 4 experiments), and ER stress levels were reduced by co-treatment of organoids with Naltrexone (Fig. 4d, 1.734 ± 0.473 to 1.017 ± 0.698, $p = 0.046$). Together, these data imply that ER stress in intestinal epithelial cells is alleviated by Naltrexone.

Next, we investigated intestinal ER stress in patients treated with LDN. Intestinal tissue biopsies were available in 13 patients prior to treatment and in 5 patients 3 months into treatment, with 3 paired samples. Sections were stained for GRP78 (for specificity of the staining, see Additional file 4: Figure S3). High levels of ER stress were observed in both the inflamed intestinal lamina propria and crypts from IBD patients (Fig. 5a). GRP78 levels decreased upon NTX treatment, most noticeably in the lamina propria, (1.14 ± 0.5 vs 0.8 ± 0.5 for lamina propria and 0.9 ± 0.4 vs 0.7 ± 0.6 for crypts) although statistical significance was not reached because of low patient numbers (Fig. 4b). However, in the 3 paired samples available, NTX treatment reduced interstitial ER stress (Fig. 4c, and examples in Fig. 4d). In toto, these data suggest that Naltrexone has a direct effect on ER stress as measured by GRP78 expression in intestinal mucosa.

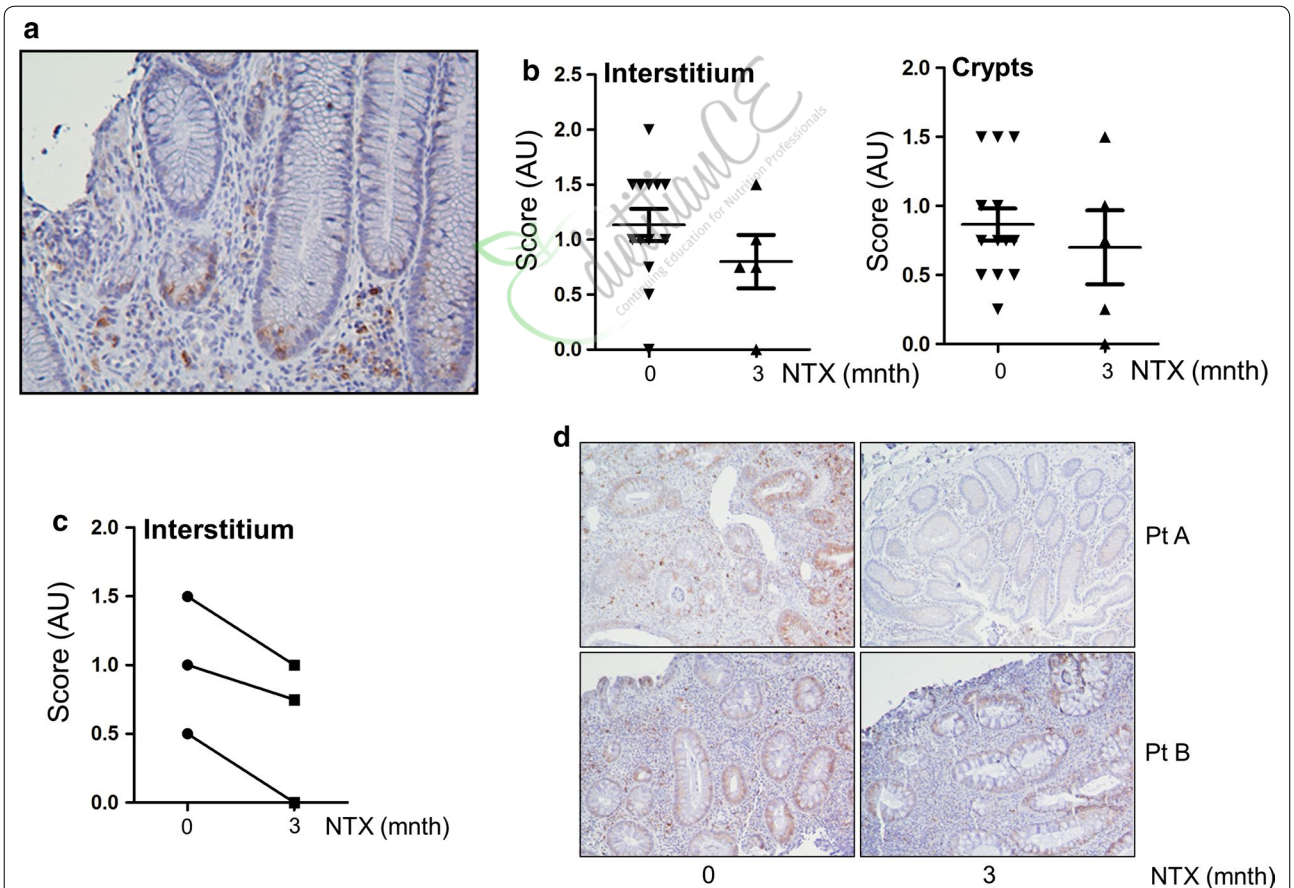

Fig. 5 High ER stress in mucosa from IBD patients is reduced by low dose Naltrexone treatment. **a** Example of GRP78, showing high ER stress marker expression in crypts as well as lamina propria. **b** GRP78 intensity was scored in lamina propria and crypts from biopsies taken from 13 patients before start of low dose Naltrexone and 5 patients 3 months into treatment. Lower levels of GRP78 expression were observed in lamina propria, although this did not reach statistical significance. **c** Paired biopsies were available from three patients. All three showed reduction of GRP78 expression in the lamina propria upon treatment with low dose Naltrexone. **d** Two paired samples are shown. Patient A was a non-responder, Patient B did show clinical response to low dose Naltrexone

Discussion

In this study, therapy refractory IBD patients receiving LDN showed clinical improvement in 74.5% of all patients and long-lasting clinical remission of in 25.5%. Furthermore, most patients achieving clinical remission also showed endoscopic improvement. The response and remission rates in this study appear slightly lower than the rates found in previously published studies (response rates of 88–89% and remission rates of 30–67% [22, 23]). These differences might be explained by differences in patient population, as the patients in our cohort had more severe disease, as reflected by the differences in previous drug exposure. Furthermore, the sample size of the previous studies was small, with only 17 and 18 patients receiving Naltrexone in the pilot study and the placebo controlled study, respectively. No serious adverse events were reported in the current study. Interestingly, we also found no elevated liver enzymes in our cohort, whereas previous studies found such abnormalities in 1.8–11.1% of patients treated with Naltrexone [22, 23]. Thus, our data suggest that LDN is safe and effective in the treatment of conventional therapy-refractory IBD patients.

While the potential benefit of Naltrexone treatment for IBD is becoming clear, the underlying mechanisms and the general role of the opioid system in IBD have so far received very little attention. An increased expression of MOR in mucosal immune cells has been shown, and one possible function of this upregulation may be compensatory pain management. Pro-inflammatory Th1 and Th17 cells produce enhanced levels of endogenous opioids during colitis in mice [31], which suppress pain signals during chronic mucosal inflammation [32]. As such, it is conceivable that part of the remission in LDN treated patients is a result of a general improvement of well-being. Interestingly, antagonists of the nociceptor receptor (involved in pain sensation) also reduced intestinal pro-inflammatory cytokine profiles and ameliorated DSS colitis in mice, suggesting that blocking pain sensors has a direct immune-modulatory effect [33]. Intriguingly, it has recently been shown that the opioid inactive (+)-isomers of Naltrexone inhibit lipopolysaccharide-induced Toll like Receptor 4 (TLR4) signaling, a bacterial-induced inflammatory pathway contributing to IBD [34, 35]. It is as yet unclear whether the Naltrexone preparations currently used in patients (and as bought for in vitro experiments) contain this opioid inactive isoform, but it is at least theoretically possible that some of the beneficial effects observed in the current study are not regulated by MOR, but rather by inhibition of TLR signaling. Furthermore, in addition to MOR, Naltrexone also has weak affinity for the κ and δ opioid receptors, and it is conceivable that some of the observed effects occur through these receptors.

The limited studies performed so far on the mechanistic effect of Naltrexone have mainly focused on immune cells. However, our study suggests that Naltrexone can also have direct beneficial consequences on epithelial barrier cells, by stimulating wound healing. These data are in accordance with the improved in vivo wound healing observed upon Naltrexone treatment in both IBD patients and diabetic mice [36]. However, while the effect of Naltrexone on wound healing in skin was shown to be a result of increased fibroblast proliferation [37], our in vitro model suggests that wound healing of intestinal epithelial barriers is modulated by improved migration rather than proliferation.

Other studies investigating the potential mechanism of LDN on inflammation have focused on immune cell cytokine production. Elevated TNFα, IL-6 and IL-12 levels have been reported to be reduced by Naltrexone in chemically induced mouse colitis models [15, 16]. In contrast, others have found that LDN enhances dendritic cell maturation and stimulates their TNFα and IL-12 production, whereas in the current study, no effect of Naltrexone on either epithelial induced IL-8 production or IL-8 and TNFα serum levels in IBD patients was observed. However, it should be noted that not all cytokines could be detected in our system, and it is possible that other cytokines, which were not studied here, are affected.

We and others have previously shown that patients carrying gene variants associated with development of IBD demonstrate increased mucosal ER stress and bacterial persistence, suggesting that intestinal ER stress contributes to IBD pathology [19, 38–40]. The cell type that appeared most affected, even in non-inflamed mucosa, were the Paneth cells, specialized anti-microbial peptide producing cells [17]. We now show that during inflammation, not only Paneth cells, but also other crypt and lamina propria cells show increased ER stress, which may reflect a general cellular stress response in the presence of pro-inflammatory cytokines or bacteria. Indeed, we demonstrate that stimulation of intestinal epithelial cells with bacteria or LPS triggers a significant upregulation of the ER stress marker GRP78. However, not all cell lines showed this effect, which may be a reflection of the genetic IBD risk factors present in these cell lines. Nevertheless, ER stress in both cell lines as well as organoids derived from IBD patients was reduced by treatment with Naltrexone, as were lamina propria GRP78 levels in biopsies from patients treated with Naltrexone, although this did not correlate with clinical response in all cases. Interestingly, genetic variants of the MOR gene *OPRM1* affect response to high doses of NTX, however to what extent

they may play a role in clinical and molecular response in IBD patients is as yet unclear [41].

Conclusion

In conclusion, our study provides additional insight into the mechanism of action of Naltrexone in intestinal inflammation, showing a direct effect of this opioid on intestinal epithelial wound healing and ER stress reduction. The clinical results are promising, and particularly given the low frequency and relative beneficial nature of side-effects, the use of LDN in therapy refractory IBD patients seems warranted. Future clinical research may also focus on the use of LDN earlier in the IBD treatment pyramid.

Is-there a place for vagus nerve stimulation in inflammatory bowel diseases?

Abstract

The vagus nerve (VN), the longest nerve of the organism that innervates the gastrointestinal tract, is a mixed nerve composed of 80% of afferent and 20% of efferent fibers. The VN has anti-inflammatory properties, in particular an anti-TNFα effect through the cholinergic anti-inflammatory pathway. The VN is a key component of the autonomic nervous system, i.e. the parasympathetic nervous system. An imbalance of the autonomic nervous system, as represented by a low vagal tone, is described in many diseases and has a pro-inflammatory role. Inflammatory bowel diseases (IBD) are chronic disorders of the gastro-intestinal tract where TNFα is a key cytokine. VN stimulation (VNS), classically used for the treatment of drug resistant epilepsy and depression, would be of interest in the treatment of IBD. We have recently reported in a 6 month follow-up pilot study that VNS improves active Crohn's disease. Preliminary data of another pilot study confirm this interest. Similarly, VNS has recently been reported to improve rheumatoid arthritis, another TNFα mediated disease. Bioelectronic Medicine, as represented by VNS, opens new therapeutic avenues in the treatment of such chronic inflammatory disorders. In the present manuscript, we will focus on the interest of VNS in IBD.

Keywords: Vagus nerve, Vagus nerve stimulation, Inflammatory bowel diseases, Cholinergic anti-inflammatory pathway

Background

Inflammatory bowel diseases (IBD) are chronic inflammatory disorders of the gastrointestinal tract involving the recto-colon for ulcerative colitis (UC) and all the digestive tract (essentially the ileum and/or colon) for Crohn's disease (CD) (Abraham & Cho, 2009). Flares are characterized by abdominal pain, diarrhea (bloody in UC), fever, weight loss, and extra-intestinal manifestations (skin, eyes, joints) with a significant impact on quality of life. About 2.2 million people in Europe and 1.5 million Americans are affected by IBD (Molodecky et al., 2012) with a regular increase of their incidence and prevalence due to the "Westernization" of our lifestyle. The pathophysiology of IBD involves genetic, immunologic and environmental factors (de Souza, 2017). The concept of medical treatment of IBD has recently evolved from steroids/immunosuppressants to biologics targeting TNFα, a key cytokine in IBD, and more recently anti-adhesion molecules and anti-IL12/23, with the aim to heal mucosa and to prevent irreversible damages of the digestive tract (Chang & Hanauer, 2017). However, these treatments don't cure the disease and are not fully effective because patients are either non-primary responders or secondarily lose response (Ben-Horin et al., 2014). In addition, these drugs are not devoid of side-effects (Bonovas et al., 2016) thus explaining that patients are reluctant and not compliant with these treatments (Lenti & Selinger, 2017), and are among the highest users of complementary and alternative medicines (Yanai et al., 2016).

Consequently, a non-drug therapy targeting an anti-inflammatory pathway and devoid of side-effects would be of interest in the treatment of IBD. Bioelectronic Medicine is a new therapeutic approach using devices to modulate electrical activity of the nervous system to restore organ function and health without the side-effects of pharmaceutical agents and avoiding compliance problems (Olofsson & Tracey, 2017). Among the nervous system, the vagus nerve (VN), the principal component

of the parasympathetic nervous system, appears as an interesting target for Bioelectronic Medicine due to its anatomical specificity at the interface of gut-brain interactions and its role in the neuro-endocrine-immune axis (Bonaz et al., 2017). VN stimulation (VNS) is presently used in the treatment of drug resistant epilepsy and depression (Milby et al., 2008) based on the widespread central projections of the VN (Ruffoli et al., 2011). More recently, VNS has been shown to improve experimental models of septic shock and colitis (Borovikova et al., 2000; Meregnani et al., 2011). Translational pilot studies have been recently performed in chronic inflammatory disorders such as CD and rheumatoid arthritis (Bonaz et al., 2016; Koopman et al., 2016). In the present review, we will focus our attention on the use of VNS in IBD, especially in CD.

Rationale for targeting the vagus nerve in inflammatory bowel diseases

The VN is the longest nerve of the organism innervating all the digestive tract for some anatomists (Delmas & Laux, 1933). It is a mixed nerve composed of 80% afferent and 20% efferent fibers (Prechtl & Powley, 1990). The VN is a key element of brain-gut interactions and of the autonomic nervous system (Bonaz et al., 2017). There is an imbalance of the autonomic nervous system in IBD that could play a role in the pathophysiology of IBD. Indeed, we have reported that vagal tone was significantly blunted in IBD in relation with negative affects and a high TNFα level (Pellissier et al., 2010; Pellissier et al., 2014). The VN, through its afferent fibers, activates the hypothalamic-pituitary adrenal (HPA) axis (Fig. 1) known to dampen peripheral inflammation through the release of glucocorticoids (Harris, 1950). Another anti-inflammatory pathway, involving vagal efferents, has been more recently described in 2000 by the group of Tracey and called the cholinergic anti-inflammatory pathway (CAP) (Pavlov et al., 2003). Indeed, the release of acetylcholine (ACh) at the distal end of the VN is able to inhibit the release of TNFα by macrophages through the link of ACh with alpha7nicotinic receptors (α7nAChR) of these macrophages (Wang et al., 2003) (Fig. 1). However, the VN does not innervate directly resident macrophages in the gut but through an interaction with nNOS-VIP-Ach interneurons with their nerve endings in close proximity of these resident macrophages (Cailotto et al., 2014). The group of Tracey has also described a vago-sympathetic pathway where, in a synergistic effect, the VN interacts with the sympathetic splenic nerve releasing norepinephrine acting on β2 receptors of splenic CD4 T-lymphocytes which release ACh to inhibit the release of TNFα by splenic macrophages through an interaction with their α7nAChR (Rosas-Ballina et al., 2008) (Fig. 1). For some authors the sympathetic nervous system, through the release of its neurotransmitter, norepinephrine, could be the efferent arm of the CAP (Martelli et al., 2016). Indeed, vagal afferents activate the central autonomic network (Benarroch, 1993) which in return, through descending pathways from the paraventricular nucleus of the hypothalamus, the A5 noradrenergic group and the C1 adrenergic group, modulates pre-ganglionic neurons of the sympathetic nervous system in the spinal cord and thus the splenic nerve (Abe et al., 2017) (Fig. 1). Consequently, the interaction of the VN with the sympathetic nervous system is of interest and targeting the anti-inflammatory effect of the VN, i.e. an anti-TNFα pathway, both through its afferent and efferent fibers would be of interest in IBD.

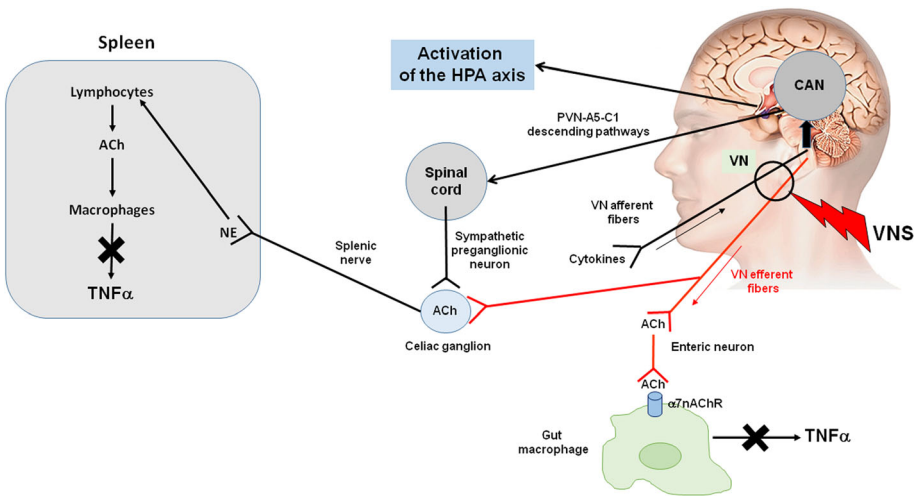

Fig. 1 Anti-inflammatory pathways of the vagus nerve. Adapted from reference (Bonaz et al., 2017). Ach, acetylcholine; CAN, central autonomic network; HPA axis, hypothalamic pituitary adrenal axis; NE, norepinephrine; TNF α, tumor necrosis alpha; VN, vagus nerve; VNS, vagus nerve stimulation; α7nAChR, alpha7 nicotinic acetylcholine receptor

How to target the vagus nerve?

Based on its dual anti-inflammatory role, the VN appears as an interesting therapeutic target for chronic inflammatory disorders such as IBD, in particular targeting the CAP. This approach can be obtained *i)* pharmacologically with α7nAChR agonists such as nicotine (Cui & Li, 2010), GTS21 (Kox et al., 2011), and AR-R17779 (van Westerloo et al., 2006), activation of the central cholinergic pathway with an AChesterase inhibitor (galantamine) (Pavlov et al., 2009) or CNI-1492, a cytokine inhibitor and synthetic guanylhydrazone mitogen-activated protein kinase blocker (Tracey, 1998), *ii)* high fat enteral feeding inducing the release of CCK that activates CCK1 vagal afferents thus activating the CAP (Luyer et al., 2005), *iii)* complementary and alternative medicines such as meditation, yoga, acupuncture, hypnosis, known to activate the VN (Keefer et al., 2013), i*v)* physical exercise (Mora et al., 2007), *v)* VNS which appears as the most interesting tool because already validated in drug resistant epilepsy and depression in human with very few side effects (Bonaz et al., 2013).

Vagus nerve stimulation in epilepsy and depression

The first VNS device for the treatment of drug-resistant epilepsy was introduced in human in 1990. VNS has been validated by the US Food and Drug Administration (FDA) for drug resistant epilepsy in 1997 and in 1994 for Europe and for depression in 2005. For these indications, the mechanism relies on an activation of vagal afferents by high frequency stimulation at 20–30 Hz (Bonaz et al., 2013). Indeed, low frequency stimulation is less efficient in epilepsy than high frequency stimulation and stimulation over 50 Hz induces damage of the VN (Schachter & Boon, 2007). Brain imaging studies in human have shown that brain regions activated were greater at high (20 Hz) than low (5 Hz) frequency VNS (Lomarev et al., 2002). The widespread projections of the NTS, the target of vagal afferents, in the brain explain the efficacy of VNS in epilepsy and depression (Ruffoli et al., 2011). The locus coeruleus (LC), the principal brain noradrenergic nucleus, is believed to mediate many of the effects of VNS in the central nervous system. The LC receives excitatory input from the NTS via the nucleus paragigantocellularis (Ruffoli et al., 2011). Lesions of the LC block the anti-epileptic and anti-depressant effects of VNS (Krahl et al., 1998). VNS increases firing rates of LC neurons and norepinephrine concentrations in the cortex and hippocampus, two projection sites of the LC (Dorr & Debonnel, 2006; Roosevelt et al., 2006) and activates the LC in a fMRI study in humans (Frangos et al., 2015). VNS may act initially and/or predominantly on the LC, and indirectly with the dorsal raphe nucleus via afferents from the LC (Dorr & Debonnel, 2006).

A reduction of seizure is observed in 50% of patients after 2 to 3 years of VNS (Morris 3rd & Mueller, 1999). In a retrospective study of VNS in 65 patients with epilepsy with a mean duration of VNS of 10 years Elliott RE et al. (Elliott et al., 2011) showed that the mean reduction in seizures at 6 months and years 1, 2, 4, 6, 8, and 10 was 35.7, 52.1, 58.3, 60.4, 65.7, 75.5, and 75.5%, respectively. Consequently, VNS is a slow acting therapy.

Vagus nerve stimulation in inflammatory bowel diseases

Based on its use in epilepsy and depression, VNS could be an interesting tool for the treatment of IBD based on pre-clinical data in rats with colitis and 2 recent clinical pilot studies targeting 2 different populations of patients with active CD either naïve of anti-TNF on inclusion or in patients resistant to biologics.

Experimental rationale

The autonomic nervous system, in particular the parasympathetic nervous system, has a role in the control of experimental colitis. Classically, vagotomy aggravates colitis (Ghia et al., 2006) and sacral nerve stimulation enhances intestinal barrier repair in acute mucosal injury of experimental colitis (Brégeon et al., 2016). The first pharmacological study targeting the CAP used Achesterase (AChE) inhibitors (physostigmine and neostigmine) prior to induce colitis in rats. Physostigmine, which crosses the blood brain barrier, induced a greater improvement of colitis than neostigmine pretreatment thus suggesting than central cholinergic pathways have a greater protective effect than peripheral pathways (Miceli & Jacobson, 2003). Based on this study and the description of the CAP, our group has performed low frequency (5 Hz) VNS in chronically implanted freely moving rats with the other parameters classically used for epilepsy, supposed to activate vagal efferents, for 5 consecutive days in rats with trinitrobenzenesulfonic acid (TNBS) colitis, classically used as an experimental model of CD (Meregnani et al., 2011). Colonic inflammation was evaluated by a global multivariate index of colitis taking into account *i)* body weight, temperature and locomotor activity, *ii)* areas of lesions and histological damage, *iii)* biological parameters such as myeloperoxidase activity, cytokine and cytokine-related mRNAs at the level of colonic damage and just above. VNS significantly improved the multivariate index of colitis (Meregnani et al., 2011). The inflammatory infiltrate just immediately above the major colonic lesion was significantly improved by VNS while a slight reduction was observed in the lesion thus arguing for a major efficacy of VNS on tissues that are less damaged (Meregnani et al., 2011). Sun et al. (Sun et al., 2013) performed chronic VNS (0.25 mA, 20 Hz, 500 ms) in a model of TNBS colitis

in rats and recorded heart rate variability (HRV) as a marker of the sympatho-vagal balance. They observed a significant improvement of colitis under VNS, a decrease of pro-inflammatory cytokines (TNFα and IL-6), and an improvement of HRV. More recently, Jin et al. (Jin et al., 2016) showed that chronic VNS improves inflammation in TNBS-treated rats by inhibiting pro-inflammatory cytokines via an autonomic mechanism; addition of noninvasive electro-acupuncture to VNS enhanced the anti-inflammatory effect of VNS.

Clinical rationale

In a translational approach, we have performed a pilot study of VNS in CD patients. We have implanted 9 patients with CD, with 8 out of 9 patients with active CD on inclusion. The patient in clinical and endoscopic remission on inclusion had received a treatment with budesonide, a topically acting corticosteroid with extensive first pass hepatic metabolism, and azathioprine, an antimetabolite therapy. This patient stopped budesonide few weeks before inclusion and azathioprine because of a pseudo-flu-like syndrome due to azathioprine. Patients between 18 and 65 years had a Crohn's disease activity index (CDAI; a research tool used to quantify symptoms of patients with CD such as abdominal pain, number of liquid or soft stools, general well-being) between 220 and 450 (i.e. moderate to severe CD; CDAI< 150: clinical remission), with a small bowel (ileum) and/or colonic CD, diagnosed for more than 3 months, naive of treatment or despite a stable treatment reference, with a C-reactive protein (CRP; acute-phase protein of hepatic origin) > 5 mg/L and/or a fecal calprotectin (a marker of intestinal inflammation) > 100 μg/g and a Crohn's disease endoscopic index of severity (CDEIS; for endoscopic assessment of mucosal disease activity. CDEIS< 6: endoscopic remission) ≥7 were prospectively included. Patients under infliximab or any other anti-TNFα agent on inclusion were not eligible. Stimulation parameters were: 10 Hz, 500 μsec pulse width, no more than 1.5 mA, 30 s ON, 5 min OFF. Intensity was progressively increased during the first month after implantation from 0.25 to 1.50 mA. All patients signed an informed consent. The study was approved by the institutional ethics committee (11-CHUG-28) and registered in ClinicalTrials.gov (Identifier: NCT01569503; First received: March 30, 2012). The primary endpoint was to induce clinical remission (CDAI< 150) and the secondary endpoints to induce biological and endoscopic remission and restore vagal tone. The first patient was implanted on April 2012 and the last one on March 2016. All the patients entered in a one year follow-up study. Only two patients were under azathioprine (2.5 mg/kg) on inclusion. VNS induced a deep (clinical-biological-endoscopical) remission in 5 of the nine patients with restored vagal tone. The patient on remission on inclusion was still in deep remission under VNS alone at 1 year. The last (9th) included patient has just reached the one year follow-up and is in flare of the disease but did not want to switch to anti-TNF because he was afraid of the side effects of anti-TNF. Two patients were removed from the study after 3 months of VNS despite a clinical improvement during the two first months of VNS and switched to infliximab and azathioprine; one of the two patients was operated (ileocecal resection). These two patients had the highest CDAI, CRP and CDEIS on inclusion as well as the 9th patient included which suggests that VNS, as a slow-acting therapy, is more indicated in moderate CD. All the 9 patients have still the device in place. Among the two patients who left the study at 3 months, the intensity was decreased to 0.5 mA for one patient and stable at 1.5 mA for the other patient. VNS was well tolerated with the classical minor side effect represented essentially by hoarseness. We did not observe any problem of infection either local or systemic and no VNS device was removed. The data on the first seven implanted patients after a 6-month follow-up were recently reported for the first time (Bonaz et al., 2016).

In a second pilot study (SetPoint Medical Corporation, ClinicalTrials.gov Identifier: NCT02311660; First received: December 3, 2014), D'Haens et al. (D'Haens et al., 2016) have reported in an abstract form the effect of VNS for 16 weeks in 8 patients with biologic-refractory small bowel and/or colonic CD. Patients had a moderate to severe CD (220 < CDAI< 450) on inclusion, a CRP ≥ 5 mg/L, a fecal calprotectin ≥200 μg/g, an endoscopic score of activity (SES-CD: Simple Endoscopic Scale for Crohn's Disease, an endoscopic score correlated with the CDEIS) with the presence of a minimal ulcer score of 2 or 3 in at least 1 segment, with a history of inadequate response and/or intolerance or adverse events to one or more TNF-alpha inhibitors (e.g.,infliximab, adalimumab, or certolizumab pegol), a 8 weeks washed out of biologics. Stimulation parameters were: 10 Hz, 250 μsec pulse, 2 mA max, for 60 s first then for 5 min. At 8 weeks, stimulations were increased if CDAI remission was not achieved. Some of the patients had prior Crohn's surgery. 8/8 had prior anti-TNF, 4/8 vedolizumab, 2/8 ustekinumab, 8/8 corticosteroids, 5/8 azathioprine, 1/8 mercaptopurine, and 4/8 methotrexate. The primary endpoint was the change in CDAI from baseline to week 16 visit: CDAI scores were reduced by 70 in 6 to 8 patients. The secondary endpoints were *i)* the rate of clinical response at week 16 visit defined as CDAI improvement from baseline of at least 70 points that was obtained in 6/8 patients, *ii)* rate of clinical remission at week 16 visit defined as CDAI≤150: 3/8 patients were in clinical remission, *iii)* change in total

SES-CD score from baseline to week 16 visit: endoscopic scores were reduced in 6 to 8. CRP and fecal calprotectin levels were reduced in patients who achieved clinical response. HRV was increased in 6 patients, consistent with an increasing parasympathetic tone. Nine serious adverse events were reported in 5/8 patients, all of which were CD-related except for 1 patient with a device-related postoperative infection.

These two pilot studies show a sign in favor of an effect of VNS in active CD and are complementary since our study involved patient naïve of biologics on inclusion and with only 2 patients under azathioprine on inclusion while in the study of D'Haens et al. (D'Haens et al., 2016) highly refractory patients were included with failure of biologics. Of course a more robust randomized control trial needs to be performed, in particular including patients who are naïve of or refractory to biologics.

Very recently, Koopman et al. (Koopman et al., 2016) have shown that VNS was able to inhibit peripheral blood production of cytokines (TNFα, IL-1β, and IL-6) and attenuate disease severity in rheumatoid arthritis, another TNF-mediated disease.

Noninvasive or invasive VNS?

Classically VNS performed in epilepsy and depression as well as in the 2 pilot studies in CD patients is invasive, generally performed by a neurosurgeon familiar with the technique with a duration of 1 h, with few side-effects. However, some patients are reluctant to surgery a fortiori in a vasculo-nervous region involving the vein and the external carotid artery which are in close contact with the VN, thus noninvasive (n) VNS would be valuable. In addition, if the device can be removed, the electrode wrapped around the VN is generally left in place although some authors removed it without major damage to the nerve and vessels (Champeaux et al., 2017). Devices stimulating the VN at the cervical level or at the auricular level have been developed. Indeed, the cymba concha of the external ear is innervated by a sensory auricular branch of the VN (Peuker & Filler, 2002) that sends projection in the NTS in cats (Nomura & Mizuno, 1984) and humans (Frangos et al., 2015). Transauricular (ta) VNS could thus activate the CAP through an inflammatory reflex. ta-VNS dampened LPS-induced inflammatory responses in rats that was suppressed by vagotomy or α7nAChR antagonist (Zhao et al., 2012). External stimulation of the left cervical VN decreased whole blood culture-derived cytokines and chemokines in healthy volunteers (Lerman et al., 2016). Two n-VNS devices, used for epilepsy, depression, and headache are available, the NEMOS one (Cerbomed, Erlangen, Germany) using an intra-auricular electrode (Stefan et al., 2012) and the GammaCore one (electroCore LLC, Basking Ridge, NJ, USA) with two stainless steel round discs functioning as skin contact surfaces (Nesbitt et al., 2015). There are presently no published data regarding the use of these two devices in inflammatory disorders of the digestive tract.

No significant serious adverse events have been reported with these noninvasive devices. By comparison to invasive VNS, n-VNS has the disadvantage of its compliance which is an important problem in the treatment of IBD. Indeed, about 30–40% of IBD patients don't take their treatment (Herman & Kane, 2015). In addition, complementary and alternative medicine-IBD users are less likely to be adherent to medical therapy than nonusers (Nguyen et al., 2016). One can wonder if it could be the same problem with these noninvasive devices. In addition, in the case of the Gammacore device, the reproducibility of the position of the discs in contact with the VN is questionable. Finally, in an experimental model of septic shock, ta-VNS was less efficient than VNS to attenuate the LPS-induced serum cytokine (TNFα, IL1β, and IL6) response (Zhao et al., 2012).

Questions-future for vagus nerve stimulation in inflammatory bowel diseases

The use of VNS in IBD, wether invasive or noninvasive, needs convincing data for health-authorities for regulatory approval and reimbursement as well as for the community of IBD physician, and patients who are expecting a nondrug therapy devoid of side-effects. Consequently a robust randomized controlled trial looking at VNS vs sham-stimulated in IBD patients is warranted. Controls should be implanted but not stimulated. Indeed, even low frequency VNS (1 Hz) discretely affected the level of c-fos expression in the rat NTS, compared to sham-operated animals (Osharina et al., 2006). Regarding the frequency of stimulation, if low frequency (5–10 Hz) is supposed to activate vagal efferents (Bonaz et al., 2013), we have reported in rats that even low frequency stimulation at 5 Hz was able to induce modifications of activation in the NTS, the first target of the VN in the brain, as well as in numerous areas of its brain projections (Reyt et al., 2010). Brain imaging studies in human as well as *c-fos* activation in the NTS and other NTS brain related nuclei have been reported in humans and animals under VNS respectively (Lomarev et al., 2002; Osharina et al., 2006). Based on the involvement of both vagal afferents and efferents in the anti-inflammatory effect of the VN one can wonder that VNS at 10 to 30 Hz would be of interest in humans. The intensity of stimulation is generally limited by side-effects such as pain in the throat which generally disappears when decreasing intensity and/or pulse width. Generally intensity beyond 1.50 mA was not well supported in our pilot study in CD patients (Bonaz et al., 2016).

Another question is the duration of the stimulation. Generally, in epilepsy and depression the parameters are 30 s ON and 5 min OFF. This is the timing that we used in our pilot study. However, Koopman et al. (Koopman et al., 2016) performed VNS for 60 s up to 4 times daily in patients with RA based on a previous work where VNS delivered once daily for 60 s attenuated joint swelling, inhibited cytokine production and conferred significant protection against synovitis and periarticular bone erosions (Levine et al., 2014). D'Haens et al. (Krahl et al., 1998) in their preliminary unpublished study also used intermittent VNS (1 to 5 min per day). However, it means that the parameters of the device need to be changed manually with the magnet generally supplied with the device that is not always convenient except if the controller is given to the patient. Consequently, a programmable device would be valuable.

Miniaturization of the VNS device is also warranted. In the same way, instead of an electrode, a VNS device which would act as an electrode by clipping it around the VN would be of interest (see setpointmedical.com; MØ1-ØØ1123). In that case, a single surgical incision would be sufficient thus reducing the duration of the surgery. Another important progress would be a device that is able to record vagal tone and able to trigger VNS in case of low vagal tone to restore a normal tone. A VNS system, AspireSRTM, already approved in Europe, and created by Cyberonics Inc. analyzes relative changes of heart rate, particularly ictal tachycardia, and responds to seizures automatically.

Anti-TNFα drugs are presently the best treatment to prevent postoperative recurrence of CD (Qiu et al., 2015). Surgery cures CD lesions and since VNS is a slow-acting therapy, it could be an interesting tool in such patients. Another possibility would be to use combotherapy (drugs + VNS) to induce mucosal healing with biologics and then VNS could take over the time of its efficacy. The two pilot studies of VNS in IBD (Bonaz et al., 2016; D'Haens et al., 2016) focused on CD but VNS in UC, which involves the recto-colon, would be also of interest. IBD occurs in childhood-adolescence in about 25% (Sawczenko et al., 2001). VNS for epilepsy in children younger than 12 years is off-label but pediatric studies have reported comparable efficacy as for adult patients (Elliott et al., 2011). Consequently, VNS in children with IBD should be of interest.

The cost of VNS was saved within 2 years following implantation of the device in drug resistant epilepsy (Boon et al., 1999). In the same way, the treatment of IBD is estimated to be reduced with VNS. The total modeled per patient infusion therapy costs in year 1 with infliximab was $38,782; drug acquisition cost was the largest total costs driver (90–93%) (Afzali et al., 2017). The cost of the device (neurostimulator + electrode) is ~ $11,000. The battery lasts between 7 and 10 years depending on the frequency of stimulation and intensity of the current. Battery life is correlated with charge, the lower pulse widths (250 and 130 μs) and their respective threshold currents conserve battery life more effectively than the longer pulse widths (500, 750, or 1000 μs) (Helmers et al., 2012). Battery demand is also affected by duty cycle and signal frequency (increases in both of these parameters will negatively affect battery longevity) (Helmers et al., 2012).

VNS is intermittent and regular as classically programmed. There is no special rule to follow in programing of VNS but adjustment to higher settings of the parameters is usually performed progressively, particularly for intensity. High stimulation (30 Hz, 30 s on, 5 min off, 500 μsec pulse width) is more effective than low stimulation (1 Hz, 30 s on, 90–180 min off, 130 μsec pulse width) in epilepsy (Schachter & Boon, 2007). Higher output current is necessary if no improvement is observed in the early phase of VNS in epilepsy; 20% of non-primary responders showed response after an increase of current intensity (Bunch et al., 2007). Consequently, in IBD such an adaptation could be performed.

In a very recent elegant study, Hulsey et al. (Hulsey et al., 2017) recorded neural activity in the LC in response to VNS over a broad range of current amplitudes, pulse frequencies, train durations, inter-train intervals, and pulse widths. Brief 0.5 s trains of VNS drive rapid, phasic firing of LC neurons at 0.1 mA. Higher current intensities and longer pulse widths drive greater increases in LC firing rate. Varying the pulse frequency substantially affects the timing, but not the total amount, of phasic LC activity. These results provide insight into VNS-evoked phasic neural activity in multiple neural structures and may be useful in guiding the selection of VNS parameters to enhance clinical efficacy.

Morphometric parameters of the VN may have a role to influence the efficacy of VNS. However, very few data are available in that area. Activation of nerve fibers during VNS depends on several factors: *i)* fibers located closer to the perimeter of the nerve and thereby closer to the VNS therapy cathode are exposed to a stronger electric field and are easier to excite than fibers located deeper in the nerve, *ii)* fibrous tissue encapsulation at the site of electrodes forms within 4–8 weeks after implantation and can increase resistance thus altering the electric field and increasing voltage requirements for fiber excitation, *iii)* fiber myelination and fiber diameter. Classically, ~20% of vagal fibers are myelinated A and B fibers and the remaining 80% are non-myelinated C-fibers; the conduction velocity of myelinated fibers is proportional to their size (Erlanger & Gasser, 1930). Vagal A-fibers are the largest and myelinated fibers and

carry afferent visceral information and motor input while vagal B-fibers are small and myelinated fibers carrying parasympathetic input. Finally, vagal C-fibers are small and unmyelinated and carry afferent visceral information. C-fibers were supposed to be involved in the effects of VNS but their destruction by capsaicin did not suppressed the effects of VNS on seizures in rats (Krahl et al., 2001) thus arguing for the involvement of myelinated A and B fibers in the effect of VNS. Fibers with larger diameters require less current to reach the stimulus thresholds for recruitment and have higher conduction velocity than fibers with smaller diameters. Therefore, as current increases, fibers are recruited in the following order: A group, B group, and C group. However, successful recruitment of fibers with the same diameter varies depending upon their proximity to the stimulus source. Selective stimulation of a group of fibers to affect only a certain portion of the brain may not be effective in many patients. Achieving full activation of the VN requires selecting the right combination of VNS therapy parameter settings. Based on a computational model, Helmers et al. (Helmers et al., 2012) have shown that a range of output current settings between 0.75 and 1.75 mA with pulse width settings of 250 or 500 μs may result in optimal stimulation. The spiral electrode wrapped around the cervical left VN does not fully encircle the VN, but wraps approximately 270 degrees around it. The bipolar helical nerve electrode is the only design that is currently approved by the FDA for VNS therapy. Consequently, higher stimulation may be required for the activation of the nerve fibers present in the area not covered by the electrode. In contrast, fibers located near the perineurium of a fascicle are exposed to a stronger electric field (Helmers et al., 2012). In addition, the large variation in epineurial connective tissue might influence the effectiveness of VNS (Helmers et al., 2012). Verlinden et al. (Verlinden et al., 2016) have shown that the right cervical VN has a 1.5 times larger effective surface area than the left nerve and that there is a broad spreading within the individual nerves. They also showed that at the right side, the mean effective surface area at the cervical level is larger than at the level inside the skull base implying that the VN receives anastomosing and 'hitchhiking' branches from areas other than the brainstem. In addition, tyrosine hydroxylase- and dopamine ß-hydroxylase-nerve fibers have been individualized in the VN, indicating a catecholaminergic neurotransmission. Consequently, a sympathetic activation could be part of the mechanism of action of VNS. There is presently no recommendation on the positioning of the electrodes, as no method has been developed to predict whether a particular fascicle or multiple fascicles within the nerve should be recruited to elicit a therapeutic response.

All the technical points developed above should be taken into consideration in clinical studies and may influence the results of these studies.

Conclusion

Based on the anti-inflammatory role of the VN, the use of VNS in the era of Bioelectromic Medicine opens new therapeutic avenues for the treatment of chronic inflammatory disorders such as IBD. Recent pilot studies have provided a sign in this direction. However, these data need to be confirmed in a more robust randomized control trial. In addition, looking at the optimal parameters for anti-inflammatory conditions is warranted. RA and psoriasis, other TNF mediated diseases, are also therapeutic targets of VNS.

"This course was developed and edited from the open access article: Colon epithelial cells luminal environment and physiopathological consequences: impact of nutrition and exercise, Nutrire - Blachier et al., (2018) 43:2. (DOI:10.1186/s41110-018-0061-6), used under the Creative Commons Attribution License."

"This course was developed and edited from the open access article: High salt diet exacerbates colitis in mice by decreasing Lactobacillus levels and butyrate production, Microbiome - Miranda et al., (2018) 6:57. (DOI:10.1186/s40168-018-0433-4), used under the Creative Commons Attribution License."

"This course was developed and edited from the open access article: A probiotic complex, rosavin, zinc, and prebiotics ameliorate intestinal inflammation in an acute colitis mouse model, Journal of Translational Medicine - Park et al., (2018) 16:37. (DOI:10.1186/s12967-018-1410-1), used under the Creative Commons Attribution License."

"This course was developed and edited from the open access article: Low dose Naltrexone for induction of remission in inflammatory bowel disease patients, Journal of Translational Medicine - Lie et al., (2018) 16:55. (DOI:10.1186/s12967-018-1427-5), used under the Creative Commons Attribution License."

"This course was developed and edited from the open access article: Is-there a place for vagus nerve stimulation in inflammatory bowel diseases?, Bioelectronic Medicine - Bruno Bonaz, (2018) 4:4. (DOI:10.1186/s42234-018-0004-9), used under the Creative Commons Attribution License."